NASA/TM-20220011967

An Analysis of the Impact of Extreme Attitude Operation on a Turbofan Engine in a Regional Jet Aircraft

Jonathan S. Litt
Glenn Research Center, Cleveland, Ohio

T. Shane Sowers
HX5, LLC, Brook Park, Ohio

Daniel A. Trowbridge
Zin Technologies, Inc., Middleburg Heights, Ohio

September 2022

NASA STI Program . . . in Profile

Since its founding, NASA has been dedicated to the advancement of aeronautics and space science. The NASA Scientific and Technical Information (STI) Program plays a key part in helping NASA maintain this important role.

The NASA STI Program operates under the auspices of the Agency Chief Information Officer. It collects, organizes, provides for archiving, and disseminates NASA's STI. The NASA STI Program provides access to the NASA Technical Report Server—Registered (NTRS Reg) and NASA Technical Report Server—Public (NTRS) thus providing one of the largest collections of aeronautical and space science STI in the world. Results are published in both non-NASA channels and by NASA in the NASA STI Report Series, which includes the following report types:

- TECHNICAL PUBLICATION. Reports of completed research or a major significant phase of research that present the results of NASA programs and include extensive data or theoretical analysis. Includes compilations of significant scientific and technical data and information deemed to be of continuing reference value. NASA counter-part of peer-reviewed formal professional papers, but has less stringent limitations on manuscript length and extent of graphic presentations.

- TECHNICAL MEMORANDUM. Scientific and technical findings that are preliminary or of specialized interest, e.g., "quick-release" reports, working papers, and bibliographies that contain minimal annotation. Does not contain extensive analysis.

- CONTRACTOR REPORT. Scientific and technical findings by NASA-sponsored contractors and grantees.

- CONFERENCE PUBLICATION. Collected papers from scientific and technical conferences, symposia, seminars, or other meetings sponsored or co-sponsored by NASA.

- SPECIAL PUBLICATION. Scientific, technical, or historical information from NASA programs, projects, and missions, often concerned with subjects having substantial public interest.

- TECHNICAL TRANSLATION. English-language translations of foreign scientific and technical material pertinent to NASA's mission.

For more information about the NASA STI program, see the following:

- Access the NASA STI program home page at http://www.sti.nasa.gov

- E-mail your question to help@sti.nasa.gov

- Fax your question to the NASA STI Information Desk at 757-864-6500

- Telephone the NASA STI Information Desk at 757-864-9658

- Write to:
  NASA STI Program
  Mail Stop 148
  NASA Langley Research Center
  Hampton, VA 23681-2199

NASA/TM-20220011967

An Analysis of the Impact of Extreme Attitude Operation on a Turbofan Engine in a Regional Jet Aircraft

Jonathan S. Litt
Glenn Research Center, Cleveland, Ohio

T. Shane Sowers
HX5, LLC, Brook Park, Ohio

Daniel A. Trowbridge
Zin Technologies, Inc., Middleburg Heights, Ohio

National Aeronautics and
Space Administration

Glenn Research Center
Cleveland, Ohio 44135

September 2022

Acknowledgments

The authors wish to thank Scott Norin of Vantage Partners, LLC, for developing the original T-MATS CF34-like engine model and the CRJ-like regional jet geometry, George Kopasakis of the NASA Glenn Research Center for designing the full envelope fan speed controller for this engine model, Jonathan Kratz, also of NASA Glenn, for converting the T-MATS engine model into parallel compressor form, and Christine Chevalier of HX5, LLC, for generating and formatting the plots. The authors also wish to thank the Airspace Operations and Safety Program/System-Wide Safety Project for funding this work.

This work was sponsored by the Airspace Operations and Safety Program at the NASA Glenn Research Center.

Level of Review: This material has been technically reviewed by technical management.

This report is available in electronic form at http://www.sti.nasa.gov/ and http://ntrs.nasa.gov/

An Analysis of the Impact of Extreme Attitude Operation on a Turbofan Engine in a Regional Jet Aircraft

Jonathan S. Litt
National Aeronautics and Space Administration
Glenn Research Center
Cleveland, Ohio 44135

T. Shane Sowers
HX5, LLC
Brook Park, Ohio 44142

Daniel A. Trowbridge
Zin Technologies, Inc.
Middleburg Heights, Ohio 44130

Abstract

The objective of this work is to characterize the variability in engine performance at extreme attitudes, resulting from the use of different standard control variables, evaluated at different points in the engine's lifecycle. This paper describes the procedure used to create a dynamic model of an aft-mounted jet engine on a T-tail regional jet aircraft. This model enables simulation of engine operation at extreme attitudes. The model was subsequently evaluated at various altitudes, Mach numbers, and power settings over a range of angles of attack and sideslip, and deterioration levels. Each case was simulated using both fan speed and engine pressure ratio as the engine control variable. The results show that the wing has a very large impact on the engine operation, overwhelming other sources of variation.

Nomenclature

ALT	Altitude
AOA	Angle of Attack
AOS	Angle of Sideslip
CFD	Computational Fluid Dynamics
c_p	Specific Heat at Constant Pressure
c_v	Specific Heat at Constant Volume
EOL	End-Of-Life, i.e., fully deteriorated
EPR	Engine Pressure Ratio (P_{T7}/P_{T2})
FAA	Federal Aviation Administration
HPC	High Pressure Compressor
HPT	High Pressure Turbine
LPT	Low Pressure Turbine
MN	Mach number
N1	Fan Speed
N2	Core Speed
NASA	National Aeronautics and Space Administration
NPSS	Numerical Propulsion System Simulation

NTSB	National Transportation Safety Board
P_0	Static Ambient Pressure
P_{T2}	Total Inlet Pressure (at the Fan Face)
P_{T7}	Total Pressure at core nozzle inlet
P_S	Static Pressure
P_T	Total Pressure
T-MATS	Toolbox for the Modeling and Analysis of Thermodynamic Systems
T_0	Static Ambient Temperature
T_S	Static Temperature
T_T	Total Temperature
T_{T2}	Total Inlet Temperature (at the Fan Face)
$T_{T4.5}$	Total Inter-Turbine Temperature (between the HPT and LPT)
α	Angle of Attack
β	Angle of Sideslip
η_d	Adiabatic efficiency of the inlet diffuser
γ	Ratio of Specific Heats $c_p/c_v = 1.4$

Introduction

The National Transportation Safety Board (NTSB) determined that the probable cause of the 2009 fatal crash of Colgan Air 3407 was an inappropriate response to a stall warning system, resulting in an aerodynamic stall from which the airplane did not recover (Ref. 1). As a result, the NTSB recommended, among other things, defining simulator fidelity requirements to support full stall recovery training during flight simulator training; this corresponded to the Commercial Aviation Safety Team's (CAST) Safety Enhancement (SE) 209: Simulator Fidelity (Ref. 2). Subsequently, Public Law 111–216 was passed requiring stall training for all Part 121 air carriers (airliners), and the Federal Aviation Administration (FAA) responded by developing appropriate rules and regulations to meet this requirement beginning in 2019 (Ref. 3). The National Aeronautics and Space Administration (NASA) collaborated with the FAA by undertaking research to define aerodynamic model parameters—along with their availability and associated uncertainties—necessary for replicating full-stall flight characteristics. NASA's efforts, which lasted from 2014 through 2018, focused specifically on development and flight simulator evaluation of a T-tail aircraft model with aft twin engines (Figure 1) to generate the necessary information, which was subsequently reported (Ref. 4).

The airframe model and integrated engine models that comprised the simulation used in Reference 4 were designed to capture the behavior of extreme attitude operation (Ref. 5). While the results reported represent the complete aircraft, this paper concentrates on the behavior of the engines, which, from the point of view of the pilot, can be obscured or overwhelmed by that of the aircraft. Furthermore, the flight simulator evaluation conducted for the FAA utilized an engine model that represented a single engine from among a population of similar engines. It did not account for engine variability or controller type, which can influence the results, and therefore this study was undertaken to better characterize the range of engine behaviors that might be experienced in a loss-of-control situation. For the purposes of this paper, the term "loss of control" refers to Loss of Control In-flight, commonly denoted LOC-I. LOC-I is the most significant cause of fatal accidents in commercial aviation. LOC-I occurs when an aircraft deviates from the intended flight path, or an adverse flight condition places an aircraft outside the normal flight envelope, with the pilot unable to maintain control of the aircraft (Ref. 6).

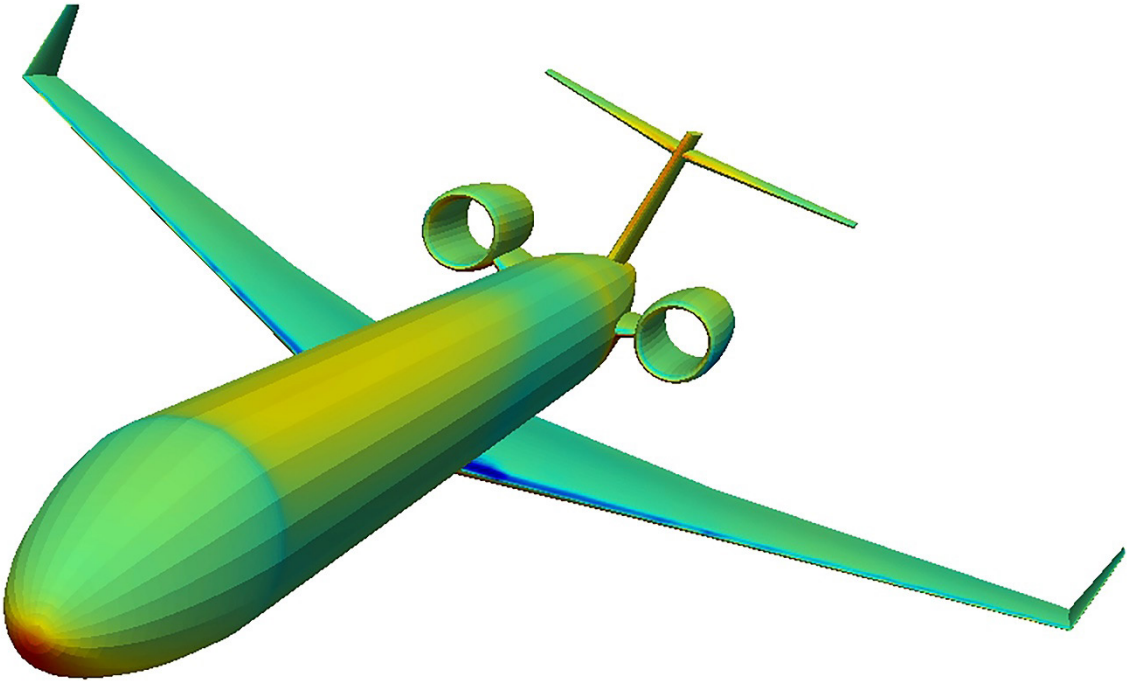

Figure 1.—Aircraft geometry model similar to a Bombardier CRJ700.

Background

Angle of attack (AOA or α) is the angle between the oncoming air or relative wind and a reference line on the airplane or wing (the angle between the horizontal plane through the aircraft's centerline and its velocity vector). It is one of the most important parameters related to airplane performance and handling because there is a limited range of AOA over which a wing can function efficiently (Ref. 7). Engines on large transport aircraft can operate at up to 30 degrees angle of attack or sideslip, which is well beyond aircraft limits (Ref. 8). Still, as AOA increases, the airflow into the engine is reduced, resulting in reduced thrust and stability. The engine is designed with an operating margin to allow for deterioration and inlet distortion; these are components of the stall/surge margin stack up (Ref. 9). This allows for a reduction in stability margin under normal AOA and allowable crosswind, (Ref. 10) although performance may not be significantly impacted. Similar to AOA, angle of sideslip (AOS or β) is the angle between the vertical plane through the aircraft's centerline and its velocity vector.

This research focuses on a T-tail regional jet aircraft configuration, with two podded turbofan engines mounted to the fuselage, above and behind the wings. The pods are attached to pylons, which positions the inlets away from the fuselage, where under normal flight conditions, the airflow is undisturbed (Ref. 11).

Early skepticism about the performance of aft-mounted engines at high angles of attack (approaching aircraft stall) and sideslip proved unwarranted. In fact, the advantages and disadvantages of such a configuration are mostly related to structural and aerodynamic performance issues of the aircraft itself (Ref. 12). Additionally, because the aircraft will enter aerodynamic stall before engine behavior is noticeably impacted, the stick pusher should prevent the engine from even approaching AOA-related stall.[1] With that said, because of the position of the engines, the airflow into the engines still has the

[1]The term "stick pusher" means a device that, at or near a stall, applies a nose down pitch force to an aircraft's control columns to attempt to decrease the aircraft's angle of attack (Public Law 111–216 Sec. 208 (c) (3)).

potential to become distorted as AOA and AOS increase, resulting in the ingestion of the wing wake, and flow blockage due to the fuselage. Anecdotal evidence of engine flameout (Ref. 13) in aircraft with aft fuselage-mounted engines indicates that dynamic interaction has the potential to be problematic. In both the PSA Airlines Flight 2386 case (Ref. 14) and the Pinnacle Airlines Flight 3701 case (Ref. 15), flameout occurred as a result of rapid AOA oscillations, when the pilots repeatedly pitched up after the stick pusher activated. Duplicating these events in simulation would potentially require modeling combustion dynamics, fuel system dynamics, and even details of the particular engine's actual control algorithm (Ref. 16), which are proprietary and engine specific. Such an undertaking goes well beyond the scope of this effort. In keeping with NASA's original role in this research, the focus here is on producing generic information concerning sources of uncertainty related to modeling of commercial T-tail aircraft behavior approaching and during stall operation.

Modeling efforts to capture the effect of inlet distortion on engine performance and stability have used the relatively simple and well-established Parallel Compressor Theory (Ref. 17). The premise involves sectioning the flow through a fan or compressor into a number of parallel streams. The flow path split is area-based and should approximate the inlet distortion pattern to be modeled. Typically, the performance map of the original compressor model is applied to each flow path after being scaled down in terms of mass flow by the relative area of the section. To resolve the parallel streams, the flow path variables are summed or averaged as appropriate to define the exit conditions. Overall mass flow is the sum of the mass flow through the individual sections. In this implementation, the overall exit value of each flow variable (e.g., pressure, temperature) is a mass flow weighted average across all sections. Note that if the inlet conditions are identical for each flow path, the parallel compressor model recovers the performance of the original compressor model regardless of how the parallel sections are defined.

Some earlier work on a different standalone engine model that specifically investigated the changes in stability and performance as a function of AOA, utilized a variation of the parallel compressor approach in which the compressor map for each sector was scaled individually with AOA, while inlet conditions were held constant (Ref. 18). This paper returns to the more traditional approach to model high AOA behavior, but the trends are shown to be similar to those presented in Reference 18. Furthermore, not only does the present work look at variations in AOS as well, but it has the added complexity of being applied to aft-mounted engines on a T-tail regional jet aircraft, meaning that there is distortion from the wings and fuselage at certain conditions.

The following sections provide a high-level overview of the engine model development approach used in this work. This is followed by a more detailed description of the model. Results generated using the model are shown next, followed by conclusions.

Overall Approach

The overall approach is briefly synopsized here, with more detail about each step below. The following sections are ordered to facilitate understanding, rather than faithfully following the steps laid out in this section. The software tools used for this effort included the Numerical Propulsion System Simulation (NPSS), an industry standard engine cycle analysis code, the Toolbox for the Modeling and Analysis of Thermodynamic Systems (T-MATS), a dynamic engine simulation tool that utilizes a Simulink-based block diagram modeling environment, and Cart3D, a high-fidelity inviscid Computational Fluid Dynamics (CFD) code analysis package. Cart3D was selected based on its ability to produce solutions quickly while capturing general trends (Ref. 19). Relative to a viscous flow solver, an inviscid code will miss detail related to boundary layer and flow separation, for instance, but is considered sufficient for this generic analysis. The use of these packages will be described in greater detail below.

What follows is a high-level description of the major steps used in the setup and analysis, with more detail provided in the subsequent sections.

Create Engine Model

1. Start with a representative NPSS model of a turbofan engine appropriate for a T-tail regional jet aircraft.
2. Convert the NPSS model to T-MATS.
3. Develop a fan speed and engine pressure ratio (EPR) controller for the engine model.
4. Modify the T-MATS model to Parallel Compressor form by partitioning the fan and compressor into quadrants in an X-configuration (i.e., top, right, bottom, and left quadrants).

Determine Inlet Conditions

5. Create a geometry model of a representative T-tail regional jet aircraft.
6. Apply CFD to visualize the static temperature and pressure disks at the installed engine fan face over a range of AOA and sideslip angles at specified altitudes and Mach numbers. These disks refer to the radial cross-sectional plane of the inlet parallel to and just in front of the fan from the point of view of the airflow.
7. Sector the temperature and pressure disks into quadrants in an X-configuration (i.e., top, right, bottom, and left quadrants).
8. Convert static values of temperature and pressure to total values and average over each quadrant.
9. Build a lookup table of average total temperatures and pressures for each quadrant as a function of altitude, Mach number, AOA, and sideslip. This includes an interpolation scheme.

Combine the Results of the Previous Steps

10. Replace the ambient conditions and inlet portions of the T-MATS parallel compressor model with the lookup table such that the interpolated total temperature and pressure values for each fan face quadrant are fed into the appropriate quadrant of the T-MATS parallel compressor model.

Perform Sensitivity Study

11. Perform slow variations in AOA and AOS at selected altitudes, Mach numbers, power settings, and deterioration levels, while maintaining fan speed.
12. Repeat tests while maintaining EPR.
13. Compare results to determine how output variables differ from run to run as inputs and controller type are modified.

The current study looks at quasi-steady state behavior of the engines during extreme attitude excursions, i.e., those that could lead to or be encountered during a loss-of-control type situation. The objective is to investigate the impact of AOA and AOS on a variety of important engine variables at different altitudes and Mach numbers, taking into account deterioration level and basic controller type, either fan speed or EPR.

With the basic steps described, the next section will provide the detail necessary to implement them.

Detailed Approach

This section contains a detailed description of the individual parts of the research and the process used to obtain the results. CFD was used to visualize the total temperature and pressure disks at the fan face. These disks were then sectored into four equal wedges (quadrants) arranged in an X-configuration, and the average total temperature and pressure for each wedge was calculated (Figure 2). These values were used as inputs to a dynamic parallel compressor turbofan engine model, i.e., one in which the fan

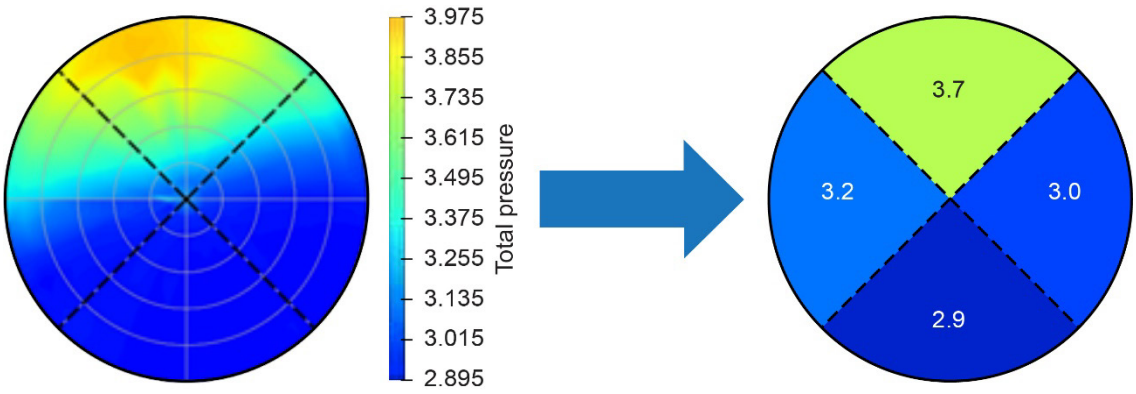

Figure 2.—Total pressure disk at fan face (left) and averaged by sector (right).

and compressor are divided into four parallel circumferential segments that extend axially through the bypass nozzle and to the combustor, respectively. Because this work focused on variations in AOA (pitch axis) and AOS (yaw axis), the disks were sectored into an X-configuration; this enabled the impact of both up and down and side to side movement to be well represented. The engine model itself was matched to NPSS data from a representative regional jet turbofan engine model at several operating points. Simulating the engine with the given inlet conditions provides a way to approximate the effect of inlet distortion and reduced airflow on thrust performance and stability. The dynamic engine model offers the option of regulating either fan speed or EPR (the two most common control variables in turbofan engines) and comparing the results to determine if controller selection causes the closed-loop behavior to differ at high AOA and sideslip. The simulation also includes the capability to model engine deterioration related to use, which has an impact on stability; this provides an additional source of uncertainty. The T-tail regional jet aircraft configuration has unique features that make it especially relevant for this study because the installed engine performance has the potential to be much more severely impacted by variations in AOA and AOS than that of wing-mounted engines.

Aircraft Model

An aircraft geometry model was created with dimensions similar to those of a Bombardier CRJ700 provided in Reference 20 (Figure 1). This is representative of a commercial T-tail regional jet aircraft. As can be seen from Figure 1, the aircraft geometry model was developed with flow through engines represented as open tubes, without propulsion effects.

Engine Model

The CRJ700 is equipped with CF34-8C5 engines. The cross section of an engine similar to a CF34-8C5 engine (Ref. 21) is shown in Figure 3. The engine has a fan, a 10-stage High Pressure Compressor (HPC), a two-stage High Pressure Turbine (HPT), and a four-stage Low Pressure Turbine (LPT).

Engine Control

The CF34 engine utilizes a fan speed (N1) control at takeoff and flight conditions (Ref. 22). Fan speed is a commonly used proxy for thrust because it is related to air mass flow, a significant contributor to thrust, and it is a relatively stable and accurate measurement. However, it is an indirect measure that is not linearly correlated with thrust, and the relationship varies with engine deterioration. EPR, which is defined as the total pressure at the core nozzle inlet divided by the total inlet pressure at the fan face,

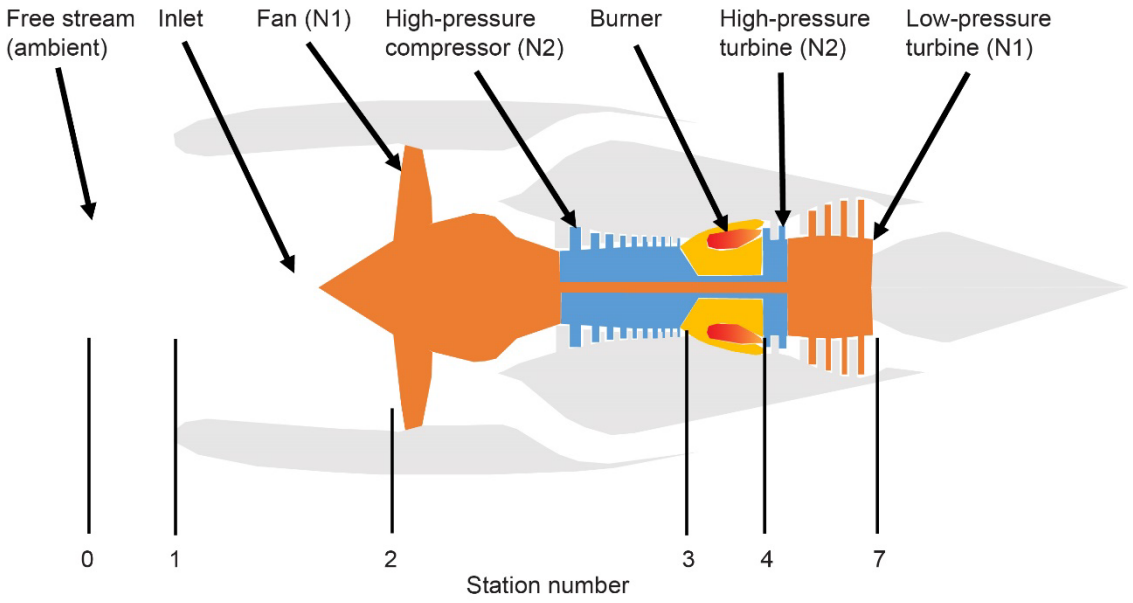

Figure 3.—Cross section of an engine similar to the CF34-8C5, showing major components and station numbers.

P_{T7}/P_{T2} (see Figure 3 for station numbers), is another common in-flight representation of thrust. EPR is a truer measure because the ratio is directly related to thrust, but the pressure measurements used for EPR calculation require filtering to avoid stability problems; this results in measurement delays. Furthermore, the exposed probes can suffer from impact damage or icing (Refs. 23 and 24). Under normal conditions, either measurement serves its purpose adequately, but under extreme attitude conditions, N1 and EPR control may produce noticeably different engine behavior (Ref. 18).

T-MATS Model

A model of the CF34-8C5 engine was created in the NPSS, a state-of-the-art aircraft engine cycle analysis simulation tool (Ref. 25). The NPSS model supplied realistic outputs at the select engine design points, providing a starting point for the creation of a dynamic T-MATS engine model.

Match to NPSS With iDesign

Performance maps of the turbomachinery components (compressors and turbines) of a jet engine are an essential piece of engine performance models. These maps typically define the relationship between corrected mass flow rate and the component's pressure ratio, and they contain the unique values for corrected shaft speed and efficiency at any given operating point (Ref. 26). The maps used in the NPSS model were sufficient to provide operating line information, but did not cover the whole operating regime. Thus, the T-MATS model used generic maps to provide a greater operating range. The NPSS engine model was converted component-by-component to T-MATS and matched at select operating points using the iDesign feature in T-MATS (Ref. 27). This tool determines map scale factors that fit the generic component maps to a design point automatically, effectively creating a model that matches performance at a specific operating point. Map scale factors for the compressor and turbine may be generated by specifying the design operating point map parameters and the actual performance values. Though generated at the design condition, scaled component maps created by this tool may be used to run the simulation in off-design conditions (Ref. 26).

Develop Controllers

The focus of this research is to determine quasi-steady state behavior of the installed closed-loop engine at extreme attitudes, thereby eliminating the effect of dynamic operation of the controller including proprietary control modes. Thus, the controller needed only to maintain the engine at its N1 or EPR set point as AOA and/or AOS slowly varied. A full envelope fan speed controller was available for the engine model, which was sufficient to maintain N1 in steady state based on a power setting. For the EPR controller design, a simple proportional integral control was used to maintain the EPR set point.

Parallelize the Model

Because the performance of the fan tip and fan hub can be dissimilar, the T-MATS fan component can be represented in several different ways depending upon the available maps (Ref. 28). The CF34 T-MATS model used in this work utilizes a single fan component representing performance of both the fan tip and the fan hub. After passing through the fan, the flow is split between the bypass and core according to the bypass ratio. To create a parallelized version of the engine, the fan, bypass nozzle, and HPC are segmented into matching quadrants. The portion of the flow through a fan quadrant that enters the core is passed to the corresponding HPC quadrant, and the remainder goes to the corresponding bypass quadrant. Beyond the bypass nozzle, the parallel flows are recombined, and beyond the HPC, the parallel flows are recombined before continuing through the remainder of the core, as shown in Figure 4.

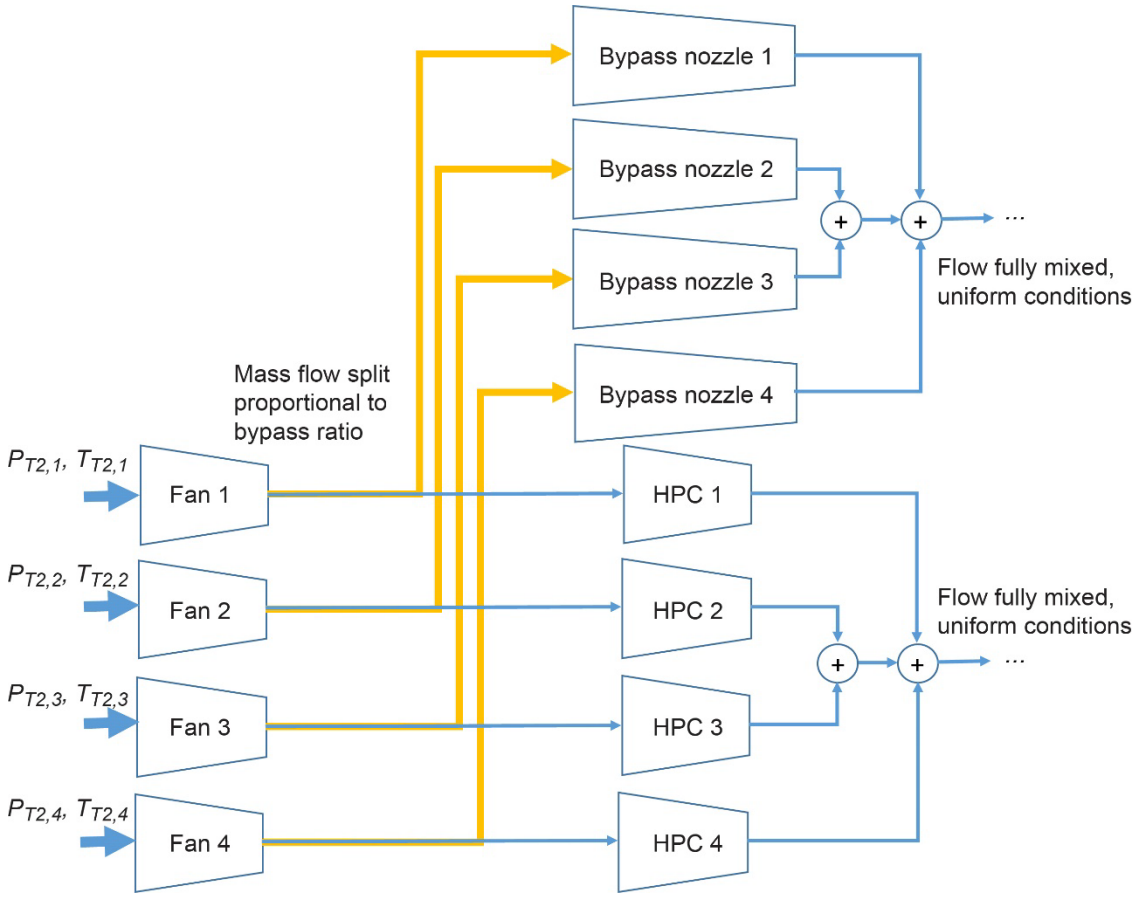

Figure 4.—Parallelized CF34 engine model, where $P_{T2,j}$ and $T_{T2,j}$ represent the inlet total pressure and temperature, respectively, for the jth quadrant.

Mass flow through each quadrant is determined by balancing the model at every time step based on its respective inlet conditions. According to parallel compressor theory, the overall compressor is assumed to become unstable (i.e., surge or rotating stall) when at least one of the parallel compressor sections is unstable. Hence, for this work, the overall compressor stall margin is calculated as the minimum of the stall margins of the four parallel compressor models (Ref. 18).

CFD Results

The Cart3D (Ref. 29) CFD code was used with the CRJ700 aircraft geometry model to visualize the total temperature and pressure disks at the engine inlet for a variety of altitude, Mach number, AOA, and sideslip conditions. It returns the static temperature and pressure on the aerodynamic interface plane at the fan face over the range of input values. Converting the static conditions at the fan face to total temperature (T_{T2}) and total pressure (P_{T2}) provides the inputs to the dynamic simulation. The total pressure predicted by the CFD at the fan face under baseline conditions (AOA and AOS values near 0) is generally less than 3 percent lower than the value in the standard altitude tables (see for example Reference 30), demonstrating that the CFD captures realistic inlet losses (Ref. 31). The predicted total temperature under the nominal conditions was within a fraction of a percent of the value in the standard altitude tables. Note that the generic T-MATS inlet component accounts for a pressure loss. The parallelized T-MATS model created for this work and described here, however, begins at the fan, forgoing the inlet since the CFD results provide station 2 conditions, including inlet losses.

Conversion of Static Temperature and Pressure to Total Temperature and Pressure

The CFD provided the static pressure and temperature as well as Mach number at the various points on the fan face using a uniform square grid. The engine model required total pressure and temperature conditions, which were calculated using the isentropic equations below. These equations calculate the pressure and temperature of the flow as if it were theoretically decelerated to stagnation without losses or heat addition (Ref. 32).

$$T_T = \left(1 + \frac{\gamma - 1}{2} MN^2\right) T_S \tag{1}$$

$$P_T = \left(1 + \frac{\gamma - 1}{2} MN^2\right)^{\gamma/(\gamma-1)} P_S \tag{2}$$

Equations (1) and (2) are the conversions from static temperature to total temperature and static pressure to total pressure, respectively. Here, MN is local Mach number, and γ is the ratio of specific heats at constant pressure and volume, assumed constant for the diffuser process. Using these equations, the static CFD results are mapped point-by-point to total values.

As an aside, it was stated in the previous section that, at AOA and AOS values near 0, the computed T_{T2} at the various flight conditions was very close to the value in the standard altitude tables, while the P_{T2} value was somewhat lower. Because the inlet does no thermodynamic work, the total temperature through the inlet is constant. However, the total pressure through the inlet changes due to loses based on adiabatic efficiency, η_d. The relevant mathematical relationships are shown in Equations (3) and (4).

$$T_{T2} = \left(1 + \frac{\gamma-1}{2} MN^2\right) T_0 \tag{3}$$

$$P_{T2} = \left(1 + \eta_d \frac{\gamma-1}{2} MN^2\right)^{\gamma/(\gamma-1)} P_0 \tag{4}$$

These equations convert the static ambient conditions to total values at the fan face. The total temperature (T_{T2}) can be computed from ambient conditions (P_0, T_0) and Mach number, while the total pressure (P_{T2}) can be computed as well, if the inlet efficiency is known (Ref. 33). Equating Equations (1) and (3), it is clear that, theoretically, the ambient static temperature matches that at the fan face. Equating Equations (2) and (4), one can observe that the static pressure at the fan face is less than that of the freestream by a factor related to the adiabatic efficiency of the inlet. This validates, at least for small AOA and AOS, that the CFD provides reasonable total temperature and pressure values at the fan face, capturing the inlet losses appropriately. It must be noted that larger values of AOA and AOS induce nonuniformity in flow conditions, including distortion of inlet total pressure and total temperature at the fan face (Ref. 34). These variations are seen in the CFD results, although their magnitudes and distributions are not validated against actual data.

For this work, Equations (1) and (2) were used to compute T_{T2} and P_{T2} directly from the static values returned by the CFD. Table 1 shows the total pressure at the fan face of the installed engine at 36,000 ft over a range of AOA and Mach number values. Comparing these pressure profiles to Figure 5, it is clear how closely they correspond. There is no real significant pressure variation until 15° AOA, then the pressure begins decreasing from the bottom up as the wing disrupts the airflow into the engine inlet. By 30° AOA, the bottom of the nacelle is obstructing the flow, while the oncoming air mass once again has an unobstructed path from behind the wing directly to the top of the fan face, which is set back well inside the nacelle (see Figure 3). This is supported by the observation that the areas of higher total pressure at 30° AOA are close in value to those same areas at 0° AOA. At higher Mach numbers, the inlet capture area, i.e., the diameter of the streamtube at infinity (see Figure 6), is smaller (Ref. 31). This is true over a wide range of AOA and AOS (Ref. 35). Thus, at higher Mach numbers, the impact of the flow blockage is expected to be more focused and intense. Conversely, at lower Mach numbers, where the inlet capture area is larger, the effect of the flow blockage is expected to be more diluted and dispersed. This manifests as a reduction in the pressure variation over the surface of the engine at lower Mach numbers, and increased variation at higher Mach numbers, with the areas of higher pressure at 30° AOA being concentrated. Sectoring and averaging for the parallel compressor implementation mitigates the pressure variation somewhat, but the difference in average pressure between sectors is still much larger for high AOA at high Mach number. A CFD visualization of the pressure variation at a vertical cut plane passing through the centerline of the engine (Figure 7) at 30° AOA shows an area of high pressure at the upper inside of the inlet, similar to what is implied by Figure 5.

TABLE 1.—INLET TOTAL PRESSURE DISTRIBUTION WITH CHANGE IN AOA FOR INSTALLED ENGINE, STARBOARD SIDE

	MN = 0.6 ALT = 36,000	*MN* = 0.4 ALT = 36,000	*MN* = 0.2 ALT = 36,000
AOA 0°	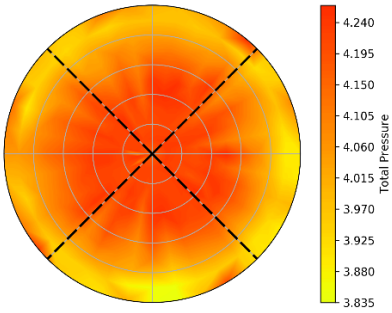	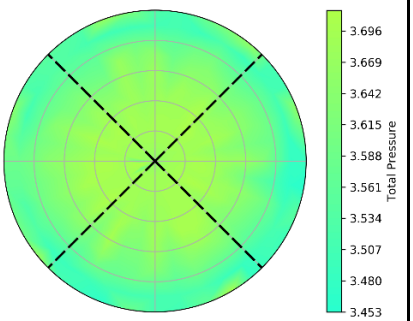	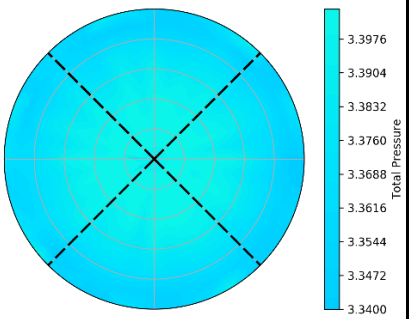
AOA 5°	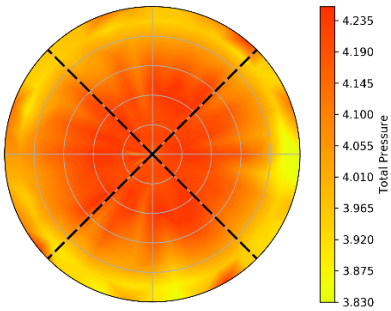	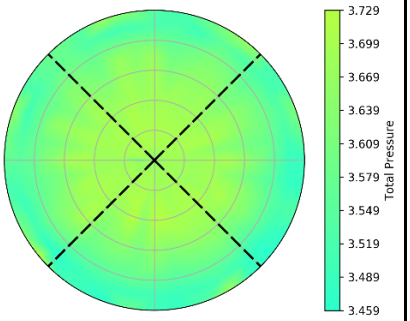	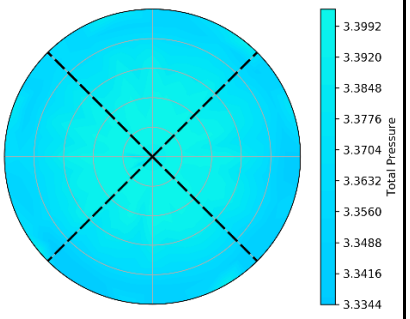
AOA 10°	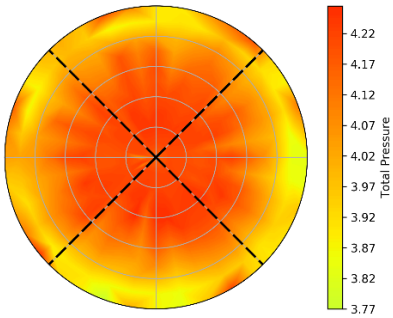	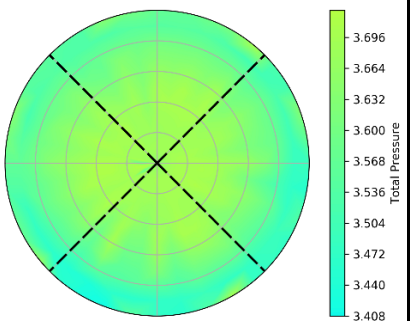	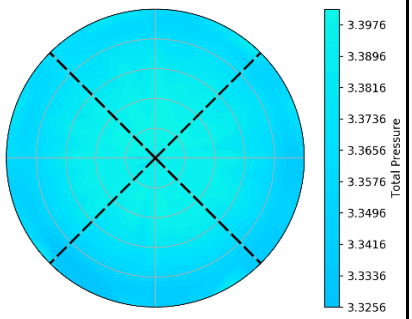
AOA 15°	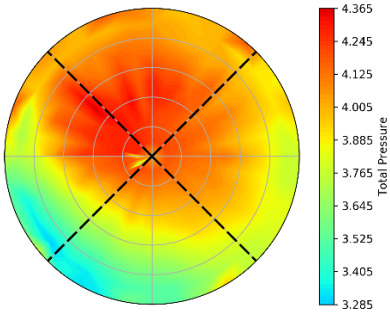	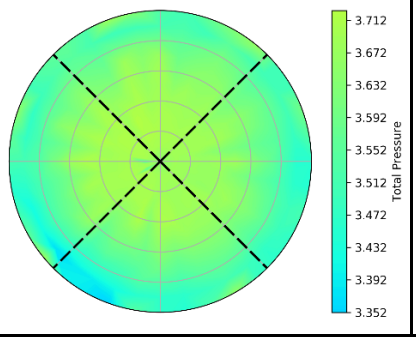	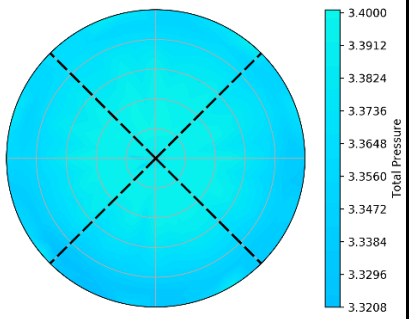

TABLE 1.—CONCLUDED.

AOA 20°	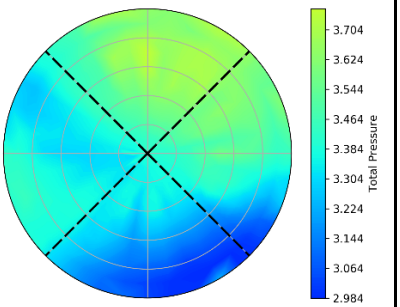	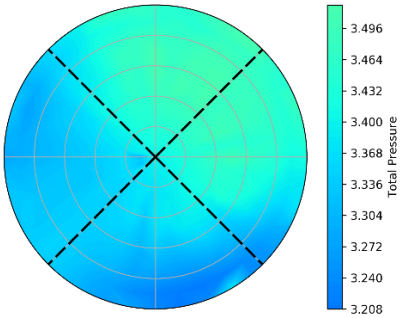	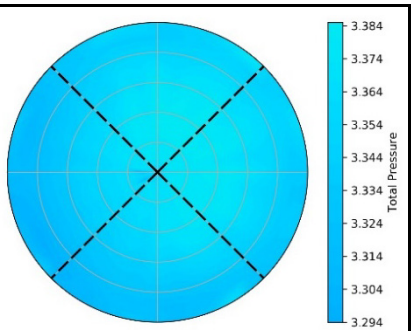
AOA 25°	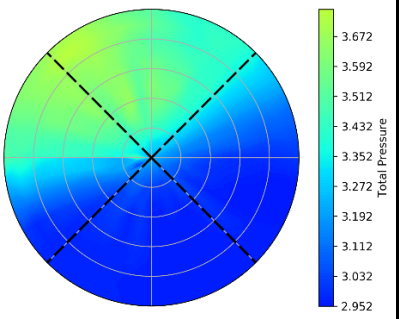	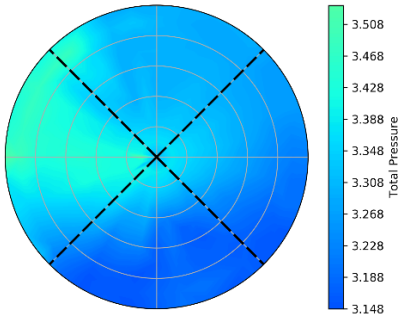	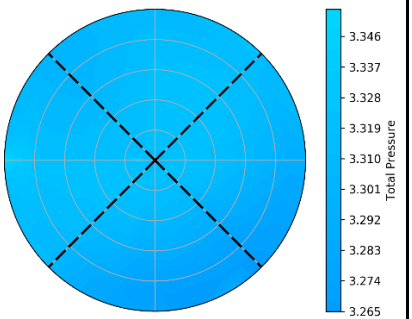
AOA 30°	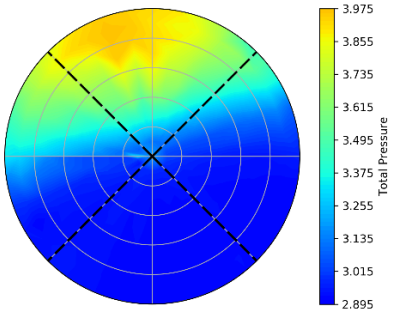	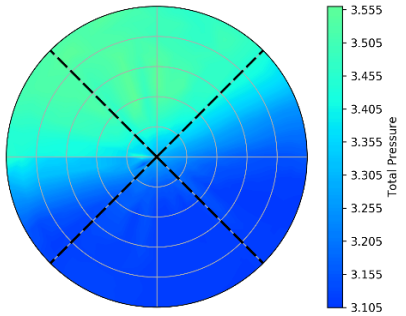	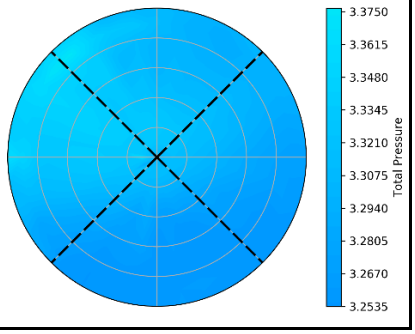

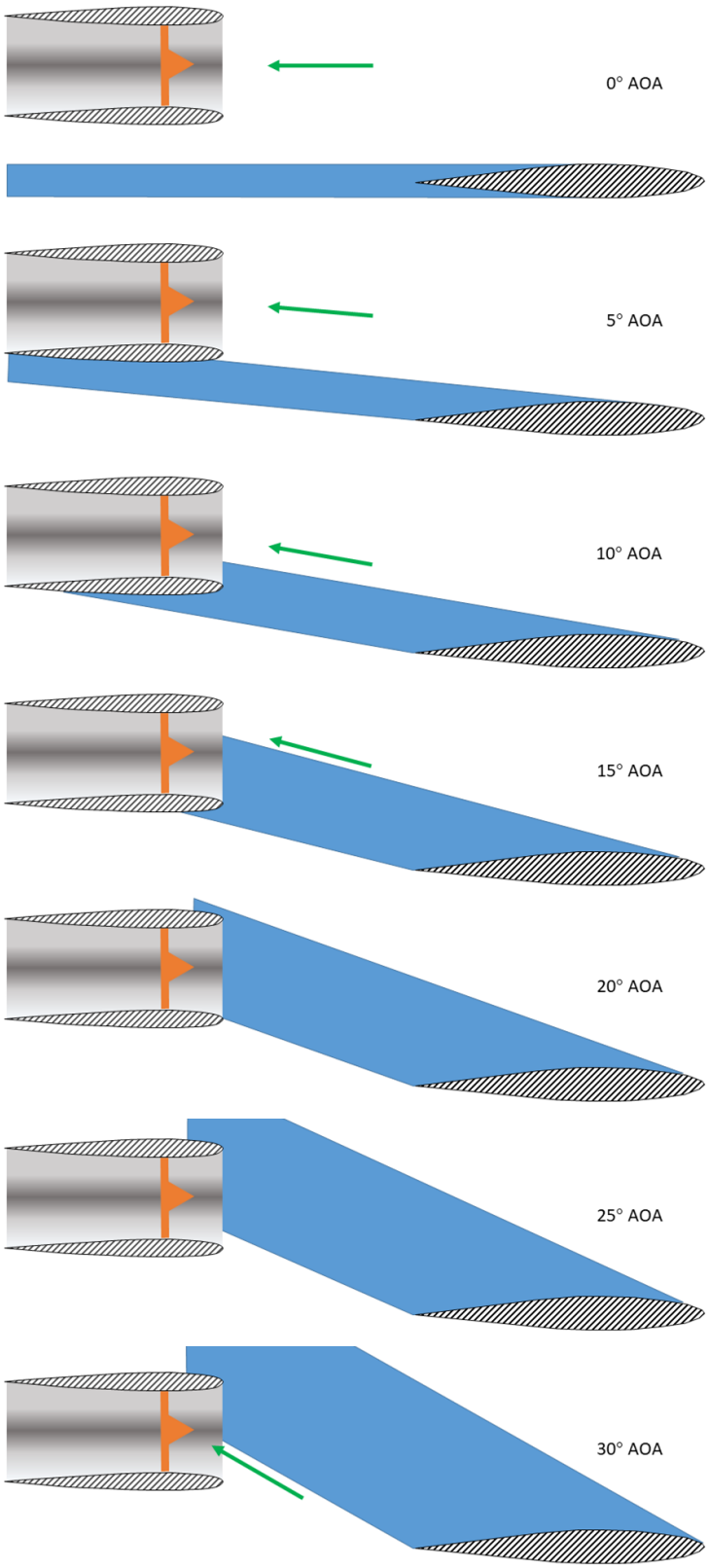

Figure 5.—Diagram indicating the obstruction of the airflow into the engine due to the wing at various values of AOA.

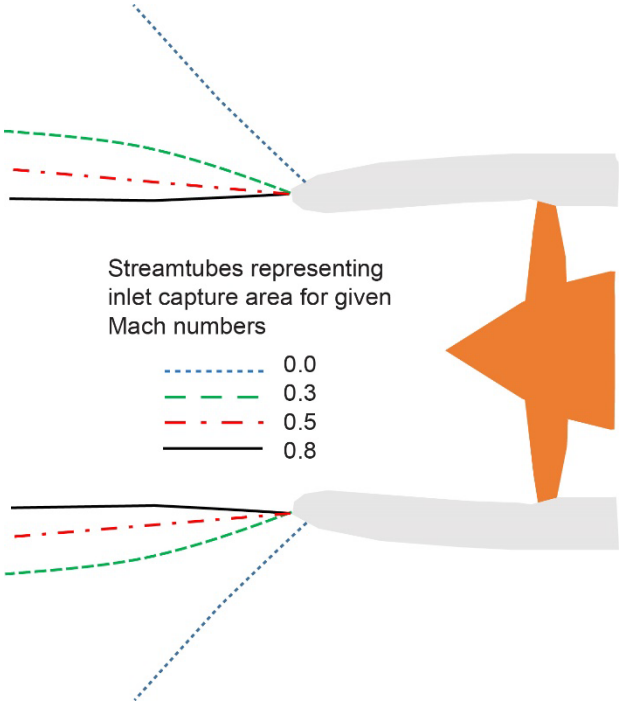

Figure 6.—Streamtubes representing inlet capture area for various Mach numbers showing decreased area with increased Mach number, based on Reference 31.

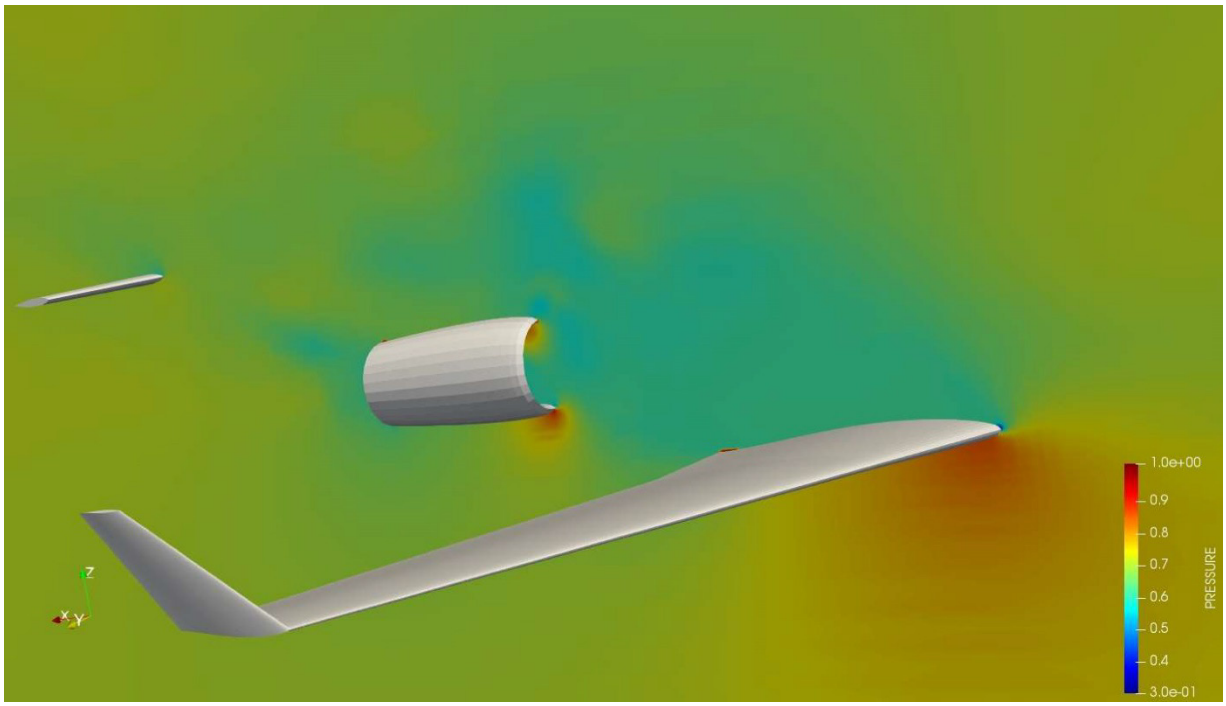

Figure 7.—CFD visualization of pressure variation at AOA = 30, AOS = 0, and Mach number = 0.6, shown at a vertical cut plane through the starboard engine.

Sector the Disk

As mentioned above, the static temperature and pressure disks at the fan face were determined using CFD and subsequently converted point-by-point to total values using Equations (1) and (2). These disks were then sectored into four equal wedges arranged in an X-configuration, as shown in Figure 2. The computed points in each sector were averaged, and these values were used as input to a dynamic parallel compressor turbofan engine model. P_{T2} and T_{T2} are key engine variables required by the control. Engine Inlet Pressure and Temperature probes (Ref. 36) are often mounted just in front of the fan, on the upper inside surface of the inlet, see for example, References 37 and 38. Thus, in this work, the average P_{T2} and T_{T2} of the upper quadrant are used for calculating engine control variables EPR and corrected N1.

Interpolation of CFD Data

With the average total temperature and pressure at the fan face available at specific values of altitude, Mach number, AOA, and AOS, an interpolation scheme was created to provide continuously variable approximations of P_{T2} and T_{T2}. This enabled the engine simulation to run transiently throughout the flight envelope over a range of attitudes. The average total temperature and pressure values computed for each sector as a function of AOA and AOS for a given *MN* and altitude are provided in the Appendix.

Modification to T-MATS Model to Accommodate Interpolation of CFD Data

Usually T-MATS engine models convert altitude and *MN* to T_{T2} and P_{T2} according to standard altitude tables (see for example Reference 30), but this generic conversion does not account for engine orientation. In the parallel compressor implementation, this calculation is replaced by the lookup table that produces the T_{T2} and P_{T2} values corresponding to the quadrants of the fan face, as a function of altitude, *MN*, AOA, and AOS.

This concludes the description of the creation of the parallel compressor model that accounts for variations in AOA and AOS. The following section presents the results obtained using the model.

Results

As an initial validation step, the behavior of the model developed in this study was compared against the results presented in Reference 18. In order to achieve this, the previously described CFD procedure was applied to the aircraft geometry model with the fuselage and wing removed, to develop total temperature and pressure tables that provide the inlet conditions to the standalone engine. In the earlier research, the standalone engine ramped through values of AOA from 0° to 21°. In this effort, an AOA sweep from 0° to 30° and back over 200 s is considered, as shown in Figure 8. Table 2 contains the results of this testing on the standalone CF34 engine model. The results are qualitatively very similar to those of Reference 18, validating, to the extent possible, that the model behavior is correct. With the model validated, the testing of the engine installed on a T-tail aircraft could begin.

To determine the effect of extreme attitude operation on the installed engine of a T-tail regional aircraft, the model was run through variations in AOA and AOS at multiple altitudes, Mach numbers, power settings, and health conditions. In this work, two power settings (Power Code or PC) were used, PC32 and PC41, which are both in the cruise range for the CRJ700. Also, two health conditions were considered: new and fully deteriorated. It should be noted that for the sake of this analysis, deviations in the health of each engine component are assumed to occur along a trajectory of which the new and fully deteriorated conditions constitute the start and end points. This deterioration profile is a representative

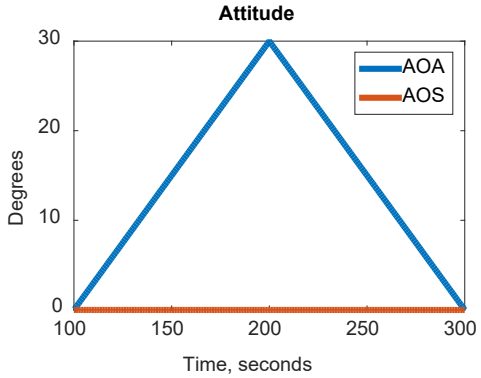

Figure 8.—AOA sweep profile.

trend of deterioration within a fleet of similar engines; any individual engine's health condition might be different due to usage and other factors (Ref. 39).

For the results shown below, all plots represent the port engine; results for the starboard engine are the same but with sideslip angle reversed. The plots show several variables, which are briefly described here.

- Net Thrust—net thrust produced by the engine, sum of core and bypass thrust minus drag (lbf)
- Bypass Thrust—gross thrust produced from the engine bypass (lbf)
- Core Thrust—gross thrust produced from the engine core (lbf)
- EPR—sensed engine pressure ratio, P_{T7}/P_{T2}, a common control variable
- N1—fan speed, a common control variable (rpm)
- N2—core speed (rpm)
- Fan Stall Margin—a measure of how close the fan is to stall (%)
- HPC Stall Margin—a measure of how close the HPC is to stall (%)
- Temperature—Inter turbine temperature, $T_{T4.5}$ (total temperature between the HPT and LPT) (°R)
- Wf—sensed fuel flow, the pounds of fuel per second consumed by the engine (pps)

The results of select simulation runs appear below. All profiles are shown at a common condition (MN = 0.6, Altitude = 20,000 ft, PC41), with allusions to results at other conditions included to emphasize specific points. A common scale is used for each of the plotted variables across all simulation runs. This allows the scenarios to be compared easily by demonstrating the relative magnitude of the deviations without overemphasizing small changes. While plotting on a common scale results in some visual detail being lost, the text provides enough analysis to give a complete picture of the situation.

AOA Sweeps

The AOA sweep maneuver begins with an AOA of 0° and slowly ramps up linearly to 30° over 100 s, then back down to 0° again over 100 s, maintaining sideslip at 0°, as shown in Figure 8. The results are shown for three cases in Table 3 to Table 5. Table 3 compares the results for an EPR controlled engine to a fan speed controlled engine. Table 4 shows the results with fan speed control on a new and fully deteriorated engine. Likewise, Table 5 shows the same results using EPR control. There are several things to notice in these results. As AOA increases, the engine moves behind the wing, relative to the airflow, but begins to reemerge by the top of the ramp. This reemergence increases the total pressure of the upper quadrant, which has a clearly visible impact on the EPR controlled engine, resulting in a thrust increase (recall that the P_{T2} sensor is in the upper quadrant). Under N1 control, the thrust appears to stop decreasing

TABLE 2.—AOA SWEEP RESULTS FOR ENGINE ONLY, PC = 41, *MN* = 0.6, ALT = 36,000, NEW ENGINE

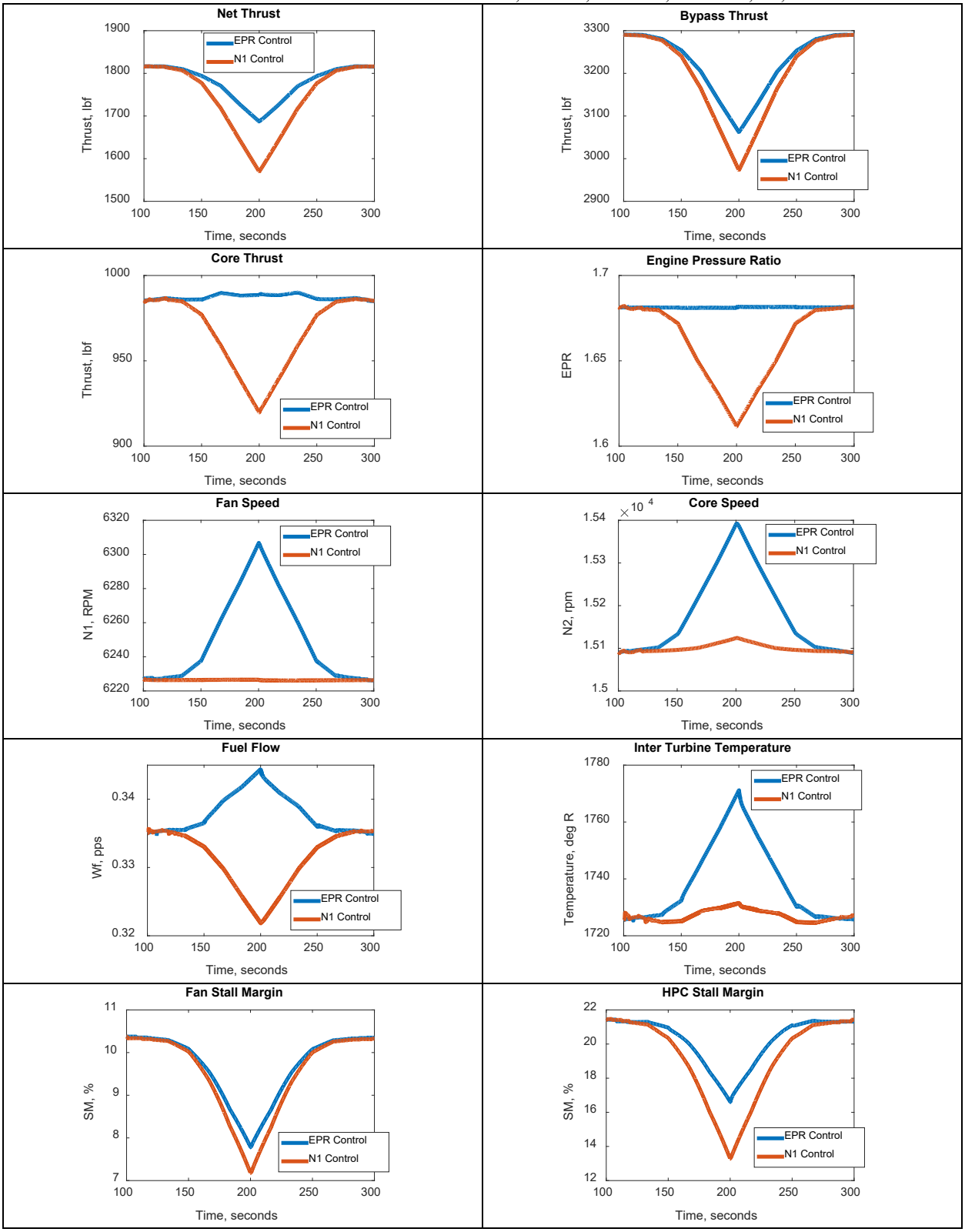

TABLE 3.—AOA SWEEP RESULTS, EPR CONTROL VS. N1 CONTROL

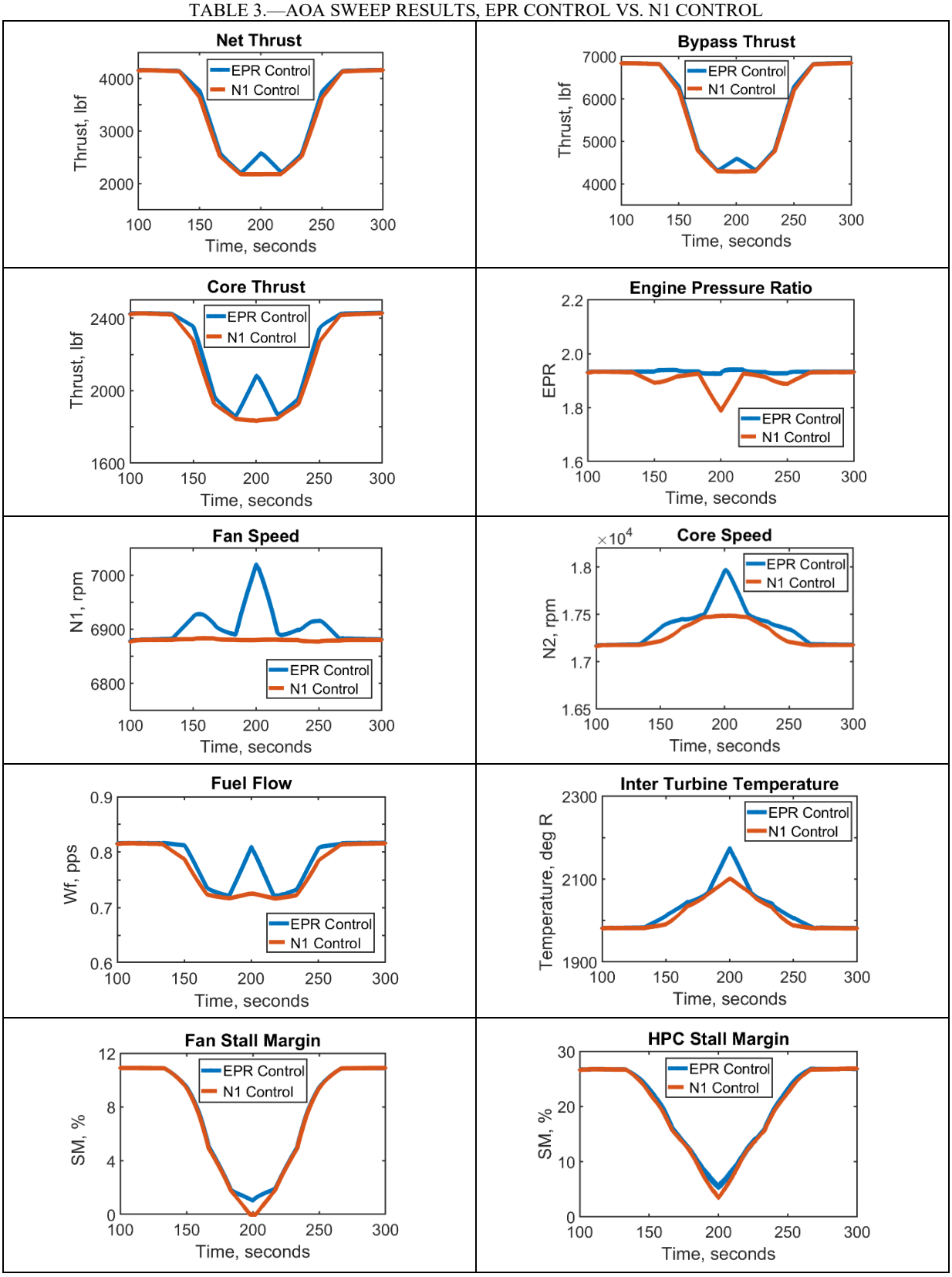

TABLE 4.—AOA SWEEP RESULTS, N1 CONTROL NEW VS. EOL ENGINE

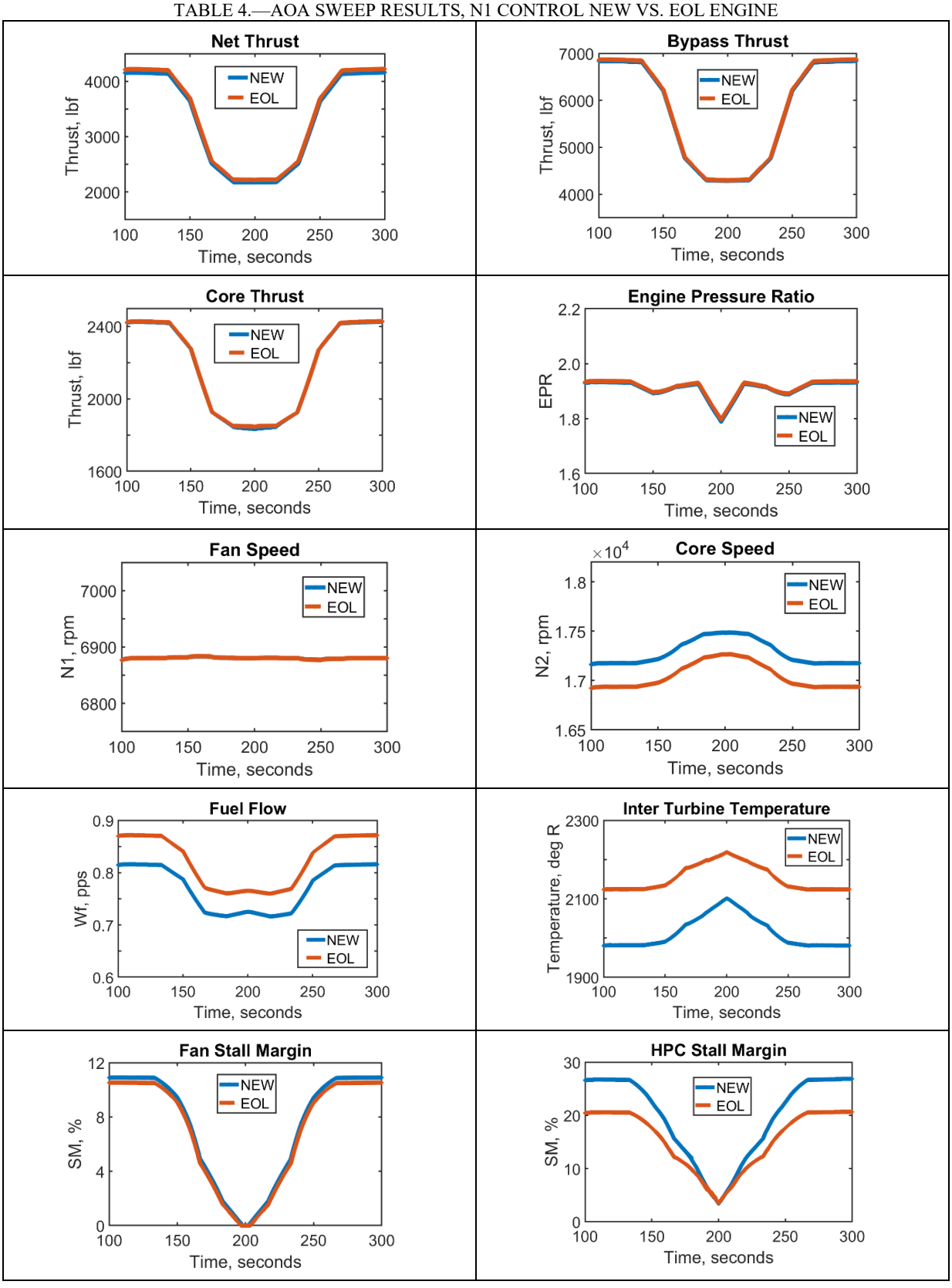

TABLE 5.—AOA SWEEP RESULTS, EPR CONTROL NEW VS. EOL ENGINE

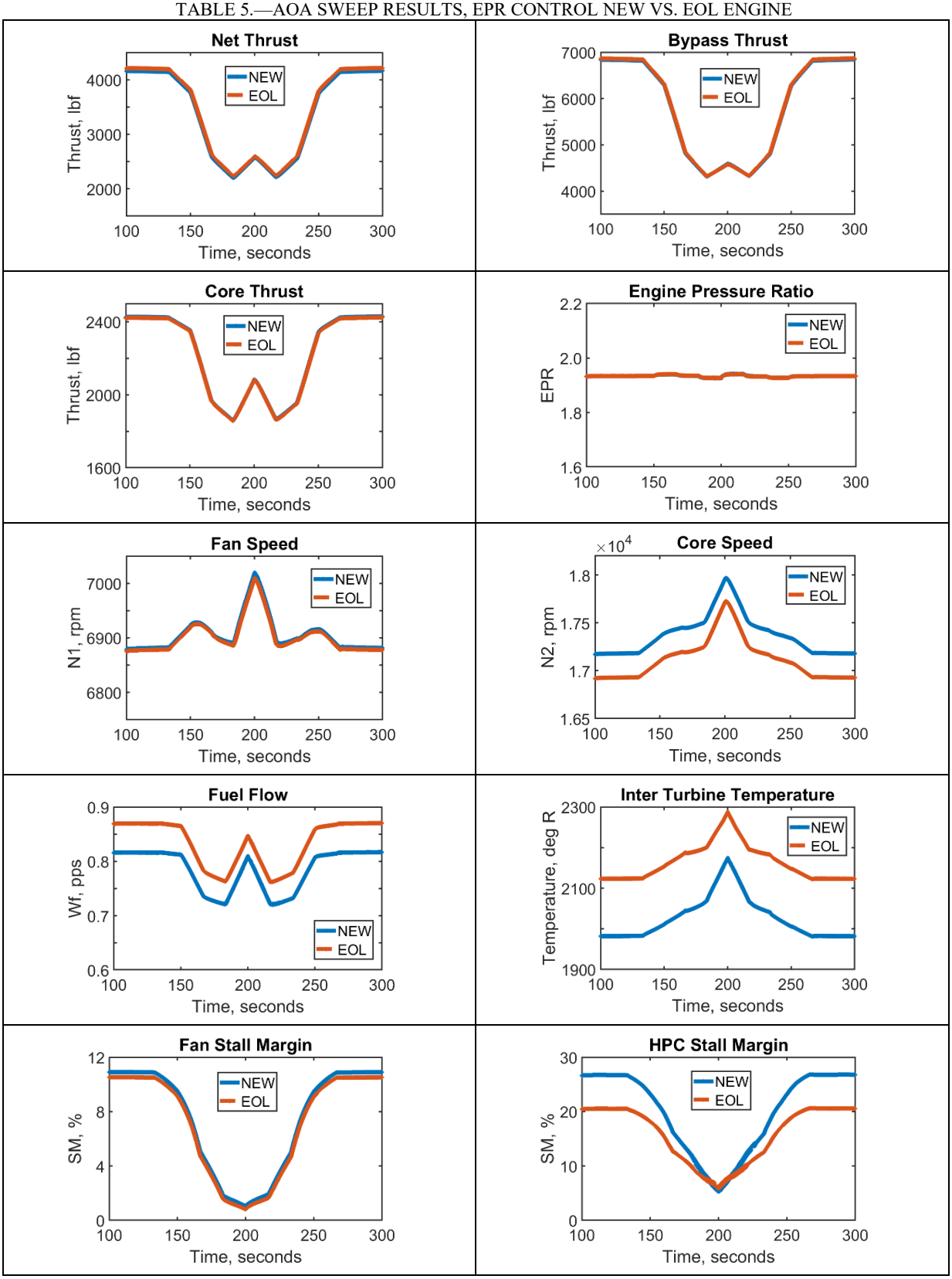

between 25° and 30° AOA, once the flow blockage due to the wing decreases. The surprising result is how similar the thrust responses are up to 25° AOA, independent of the type of controller (EPR or N1). A previous study on a standalone engine (Ref. 18) and similar testing on the standalone CF34 model (Table 2) showed that EPR control maintains thrust at high AOA significantly better than N1 control does. However, when the effect of the wing on the T-tail aircraft is taken into account, the reduction in P_{T2} leads to a corresponding reduction in P_{T7}, such that target EPR is maintained even while thrust is reduced by nearly 50 percent near the maximum AOA. It is only near 30° AOA that P_{T2} begins to increase, and the EPR control increases thrust with a corresponding spike in N1, N2, fuel flow and temperature. It is also interesting to note that EPR control maintains core thrust slightly better than N1 control, resulting in an increase in N1 at about 10° AOA, but dropping off again at about 15° AOA, and reversing again at 25° AOA. These variations in N1 under EPR control can be attributed to the flow through four compressor quadrants as the pressure in the lower three quadrants drops off rapidly with AOA compared to that of the upper quadrant. EPR control also has a slightly lower reduction in both fan and HPC stall margin at 30° AOA than N1 control.

The deterioration cases for both controller types are quite unremarkable. Deterioration tends to shift uncontrolled variables in directions that indicate less efficient operation. Here there is a small increase (about 1.5 percent) in thrust due to much larger increases in fuel flow and temperature (in the 5 to 10 percent range), allowing core speed to drop slightly. In both the fan speed and EPR control case, there is very little change in the one of those two variables that is not controlled. Fan stall margin was essentially unchanged from the new engine case, and while a large deterioration-induced shift occurred in the nominal HPC stall margin, it converged with that of the new engine at high AOA, for both controller types.

At other flight conditions, the thrust loss profile under N1 control retained the same U-shaped characteristic. Under EPR control at lower Mach numbers, the thrust responses resembled those under N1 control: they reduced to a minimum at 30° AOA, then started increasing again with decreasing AOA. It was only at higher Mach numbers that the characteristic W shape appeared in the response. This was independent of altitude and power code.

AOS Sweeps

The AOS linear sweep consists of a ramp in sideslip angle from 0° to 20°, then back through 0° to –20°, and back to 0° again, while holding AOA at 0°, all over 200 s, as shown in Figure 9. This keeps the engine on the windward side of the aircraft for the first half of the sweep, and on the leeward side for the second half. Table 6 to Table 8 show the impact of the fuselage on the engine's performance and operability. The thrust reduction is not anywhere near as significant when the engine is positioned into the wind, even at a large sideslip angle, as when the airflow is blocked by the fuselage. There is a small drop in thrust of about 1 percent when the sideslip angle approaches 20°, nearly all of which can be attributed to bypass thrust, as the core thrust remains relatively constant. This is true for both N1 and EPR control. Once the engine rotates back and moves past 0° AOS, there is an immediate and severe drop in thrust, in the neighborhood of 7 percent at the maximum sideslip deviation. Here N1 control does noticeably better than EPR control at maintaining thrust, especially from the core, although the reduction is still significant. This can again be attributed to the reduction in P_{T2} with AOS, especially on the leeward side, which allows EPR to be maintained with reduced thrust. Thus, under EPR control, N1 decreases, although the drop is well under 1 percent even at high AOS. Unlike with the AOA sweep, the thrust loss with AOS does not show signs of bottoming out, and indeed the fuselage presents a flow blockage that does not dissipate with increasing AOS. It is interesting that with either type of control, N2 increases with sideslip angle as the engine turns on the windward side, but on the leeward side, N2 increases with AOS under N1

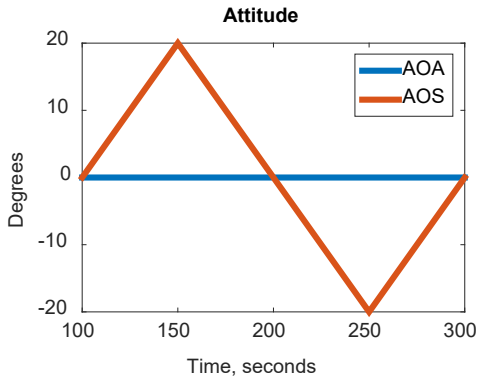

Figure 9.—AOS sweep profile.

control, but decreases with AOS under EPR control. Inter turbine temperature, ($T_{T4.5}$) follows the same pattern, although fuel flow reduces in both cases, just less so under N1 control. Fan and HPC stall margins both decrease slightly with AOS; controller type seems to have little impact on that. Interestingly, the loss of thrust due to a large deviation in AOS, even on the leeward side, is much less than for an AOA excursion.

Again, the cases with a deteriorated engine relative to a new engine did not produce any surprising results. There was a fairly constant shift in all but the controlled variables, with a slight thrust increase due to a fuel flow and temperature increase, and a slight decrease in N2. Fan and HPC stall margins decreased slightly with deterioration, and the shift remained about constant throughout the profile. It is interesting to note that the deterioration-related shift in the thrust variables is small compared to the dynamic change due to variation in AOS, but for N2, $T_{T4.5}$, and fuel flow, the opposite is true, i.e., the change through the profile is much smaller than the shift due to deterioration.

Qualitatively similar results are produced at other flight conditions. Notable differences are that at lower Mach numbers, the thrust drop at maximum AOS excursion is significantly less, about 1 to 2 percent on the windward side, and a little higher, 2 to 3 percent, on the leeward side. Altitude and power setting seem to have a much smaller effect than Mach number on the thrust loss.

TABLE 6.—AOS SWEEP RESULTS, EPR CONTROL VS N1 CONTROL

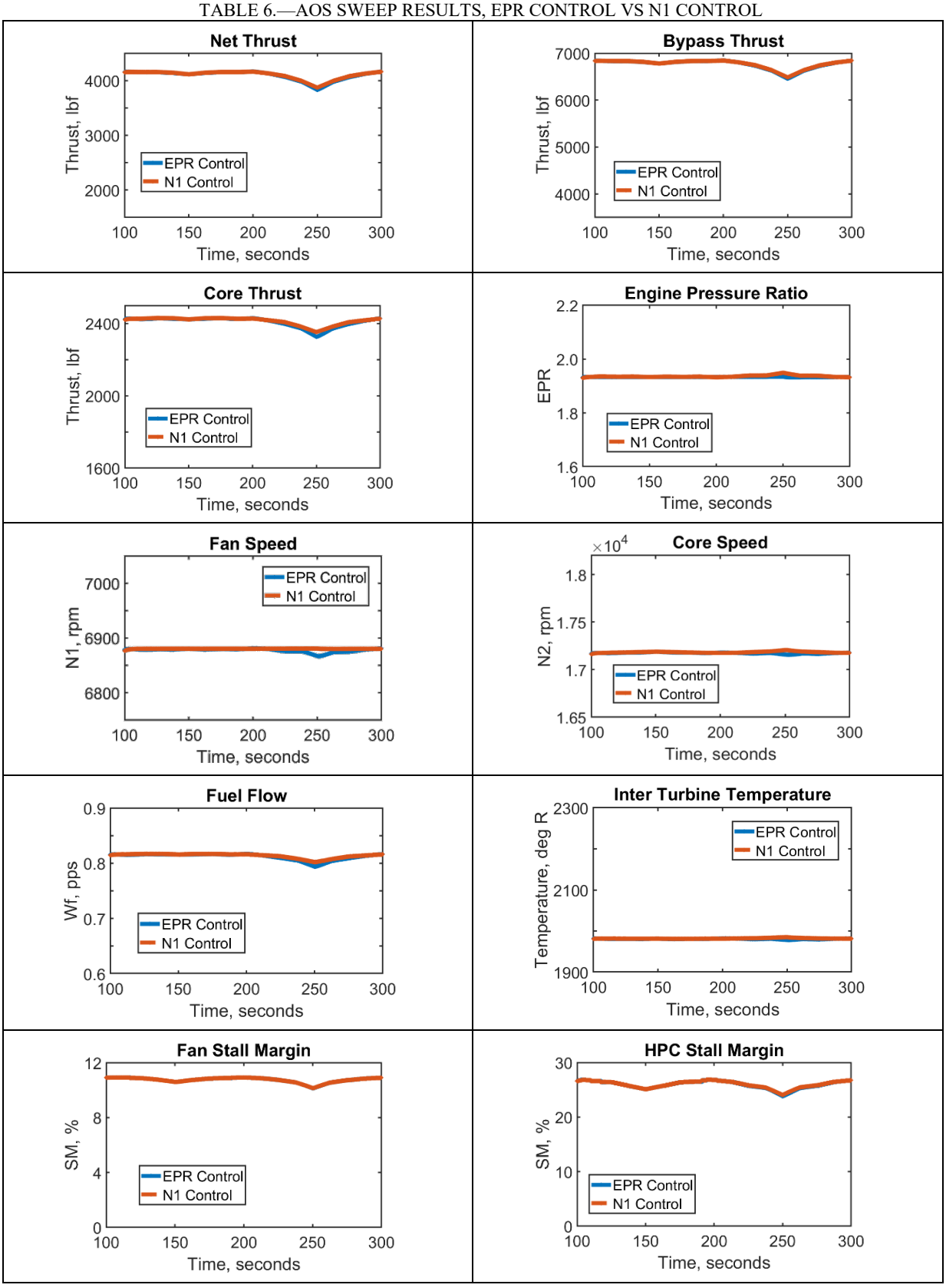

TABLE 7.—AOS SWEEP RESULTS, N1 CONTROL NEW VS. EOL ENGINE

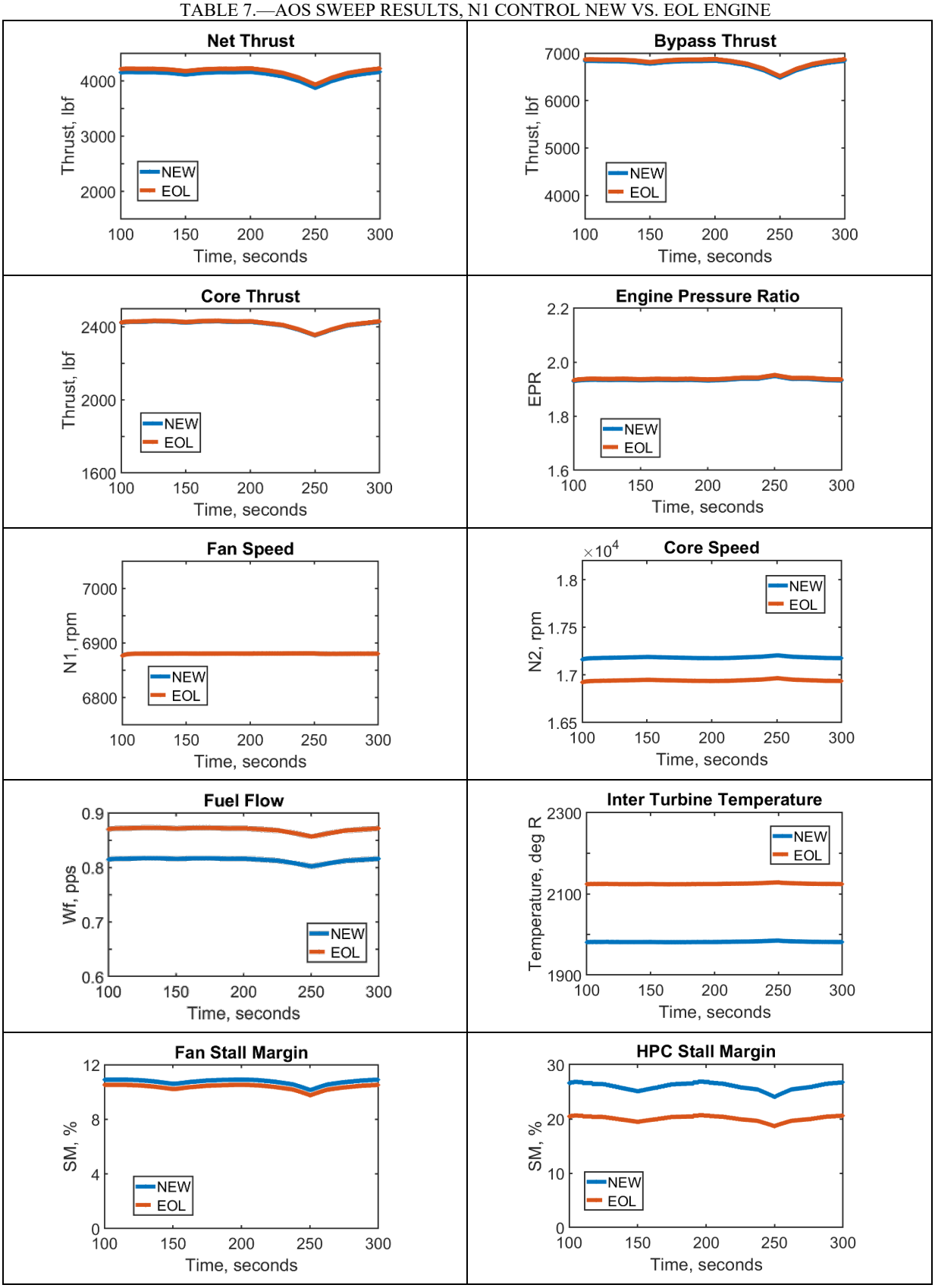

TABLE 8.—AOS SWEEP RESULTS, EPR CONTROL NEW VS. EOL ENGINE

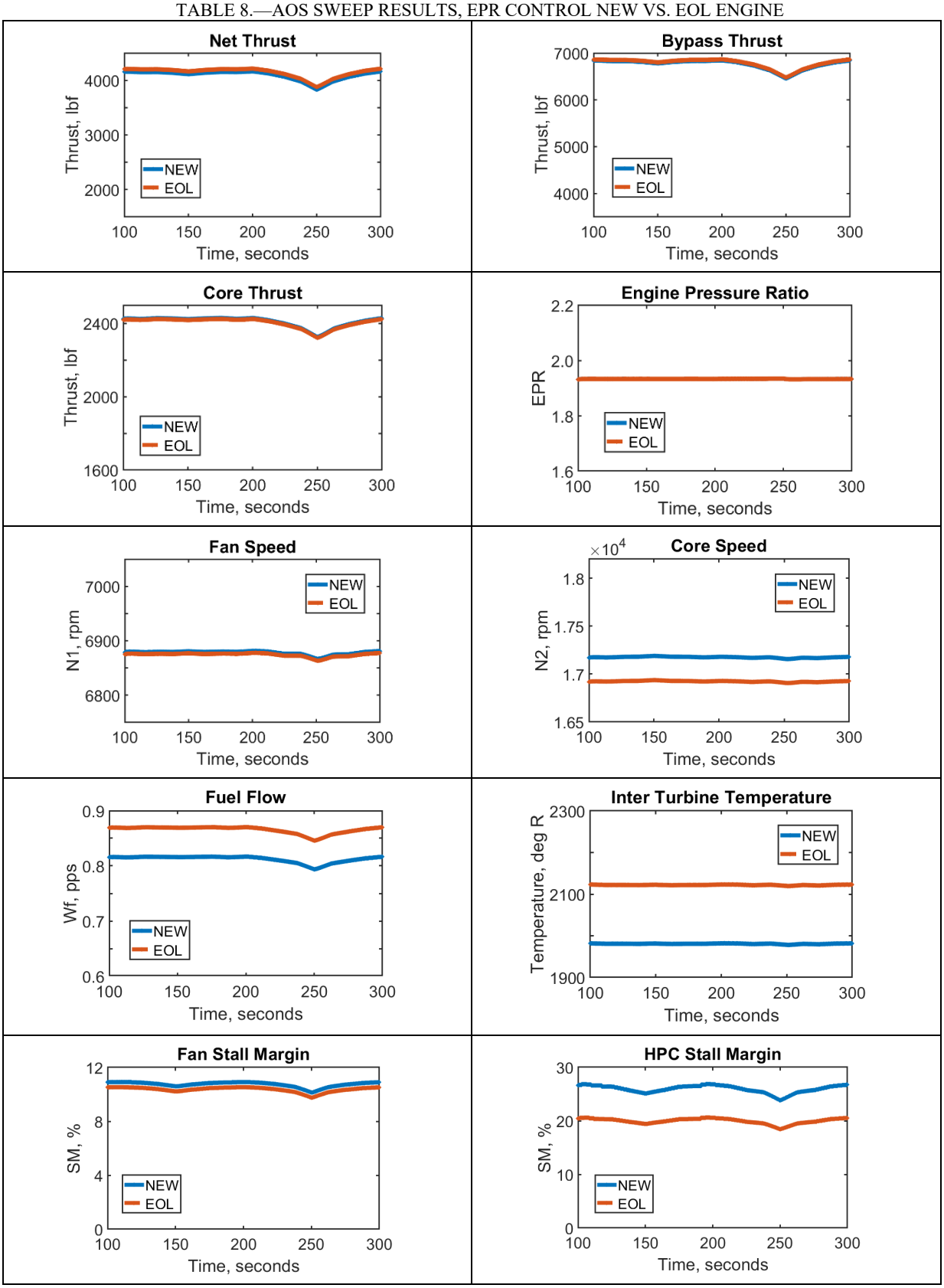

AOA and AOS Ovals

Engine performance during a combined AOA and AOS "oval maneuver" was also evaluated. In this profile the engine starts out at the nominal condition of AOA and AOS at 0°. It's attitude then traces out an oval during which AOA goes from 0° to 30° and back in a sinusoidal profile (a full period), while AOS sweeps sinusoidally from 0° to –20°, back through 0° to 20°, then back to 0° (a full period), as shown in Figure 10. Thus, the maximum AOS in each direction coincides with an AOA of about 15° (Figure 11). Table 9 shows the results of the oval maneuver comparing N1 and EPR control while Table 10 and Table 11 show the same cases comparing the controllers for new and deteriorated engines. From the previous tests it was seen that deviations in AOA have a much larger impact than those in AOS. This is borne out again in this case, as the thrust results look broadly similar to the AOA excursion cases (Table 3 through Table 5) with asymmetrical deviation due to AOS variation; this is especially noticeable under N1 control. The maximum thrust loss is over 50 percent. Comparing the controllers, under N1 control, the thrusts, N2, temperature, and fuel flow all look like smoothed versions of their counterparts under EPR control, i.e., the general shape is tracked but without the rapid swings associated with this input profile under EPR control. Under N1 control, the fan and HPC stall margins are slightly more reduced than for EPR control.

With deterioration, the thrusts are slightly increased with either controller at the cost of increased fuel and temperature. Fan stall margin has a slight downward shift, while HPC stall margin has a significant shift down near the nominal attitude, but converges with that of the new engine at extreme conditions.

At lower Mach numbers, the thrust variation was much smoother. Under EPR control, the thrust responses approached a slightly skewed W shape, while under N1 control they took on an asymmetrical U form, very reminiscent of the AOA sweep cases with the effect of AOS almost negligible. Again, power code and altitude had much less of an impact than Mach number.

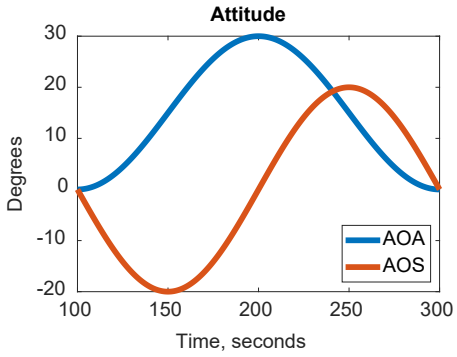

Figure 10.—AOA and AOS sinusoidal sweep profile.

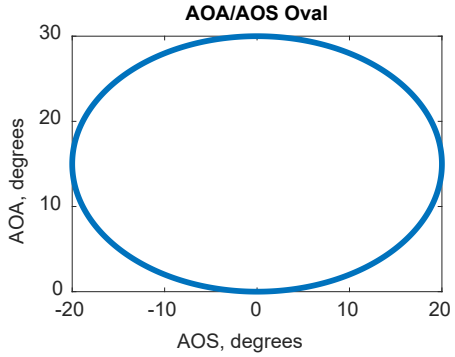

Figure 11.—Oval AOA and AOS profile.

TABLE 9.—AOA /AOS OVAL RESULTS, EPR CONTROL VS. N1 CONTROL

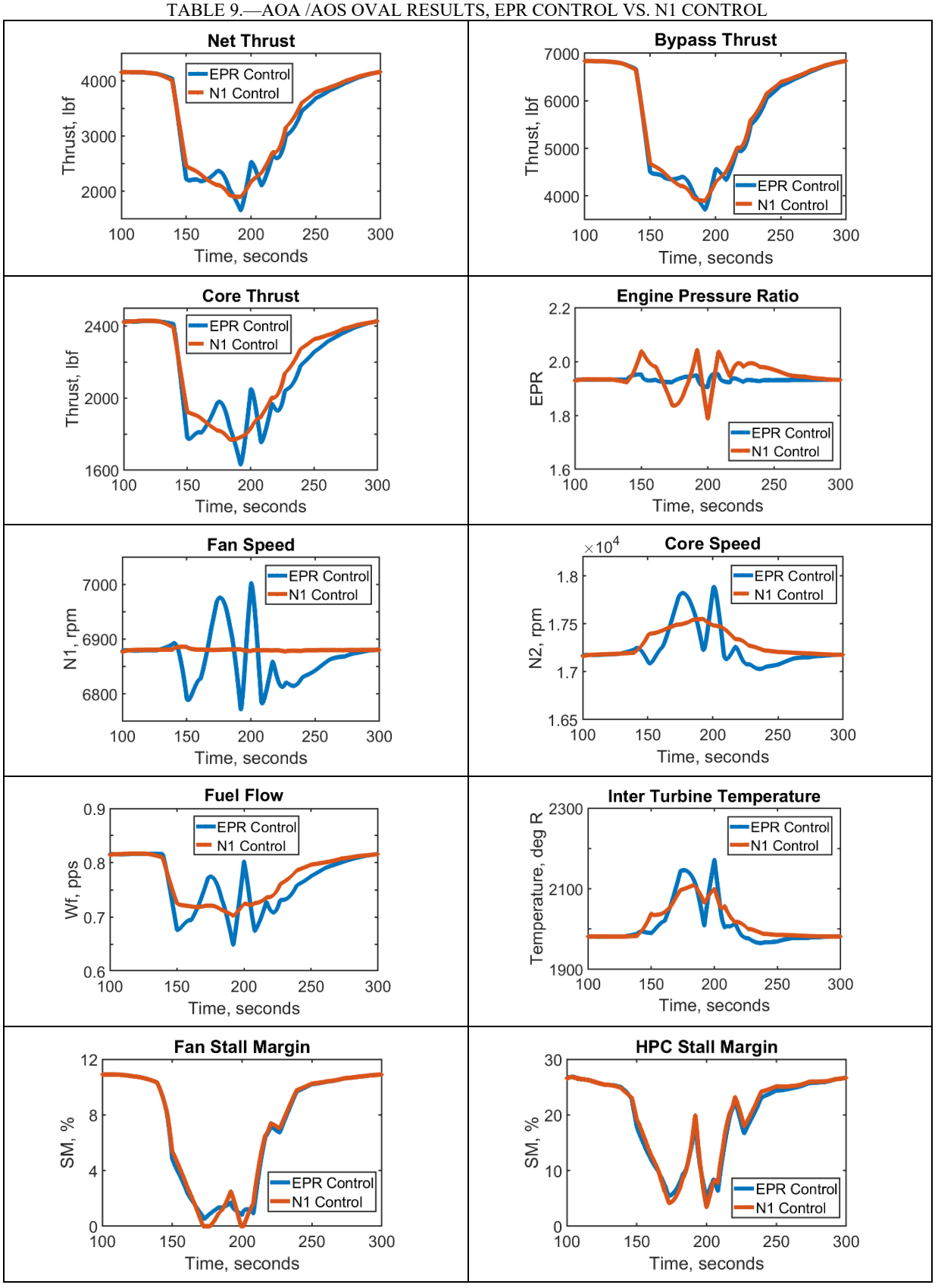

TABLE 10.—AOA/AOS OVAL RESULTS, N1 CONTROL NEW VS. EOL ENGINE

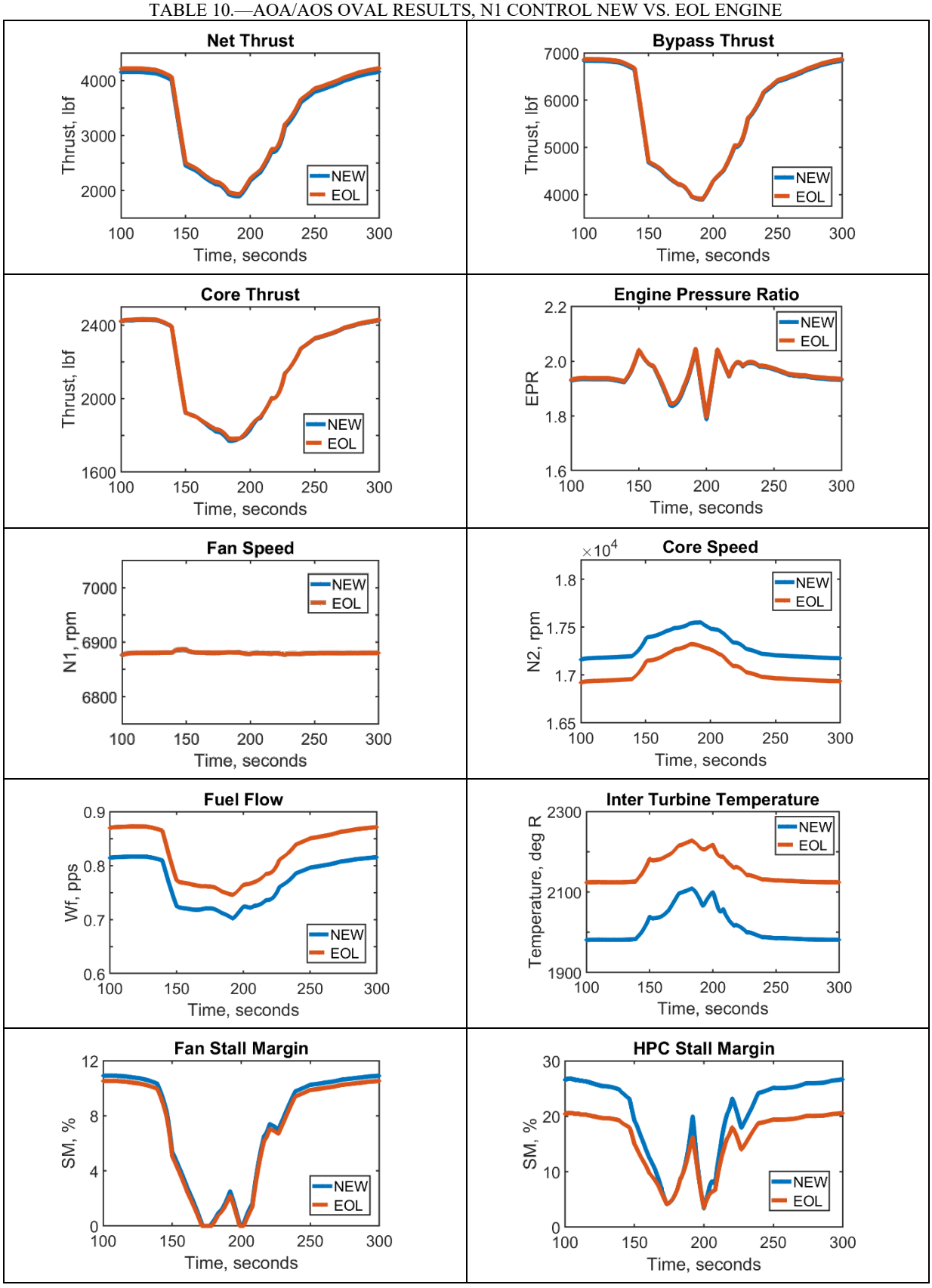

TABLE 11.—AOA/AOS OVAL RESULTS, EPR CONTROL NEW VS. EOL ENGINE

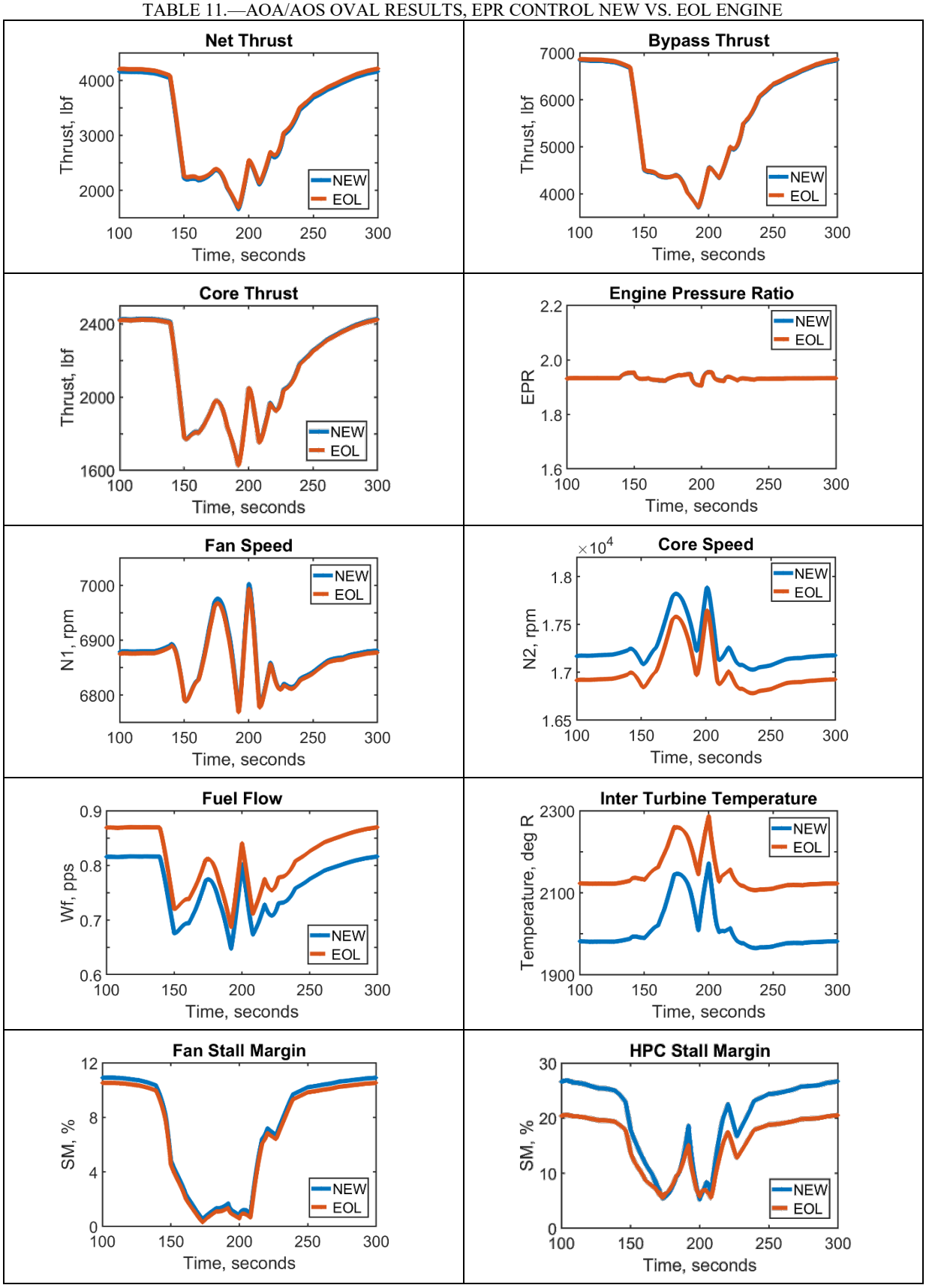

Discussion

Beyond controller type and engine health, other factors that impact engine operation, such as ambient temperature variation, were not examined; they will tend to shift trends up or down (similar to the impact of component health condition) with known effect and should not significantly impact the trends themselves at a fixed altitude and Mach number. Unlike the engine health condition, deviations in variables such as ambient temperature are accounted for through parameter correction (Ref. 40), minimizing their impact on engine control.

The testing and evaluation pointed out several systematic issues to be aware of, although they did not fundamentally impact the results: A linear interpolation scheme was used to determine total temperature and pressure points in between the table values. This resulted in two specific issues, one obvious and one more subtle. The obvious one is that rather than being smooth, some of the plots consist of relatively straight lines between the breakpoints, which correspond to the table values. This is only a cosmetic concern because the shape of the curve is broadly captured. The other has to do with the EPR set point. Because the interpolation routine was used to set input conditions between table breakpoints, variable values under EPR control did not correspond to their values under fan speed control except at the breakpoints because P_{T2} and T_{T2} were being approximated. Running the tests at the altitude/MN breakpoints eliminated the problem. Both issues could be resolved by using more breakpoints. Related to this is that at high AOA where total pressure in the upper quadrant begins to increase (between 20° and 30° AOA), a finer set of breakpoints would have given a better indication of where this occurs.

There is a small but noticeable amount of variation in the controlled variables (N1 and EPR) during the AOA and AOS profiles, which is especially apparent in the EPR plot in Table 11. The variation is much more prominent with AOA (Table 4 and Table 5) than with AOS (Table 7 and Table 8) and can be attributed to the interpolation of the inlet conditions, which are changing throughout the profile. Recall that the total temperature and pressure values used for computing EPR and for parameter correction are those from the upper quadrant. Use of a single location for inlet parameter sensing can affect performance when inlet flow distortion, especially temperature distortion, is present. This is because the temperature signal needed for calculating the corrected speed will be affected by inlet temperature distortion (Ref. 41). For the condition shown (MN = 0.6, Altitude 20,000 ft), T_{T2}, which is used to correct N1, varies about twice as much with AOA over the given range than with AOS (see the tables in the Appendix). Although the difference is only a few degrees Rankine, this results in a larger variation in the correction factor for AOA. As the attitude sweeps progress, the controller must adjust measured fan speed to track the corrected fan speed setpoint, which remains constant. The variation in the fan speed is barely noticeable, and its impact on other variables appears negligible. The situation with EPR is quite different. Because EPR is a ratio, correction does not come into play. The total pressure of the upper quadrant, where P_{T2} is obtained, changes relatively little over the range of variation in AOA or AOS. In contrast, P_{T7} is a function of the total pressure in all four quadrants, some of which show significantly more variation with AOA and AOS than does “measured” P_{T2}. Thus, the computed EPR changes as the sweeps progress, and the controller must continuously adjust P_{T7} to maintain the setpoint. These small variations in EPR likely have some impact on the output variables, but it is minor compared to the variations due to other sources and thus does not qualitatively change the results. This is clear from noticing how the changes in the controlled variable (EPR or N1) are dwarfed by the changes due to the sweeps when the other variable is controlled (Table 3, Table 6, and Table 9). Thus, while some of this variation in the controlled variable is a result of the parallel compressor implementation, it highlights a more general observation about EPR control. That is that P_{T2} from the upper quadrant does not necessarily represent the total pressure at the fan face as a whole, and using it as a control variable may in fact be the cause of much of the variation in

other variables during the extreme portions of the attitude sweeps (compare the difference in N1 and EPR control between about 150 and 250 s in Table 9).

The tendency of the fan stall margin to reduce to zero in this simulation is most likely due to fan operating unrealistically close to stall to begin with. Better component maps in general would improve the realism of the results, but the objective of the research is to identify representative trends for T-tail aircraft with aft-mounted engines, so the trends are of more interest than specific numbers.

Some small oscillations and quantization of the results are visible in certain variables (hardly noticeable at the scale of the plots shown here), mostly at the high AOA conditions and during the AOS sweeps. These are attributed to failure of the T-MATS simulation to fully converge at each time step, resulting in the solution, i.e., the output variables, jumping between values. It is likely that allowing more iterations per time step or loosening the convergence tolerance would resolve this.

It is important to understand that both the engine and the airframe models are only representative and thus the results should not be considered quantitatively accurate for how such an airframe/engine combination will actually perform. The intent is to generate qualitatively realistic results that can be applied to T-tail regional jet aircraft in general.

Conclusions

The point of the research is to expose trends in engine operation at extreme attitudes as a way to capture uncertainties for modeling aircraft behavior. The work was undertaken using a reverse approach: starting with sources of uncertainty from a pilot's perspective (e.g., controller type and engine health) that are, in fact, precisely known or can at least be bounded, and using them to characterize the variation in engine performance. Thus, both general trends and deviations from the trends can be observed.

For the aft-mounted jet engine on a T-tail regional jet aircraft under study, it was noted that AOA has a much more significant impact on thrust reduction than AOS; this is interesting because the fuselage appears to present a much larger flow blockage than the wing.

The results shown are illustrative and should not be construed to represent an actual airframe/engine combination. However, the trends shown do provide a reasonable approximation of the types of engine behavior that can be expected for a T-tail regional jet aircraft in extreme attitude situations.

Relating this effort back to the original study in support of flight simulator training, the takeaway is that for the T-tail aircraft with aft-mounted engines, there is little difference between fan speed and EPR control when it comes to installed operation. Interestingly, this seems to be because of the interference of the wing as AOA increases, since previous research showed that controller type makes a significant difference with a standalone engine. Here that difference only manifested above 25° AOA. Furthermore, engine performance was not noticeably changed until AOA exceeded 10°. This is about where the stick pusher activates in these T-tail regional jet aircraft, meaning that under normal AOA excursions, the pilot will see no difference in engine performance. Even if the stick pusher is overridden or inoperative, although thrust may drop off significantly, there will be essentially no difference due to controller selection until about 25° AOA, and then only at high Mach number. Deterioration resulted in a reduced stall margin, which is to be expected, but otherwise there was no difference in trends between a deteriorated engine and a new engine during similar attitude excursions.

Appendix

Average Total Temperature and Pressure Values for Each Sector as a Function of AOA and AOS for a Given *MN* and Altitude

Below are tables of the average total inlet temperature and pressure values computed for each quadrant of an aft-mounted engine installed on a T-tail regional jet aircraft, as a function of AOA and AOS, for a given Mach number and altitude. Tables for the starboard engine are shown; note that the tables for port side are mirror images (relative to AOS) of those for the starboard side.

Total Temperature--Starboard Side

MN = 0.2

ALT = 0

QUADRANT = TOP

ANGLE OF ATTACK (AOA) \ ANGLE OF SIDESLIP (AOS)	-20	-15	-10	-5	0	5	10	15	20
0	522.78	522.78	522.83	522.89	523.02	523.01	523.00	523.03	522.93
5	522.77	522.80	522.93	523.06	523.02	523.12	523.04	523.04	523.00
10	522.67	522.77	522.91	523.04	523.15	523.19	523.21	523.12	523.08
15	522.73	522.65	522.88	523.03	523.18	523.21	523.19	523.14	523.15
20	522.77	522.71	522.92	523.09	523.05	523.14	522.61	522.25	522.04
25	522.91	522.65	522.90	522.76	522.80	522.35	522.62	523.10	523.18
30	521.95	522.97	522.73	522.64	522.99	523.52	522.90	522.50	522.60

QUADRANT = RIGHT

ANGLE OF ATTACK (AOA) \ ANGLE OF SIDESLIP (AOS)	-20	-15	-10	-5	0	5	10	15	20
0	522.48	522.55	522.68	522.73	523.02	523.05	523.23	523.26	523.25
5	522.60	522.64	522.64	523.01	522.96	523.09	523.24	523.26	523.20
10	522.49	522.66	522.72	522.96	522.96	523.13	523.20	523.16	523.16
15	522.61	522.54	522.59	522.81	522.96	523.17	523.16	522.99	522.89
20	522.60	522.59	522.45	522.71	523.01	522.93	522.71	522.67	522.31
25	522.76	522.66	522.54	522.39	522.28	522.15	522.29	522.39	522.35
30	522.16	522.81	522.42	522.10	522.31	522.32	521.88	521.84	522.03

QUADRANT = BOTTOM

ANGLE OF ATTACK (AOA) \ ANGLE OF SIDESLIP (AOS)	-20	-15	-10	-5	0	5	10	15	20
0	522.90	523.07	523.10	523.12	523.07	523.01	522.95	522.87	522.82
5	522.96	523.08	523.08	523.14	523.13	522.94	522.84	522.70	522.62
10	523.01	523.09	523.08	523.16	523.01	522.80	522.66	522.56	522.52
15	523.00	523.04	523.00	523.26	523.04	522.62	522.36	522.29	522.23
20	522.88	522.96	522.89	522.87	522.52	522.29	521.86	522.24	522.33
25	523.03	522.73	522.38	521.98	522.33	522.36	522.37	522.47	522.57
30	522.43	522.48	522.27	522.34	522.22	522.06	521.46	521.56	521.84

QUADRANT = LEFT

ANGLE OF ATTACK (AOA) \ ANGLE OF SIDESLIP (AOS)	-20	-15	-10	-5	0	5	10	15	20
0	523.14	523.28	523.25	523.16	523.06	522.90	522.64	522.50	522.29
5	523.16	523.23	523.15	523.23	523.15	522.85	522.62	522.51	522.41
10	523.16	523.26	523.32	523.22	523.13	522.79	522.71	522.55	522.63
15	523.22	523.21	523.33	523.33	523.07	522.74	522.60	522.57	522.43
20	523.08	523.29	523.32	523.43	522.89	522.43	521.91	522.14	522.40
25	523.21	522.72	522.86	522.38	522.77	523.05	522.73	522.65	522.51
30	522.82	522.87	522.48	523.17	523.06	522.36	521.54	521.68	521.83

Total Temperature--Starboard Side

MN = 0.2

ALT = 10000

QUADRANT = TOP

ANGLE OF ATTACK (AOA) \ ANGLE OF SIDESLIP (AOS)	-20	-15	-10	-5	0	5	10	15	20
0	486.81	486.81	486.85	486.91	487.03	487.02	487.01	487.04	486.95
5	486.79	486.82	486.95	487.07	487.03	487.13	487.05	487.05	487.01
10	486.71	486.79	486.93	487.05	487.15	487.19	487.21	487.13	487.08
15	486.76	486.69	486.90	487.04	487.18	487.21	487.19	487.15	487.16
20	486.80	486.74	486.94	487.10	487.06	487.14	486.65	486.31	486.11
25	486.93	486.68	486.92	486.79	486.83	486.40	486.66	487.10	487.18
30	486.04	486.99	486.76	486.68	487.00	487.49	486.92	486.55	486.64

QUADRANT = RIGHT

ANGLE OF ATTACK (AOA) \ ANGLE OF SIDESLIP (AOS)	-20	-15	-10	-5	0	5	10	15	20
0	486.53	486.59	486.71	486.76	487.03	487.06	487.22	487.25	487.25
5	486.64	486.68	486.67	487.02	486.98	487.10	487.24	487.26	487.20
10	486.54	486.69	486.75	486.98	486.97	487.14	487.20	487.16	487.16
15	486.65	486.58	486.63	486.84	486.98	487.18	487.16	487.01	486.91
20	486.64	486.63	486.50	486.74	487.03	486.95	486.74	486.70	486.36
25	486.79	486.69	486.58	486.44	486.34	486.22	486.35	486.44	486.41
30	486.23	486.83	486.47	486.18	486.36	486.38	485.97	485.93	486.11

QUADRANT = BOTTOM

ANGLE OF ATTACK (AOA) \ ANGLE OF SIDESLIP (AOS)	-20	-15	-10	-5	0	5	10	15	20
0	486.92	487.08	487.10	487.13	487.07	487.02	486.96	486.90	486.84
5	486.97	487.08	487.09	487.15	487.14	486.96	486.86	486.74	486.66
10	487.02	487.10	487.09	487.16	487.02	486.83	486.70	486.60	486.56
15	487.01	487.05	487.01	487.26	487.05	486.66	486.42	486.36	486.30
20	486.90	486.98	486.91	486.89	486.56	486.35	485.95	486.30	486.38
25	487.04	486.76	486.44	486.06	486.38	486.42	486.42	486.51	486.61
30	486.48	486.53	486.33	486.40	486.28	486.14	485.58	485.67	485.93

QUADRANT = LEFT

ANGLE OF ATTACK (AOA) \ ANGLE OF SIDESLIP (AOS)	-20	-15	-10	-5	0	5	10	15	20
0	487.14	487.27	487.25	487.16	487.07	486.92	486.68	486.55	486.35
5	487.16	487.23	487.16	487.22	487.16	486.87	486.66	486.56	486.46
10	487.16	487.26	487.31	487.22	487.14	486.81	486.75	486.60	486.67
15	487.22	487.20	487.32	487.32	487.08	486.77	486.64	486.61	486.48
20	487.08	487.29	487.31	487.42	486.91	486.48	486.00	486.21	486.45
25	487.21	486.75	486.89	486.43	486.80	487.05	486.76	486.69	486.56
30	486.85	486.89	486.53	487.17	487.07	486.41	485.65	485.78	485.92

Total Temperature--Starboard Side

MN = 0.2

ALT = 20000

QUADRANT = TOP

ANGLE OF ATTACK (AOA) \ ANGLE OF SIDESLIP (AOS)	-20	-15	-10	-5	0	5	10	15	20
0	450.90	450.90	450.94	450.99	451.10	451.09	451.08	451.12	451.03
5	450.89	450.91	451.03	451.14	451.11	451.19	451.12	451.12	451.08
10	450.81	450.89	451.01	451.13	451.22	451.25	451.27	451.19	451.15
15	450.85	450.79	450.98	451.11	451.24	451.27	451.25	451.21	451.22
20	450.89	450.84	451.02	451.17	451.13	451.21	450.75	450.44	450.25
25	451.01	450.78	451.00	450.88	450.92	450.52	450.76	451.17	451.24
30	450.18	451.06	450.85	450.78	451.07	451.53	451.00	450.65	450.74

QUADRANT = RIGHT

ANGLE OF ATTACK (AOA) \ ANGLE OF SIDESLIP (AOS)	-20	-15	-10	-5	0	5	10	15	20
0	450.64	450.70	450.81	450.85	451.11	451.13	451.28	451.31	451.31
5	450.74	450.78	450.77	451.09	451.05	451.17	451.29	451.31	451.26
10	450.65	450.79	450.85	451.05	451.05	451.20	451.26	451.23	451.22
15	450.75	450.69	450.73	450.93	451.05	451.24	451.22	451.08	450.99
20	450.74	450.73	450.61	450.84	451.10	451.03	450.84	450.80	450.49
25	450.88	450.79	450.69	450.56	450.46	450.35	450.47	450.56	450.53
30	450.36	450.92	450.58	450.31	450.49	450.50	450.12	450.08	450.25

QUADRANT = BOTTOM

ANGLE OF ATTACK (AOA) \ ANGLE OF SIDESLIP (AOS)	-20	-15	-10	-5	0	5	10	15	20
0	451.00	451.15	451.17	451.19	451.14	451.10	451.04	450.98	450.93
5	451.05	451.15	451.16	451.21	451.20	451.03	450.95	450.83	450.76
10	451.10	451.16	451.16	451.22	451.10	450.92	450.80	450.71	450.67
15	451.09	451.12	451.09	451.31	451.12	450.76	450.54	450.48	450.43
20	450.98	451.06	450.99	450.97	450.67	450.47	450.11	450.43	450.50
25	451.11	450.85	450.55	450.20	450.50	450.53	450.54	450.62	450.71
30	450.59	450.64	450.46	450.52	450.41	450.28	449.76	449.84	450.08

QUADRANT = LEFT

ANGLE OF ATTACK (AOA) \ ANGLE OF SIDESLIP (AOS)	-20	-15	-10	-5	0	5	10	15	20
0	451.21	451.33	451.30	451.23	451.14	451.00	450.78	450.66	450.47
5	451.22	451.29	451.22	451.28	451.22	450.96	450.76	450.66	450.58
10	451.22	451.31	451.37	451.28	451.20	450.90	450.84	450.70	450.77
15	451.28	451.26	451.37	451.37	451.15	450.86	450.74	450.72	450.59
20	451.15	451.34	451.36	451.46	451.00	450.60	450.15	450.35	450.57
25	451.27	450.85	450.97	450.55	450.89	451.13	450.85	450.78	450.66
30	450.93	450.97	450.64	451.23	451.14	450.53	449.82	449.95	450.07

Total Temperature--Starboard Side

MN = 0.2

ALT = 30000

QUADRANT = TOP

ANGLE OF ATTACK (AOA) \ ANGLE OF SIDESLIP (AOS)	-20	-15	-10	-5	0	5	10	15	20
0	415.02	415.02	415.06	415.11	415.21	415.21	415.20	415.23	415.15
5	415.01	415.04	415.15	415.25	415.22	415.30	415.23	415.23	415.20
10	414.94	415.01	415.13	415.23	415.32	415.35	415.37	415.30	415.26
15	414.98	414.93	415.11	415.22	415.34	415.37	415.35	415.31	415.32
20	415.02	414.97	415.14	415.27	415.24	415.31	414.89	414.60	414.43
25	415.13	414.92	415.12	415.01	415.04	414.68	414.90	415.28	415.35
30	414.37	415.18	414.99	414.91	415.19	415.61	415.12	414.80	414.88

QUADRANT = RIGHT

ANGLE OF ATTACK (AOA) \ ANGLE OF SIDESLIP (AOS)	-20	-15	-10	-5	0	5	10	15	20
0	414.79	414.84	414.94	414.98	415.22	415.24	415.38	415.40	415.40
5	414.88	414.91	414.91	415.20	415.17	415.27	415.39	415.41	415.36
10	414.80	414.93	414.98	415.17	415.16	415.31	415.36	415.33	415.32
15	414.89	414.83	414.87	415.05	415.17	415.34	415.32	415.19	415.11
20	414.88	414.87	414.76	414.97	415.21	415.15	414.97	414.94	414.65
25	415.01	414.93	414.83	414.71	414.62	414.52	414.64	414.71	414.68
30	414.53	415.05	414.74	414.49	414.65	414.66	414.31	414.28	414.43

QUADRANT = BOTTOM

ANGLE OF ATTACK (AOA) \ ANGLE OF SIDESLIP (AOS)	-20	-15	-10	-5	0	5	10	15	20
0	415.12	415.25	415.28	415.30	415.25	415.21	415.16	415.10	415.05
5	415.17	415.26	415.26	415.31	415.31	415.15	415.07	414.96	414.90
10	415.21	415.27	415.26	415.32	415.21	415.04	414.93	414.85	414.82
15	415.20	415.23	415.20	415.41	415.23	414.89	414.69	414.64	414.59
20	415.10	415.17	415.11	415.09	414.82	414.63	414.30	414.60	414.66
25	415.22	414.99	414.71	414.39	414.66	414.69	414.70	414.77	414.86
30	414.75	414.79	414.62	414.68	414.58	414.46	413.98	414.05	414.28

QUADRANT = LEFT

ANGLE OF ATTACK (AOA) \ ANGLE OF SIDESLIP (AOS)	-20	-15	-10	-5	0	5	10	15	20
0	415.31	415.42	415.40	415.33	415.24	415.12	414.92	414.80	414.63
5	415.33	415.38	415.32	415.38	415.32	415.08	414.90	414.81	414.73
10	415.33	415.41	415.46	415.37	415.31	415.03	414.97	414.84	414.91
15	415.37	415.36	415.46	415.46	415.26	414.99	414.88	414.86	414.75
20	415.26	415.43	415.45	415.54	415.12	414.75	414.34	414.52	414.72
25	415.36	414.98	415.09	414.71	415.02	415.24	414.98	414.92	414.81
30	415.06	415.09	414.79	415.34	415.25	414.69	414.04	414.15	414.27

Total Temperature--Starboard Side

MN = 0.2

ALT = 36000

QUADRANT = TOP

ANGLE OF ATTACK (AOA) \ ANGLE OF SIDESLIP (AOS)	-20	-15	-10	-5	0	5	10	15	20
0	393.53	393.53	393.57	393.61	393.71	393.70	393.69	393.72	393.65
5	393.52	393.54	393.65	393.74	393.71	393.79	393.73	393.73	393.69
10	393.45	393.52	393.63	393.73	393.81	393.84	393.86	393.79	393.75
15	393.49	393.44	393.61	393.72	393.83	393.86	393.84	393.80	393.81
20	393.52	393.48	393.64	393.76	393.73	393.80	393.40	393.13	392.97
25	393.63	393.43	393.62	393.52	393.55	393.21	393.41	393.77	393.84
30	392.91	393.68	393.50	393.43	393.69	394.09	393.62	393.32	393.40

QUADRANT = RIGHT

ANGLE OF ATTACK (AOA) \ ANGLE OF SIDESLIP (AOS)	-20	-15	-10	-5	0	5	10	15	20
0	393.31	393.36	393.45	393.49	393.71	393.74	393.87	393.89	393.89
5	393.40	393.43	393.42	393.70	393.67	393.76	393.88	393.89	393.84
10	393.31	393.44	393.49	393.67	393.66	393.80	393.85	393.82	393.81
15	393.40	393.35	393.39	393.55	393.67	393.83	393.81	393.69	393.61
20	393.40	393.39	393.28	393.48	393.71	393.65	393.48	393.45	393.17
25	393.51	393.44	393.35	393.23	393.15	393.06	393.16	393.24	393.21
30	393.06	393.55	393.26	393.02	393.18	393.19	392.85	392.82	392.97

QUADRANT = BOTTOM

ANGLE OF ATTACK (AOA) \ ANGLE OF SIDESLIP (AOS)	-20	-15	-10	-5	0	5	10	15	20
0	393.62	393.75	393.77	393.79	393.75	393.71	393.66	393.60	393.56
5	393.66	393.75	393.76	393.80	393.80	393.65	393.57	393.47	393.41
10	393.71	393.76	393.76	393.81	393.70	393.55	393.44	393.37	393.33
15	393.70	393.73	393.70	393.89	393.73	393.41	393.22	393.17	393.12
20	393.61	393.67	393.61	393.60	393.34	393.16	392.84	393.13	393.19
25	393.72	393.49	393.23	392.93	393.19	393.22	393.22	393.30	393.37
30	393.27	393.31	393.15	393.20	393.11	392.99	392.54	392.61	392.82

QUADRANT = LEFT

ANGLE OF ATTACK (AOA) \ ANGLE OF SIDESLIP (AOS)	-20	-15	-10	-5	0	5	10	15	20
0	393.80	393.91	393.89	393.82	393.74	393.62	393.43	393.32	393.16
5	393.82	393.87	393.81	393.87	393.81	393.58	393.41	393.33	393.25
10	393.82	393.89	393.94	393.86	393.80	393.54	393.48	393.36	393.42
15	393.86	393.85	393.94	393.94	393.75	393.50	393.39	393.37	393.27
20	393.75	393.92	393.93	394.02	393.62	393.27	392.88	393.05	393.24
25	393.85	393.49	393.60	393.23	393.53	393.73	393.49	393.43	393.33
30	393.56	393.60	393.31	393.83	393.74	393.21	392.60	392.71	392.81

Total Temperature--Starboard Side

MN = 0.4

ALT = 0

QUADRANT = TOP

ANGLE OF ATTACK (AOA) \ ANGLE OF SIDESLIP (AOS)	-20	-15	-10	-5	0	5	10	15	20
0	534.76	535.04	534.93	535.13	535.41	535.75	535.94	535.76	535.55
5	534.82	534.91	535.31	535.60	536.24	536.29	536.26	535.97	535.64
10	534.62	534.94	535.55	536.18	536.40	536.30	536.38	535.75	535.85
15	534.08	534.60	535.20	536.20	536.69	536.63	536.65	536.75	534.22
20	533.85	534.02	535.01	535.01	536.22	535.81	534.23	533.86	536.11
25	533.95	534.21	533.55	535.55	535.65	536.01	535.88	535.68	535.03
30	533.70	531.41	534.09	534.01	534.88	534.66	534.67	534.57	534.52

QUADRANT = RIGHT

ANGLE OF ATTACK (AOA) \ ANGLE OF SIDESLIP (AOS)	-20	-15	-10	-5	0	5	10	15	20
0	533.90	534.28	534.15	534.98	535.81	536.33	536.39	536.12	535.79
5	533.89	534.12	534.82	535.36	535.73	536.22	536.56	535.97	535.44
10	533.82	534.41	534.69	535.12	535.80	536.67	536.60	535.61	535.79
15	533.66	534.27	534.40	535.45	535.78	537.29	536.89	536.23	535.65
20	533.31	534.54	533.74	533.85	535.50	535.02	534.31	533.91	533.66
25	532.65	533.08	533.22	532.37	533.59	531.97	531.17	530.79	531.43
30	533.25	532.51	533.27	532.47	531.73	532.45	530.68	531.65	531.81

QUADRANT = BOTTOM

ANGLE OF ATTACK (AOA) \ ANGLE OF SIDESLIP (AOS)	-20	-15	-10	-5	0	5	10	15	20
0	535.67	535.93	536.17	536.42	536.14	536.05	535.35	535.02	534.71
5	535.39	536.00	536.03	536.19	535.73	535.56	534.91	534.62	534.36
10	535.62	536.03	535.89	535.96	535.74	535.39	534.64	534.22	534.23
15	535.89	535.97	535.75	536.61	536.20	534.45	533.54	533.01	534.25
20	536.22	536.34	534.77	533.58	533.84	533.87	534.65	533.89	531.75
25	535.71	533.42	533.29	533.15	532.05	531.61	530.99	530.65	531.71
30	532.73	533.28	533.73	532.18	532.56	532.56	531.04	531.74	532.53

QUADRANT = LEFT

ANGLE OF ATTACK (AOA) \ ANGLE OF SIDESLIP (AOS)	-20	-15	-10	-5	0	5	10	15	20
0	536.59	536.50	536.77	536.59	536.09	535.11	534.67	534.13	533.88
5	536.29	536.42	536.37	536.53	535.59	535.05	534.42	534.11	533.78
10	536.18	536.57	536.53	536.50	535.67	534.83	533.71	534.06	534.29
15	536.51	536.66	536.60	536.82	535.73	535.43	534.25	533.12	532.71
20	536.55	536.44	536.67	535.84	535.38	534.47	535.48	535.03	533.76
25	536.18	534.56	534.42	535.69	535.81	532.96	531.83	531.39	531.32
30	532.00	535.12	534.37	535.35	532.77	532.65	530.56	531.25	531.29

Total Temperature--Starboard Side

MN = 0.4

ALT = 10000

QUADRANT = TOP

ANGLE OF ATTACK (AOA) \ ANGLE OF SIDESLIP (AOS)	-20	-15	-10	-5	0	5	10	15	20
0	497.97	498.23	498.13	498.32	498.58	498.90	499.08	498.90	498.72
5	498.03	498.12	498.49	498.76	499.36	499.40	499.38	499.11	498.79
10	497.84	498.15	498.71	499.30	499.51	499.41	499.48	498.89	498.99
15	497.34	497.83	498.39	499.32	499.78	499.72	499.73	499.82	497.47
20	497.13	497.28	498.21	498.20	499.33	498.95	497.47	497.13	499.22
25	497.22	497.46	496.84	498.70	498.79	499.13	499.01	498.82	498.21
30	496.98	494.84	497.34	497.27	498.08	497.87	497.88	497.79	497.75

QUADRANT = RIGHT

ANGLE OF ATTACK (AOA) \ ANGLE OF SIDESLIP (AOS)	-20	-15	-10	-5	0	5	10	15	20
0	497.17	497.53	497.41	498.18	498.95	499.44	499.49	499.24	498.93
5	497.16	497.38	498.04	498.54	498.88	499.34	499.65	499.11	498.61
10	497.10	497.65	497.91	498.31	498.95	499.76	499.69	498.77	498.93
15	496.95	497.52	497.64	498.62	498.93	500.34	499.95	499.34	498.80
20	496.62	497.77	497.02	497.13	498.65	498.21	497.55	497.17	496.94
25	496.00	496.41	496.54	495.74	496.87	495.37	494.62	494.27	494.86
30	496.55	495.87	496.58	495.83	495.14	495.81	494.16	495.06	495.22

QUADRANT = BOTTOM

ANGLE OF ATTACK (AOA) \ ANGLE OF SIDESLIP (AOS)	-20	-15	-10	-5	0	5	10	15	20
0	498.82	499.07	499.29	499.52	499.26	499.18	498.53	498.22	497.93
5	498.56	499.13	499.15	499.31	498.88	498.72	498.12	497.84	497.61
10	498.78	499.15	499.03	499.10	498.89	498.57	497.87	497.47	497.48
15	499.03	499.10	498.90	499.70	499.32	497.68	496.83	496.34	497.50
20	499.34	499.44	497.98	496.86	497.11	497.14	497.86	497.16	495.16
25	498.85	496.72	496.60	496.46	495.44	495.03	494.45	494.13	495.12
30	496.07	496.59	497.01	495.56	495.91	495.91	494.50	495.15	495.88

QUADRANT = LEFT

ANGLE OF ATTACK (AOA) \ ANGLE OF SIDESLIP (AOS)	-20	-15	-10	-5	0	5	10	15	20
0	499.67	499.59	499.84	499.68	499.21	498.30	497.90	497.39	497.15
5	499.40	499.52	499.48	499.62	498.75	498.24	497.66	497.37	497.06
10	499.30	499.66	499.63	499.60	498.82	498.04	497.00	497.33	497.54
15	499.61	499.74	499.69	499.90	498.88	498.60	497.50	496.44	496.06
20	499.64	499.54	499.75	498.98	498.54	497.69	498.63	498.22	497.03
25	499.29	497.78	497.65	498.83	498.94	496.29	495.23	494.82	494.76
30	495.40	498.31	497.61	498.51	496.11	495.99	494.05	494.70	494.73

Total Temperature--Starboard Side

MN = 0.4

ALT = 20000

QUADRANT = TOP

ANGLE OF ATTACK (AOA) \ ANGLE OF SIDESLIP (AOS)	-20	-15	-10	-5	0	5	10	15	20
0	461.24	461.48	461.39	461.57	461.80	462.10	462.26	462.10	461.93
5	461.29	461.37	461.72	461.97	462.52	462.57	462.54	462.29	462.00
10	461.12	461.40	461.92	462.47	462.66	462.57	462.64	462.09	462.18
15	460.66	461.10	461.62	462.49	462.91	462.86	462.87	462.95	460.77
20	460.46	460.60	461.46	461.45	462.49	462.14	460.77	460.46	462.39
25	460.54	460.77	460.19	461.91	461.99	462.31	462.20	462.03	461.46
30	460.32	458.34	460.65	460.59	461.34	461.15	461.15	461.07	461.03

QUADRANT = RIGHT

ANGLE OF ATTACK (AOA) \ ANGLE OF SIDESLIP (AOS)	-20	-15	-10	-5	0	5	10	15	20
0	460.50	460.83	460.72	461.44	462.15	462.60	462.65	462.42	462.13
5	460.49	460.69	461.30	461.76	462.08	462.51	462.79	462.29	461.83
10	460.43	460.94	461.18	461.55	462.14	462.89	462.83	461.98	462.13
15	460.30	460.82	460.93	461.84	462.12	463.43	463.07	462.51	462.01
20	459.99	461.05	460.36	460.46	461.87	461.46	460.84	460.50	460.28
25	459.41	459.79	459.91	459.17	460.22	458.83	458.14	457.81	458.36
30	459.92	459.29	459.95	459.25	458.61	459.24	457.71	458.54	458.68

QUADRANT = BOTTOM

ANGLE OF ATTACK (AOA) \ ANGLE OF SIDESLIP (AOS)	-20	-15	-10	-5	0	5	10	15	20
0	462.02	462.26	462.46	462.67	462.43	462.36	461.76	461.47	461.21
5	461.78	462.31	462.33	462.48	462.08	461.94	461.37	461.12	460.90
10	461.99	462.34	462.22	462.28	462.09	461.79	461.14	460.78	460.79
15	462.22	462.28	462.10	462.84	462.49	460.97	460.18	459.72	460.80
20	462.50	462.60	461.25	460.21	460.44	460.46	461.14	460.48	458.63
25	462.05	460.08	459.97	459.84	458.89	458.51	457.98	457.68	458.59
30	459.48	459.95	460.34	459.00	459.33	459.33	458.02	458.62	459.30

QUADRANT = LEFT

ANGLE OF ATTACK (AOA) \ ANGLE OF SIDESLIP (AOS)	-20	-15	-10	-5	0	5	10	15	20
0	462.82	462.74	462.97	462.82	462.39	461.54	461.17	460.70	460.48
5	462.56	462.67	462.64	462.77	461.96	461.49	460.95	460.68	460.40
10	462.47	462.80	462.77	462.75	462.03	461.30	460.34	460.64	460.84
15	462.75	462.88	462.83	463.02	462.08	461.82	460.80	459.82	459.46
20	462.78	462.69	462.88	462.17	461.77	460.98	461.85	461.47	460.37
25	462.46	461.06	460.94	462.03	462.13	459.68	458.70	458.32	458.26
30	458.85	461.55	460.90	461.74	459.51	459.41	457.60	458.21	458.24

Total Temperature--Starboard Side

MN = 0.4

ALT = 30000

QUADRANT = TOP

ANGLE OF ATTACK (AOA) \ ANGLE OF SIDESLIP (AOS)	-20	-15	-10	-5	0	5	10	15	20
0	424.54	424.76	424.67	424.84	425.05	425.33	425.48	425.33	425.17
5	424.59	424.66	424.97	425.21	425.72	425.76	425.73	425.50	425.24
10	424.43	424.69	425.16	425.67	425.84	425.76	425.83	425.32	425.41
15	424.00	424.41	424.89	425.69	426.08	426.03	426.04	426.11	424.11
20	423.82	423.95	424.74	424.74	425.69	425.37	424.11	423.82	425.61
25	423.90	424.10	423.58	425.16	425.24	425.53	425.43	425.27	424.75
30	423.69	421.87	424.00	423.94	424.63	424.46	424.46	424.38	424.35

QUADRANT = RIGHT

ANGLE OF ATTACK (AOA) \ ANGLE OF SIDESLIP (AOS)	-20	-15	-10	-5	0	5	10	15	20
0	423.85	424.16	424.06	424.72	425.37	425.79	425.83	425.62	425.35
5	423.85	424.03	424.59	425.02	425.31	425.70	425.97	425.50	425.08
10	423.79	424.26	424.48	424.83	425.37	426.06	426.00	425.22	425.36
15	423.67	424.15	424.25	425.09	425.35	426.55	426.23	425.71	425.25
20	423.39	424.36	423.73	423.82	425.12	424.74	424.18	423.86	423.66
25	422.86	423.21	423.32	422.64	423.60	422.32	421.69	421.38	421.89
30	423.33	422.75	423.36	422.72	422.13	422.70	421.30	422.06	422.19

QUADRANT = BOTTOM

ANGLE OF ATTACK (AOA) \ ANGLE OF SIDESLIP (AOS)	-20	-15	-10	-5	0	5	10	15	20
0	425.26	425.47	425.66	425.86	425.64	425.56	425.01	424.75	424.50
5	425.04	425.52	425.54	425.67	425.31	425.18	424.66	424.43	424.23
10	425.22	425.55	425.43	425.50	425.32	425.04	424.45	424.11	424.12
15	425.44	425.50	425.33	426.01	425.69	424.29	423.57	423.15	424.13
20	425.70	425.79	424.55	423.60	423.81	423.83	424.45	423.85	422.15
25	425.29	423.47	423.37	423.26	422.39	422.03	421.54	421.27	422.11
30	422.92	423.36	423.72	422.49	422.79	422.79	421.58	422.14	422.76

QUADRANT = LEFT

ANGLE OF ATTACK (AOA) \ ANGLE OF SIDESLIP (AOS)	-20	-15	-10	-5	0	5	10	15	20
0	425.99	425.92	426.13	425.99	425.59	424.82	424.47	424.04	423.84
5	425.76	425.86	425.82	425.94	425.20	424.77	424.27	424.02	423.76
10	425.67	425.98	425.95	425.92	425.26	424.59	423.71	423.99	424.16
15	425.93	426.04	426.00	426.18	425.31	425.07	424.14	423.23	422.91
20	425.96	425.88	426.05	425.40	425.03	424.30	425.11	424.75	423.74
25	425.66	424.38	424.27	425.27	425.37	423.11	422.21	421.86	421.80
30	422.35	424.83	424.23	425.00	422.95	422.86	421.20	421.75	421.78

Total Temperature--Starboard Side

MN = 0.4

ALT = 36000

QUADRANT = TOP

ANGLE OF ATTACK (AOA) \ ANGLE OF SIDESLIP (AOS)	-20	-15	-10	-5	0	5	10	15	20
0	402.54	402.75	402.67	402.83	403.03	403.29	403.43	403.29	403.14
5	402.59	402.66	402.96	403.18	403.66	403.70	403.68	403.46	403.20
10	402.44	402.68	403.14	403.61	403.78	403.70	403.76	403.29	403.37
15	402.04	402.43	402.88	403.63	404.00	403.95	403.97	404.04	402.14
20	401.86	401.99	402.73	402.73	403.65	403.34	402.15	401.88	403.56
25	401.94	402.13	401.64	403.14	403.22	403.49	403.40	403.24	402.75
30	401.75	400.02	402.04	401.99	402.64	402.47	402.48	402.40	402.37

QUADRANT = RIGHT

ANGLE OF ATTACK (AOA) \ ANGLE OF SIDESLIP (AOS)	-20	-15	-10	-5	0	5	10	15	20
0	401.90	402.19	402.09	402.71	403.33	403.73	403.77	403.57	403.32
5	401.89	402.06	402.59	403.00	403.28	403.65	403.90	403.46	403.06
10	401.84	402.28	402.49	402.82	403.33	403.98	403.93	403.19	403.32
15	401.72	402.18	402.27	403.07	403.31	404.45	404.15	403.65	403.22
20	401.45	402.38	401.78	401.86	403.10	402.75	402.21	401.91	401.72
25	400.96	401.28	401.39	400.75	401.67	400.45	399.85	399.56	400.04
30	401.41	400.86	401.43	400.82	400.27	400.81	399.48	400.21	400.33

QUADRANT = BOTTOM

ANGLE OF ATTACK (AOA) \ ANGLE OF SIDESLIP (AOS)	-20	-15	-10	-5	0	5	10	15	20
0	403.23	403.43	403.61	403.79	403.58	403.52	402.99	402.74	402.51
5	403.02	403.48	403.50	403.62	403.27	403.15	402.66	402.44	402.25
10	403.20	403.50	403.39	403.45	403.28	403.02	402.46	402.14	402.15
15	403.40	403.45	403.29	403.94	403.63	402.31	401.63	401.23	402.17
20	403.65	403.73	402.56	401.66	401.86	401.88	402.47	401.90	400.29
25	403.26	401.54	401.44	401.34	400.51	400.18	399.71	399.46	400.25
30	401.02	401.43	401.77	400.61	400.89	400.89	399.75	400.28	400.87

QUADRANT = LEFT

ANGLE OF ATTACK (AOA) \ ANGLE OF SIDESLIP (AOS)	-20	-15	-10	-5	0	5	10	15	20
0	403.92	403.85	404.06	403.92	403.54	402.81	402.48	402.07	401.88
5	403.70	403.79	403.76	403.88	403.17	402.76	402.29	402.05	401.81
10	403.61	403.91	403.88	403.86	403.23	402.59	401.75	402.02	402.19
15	403.87	403.97	403.93	404.10	403.27	403.05	402.16	401.31	401.00
20	403.89	403.81	403.98	403.36	403.02	402.33	403.09	402.76	401.80
25	403.62	402.39	402.29	403.25	403.34	401.19	400.34	400.01	399.96
30	400.47	402.82	402.26	402.99	401.05	400.96	399.39	399.91	399.94

Total Temperature--Starboard Side

MN = 0.6

ALT = 0

QUADRANT = TOP

ANGLE OF ATTACK (AOA)	ANGLE OF SIDESLIP (AOS)								
	-20	-15	-10	-5	0	5	10	15	20
0	555.31	556.15	556.60	557.16	557.95	557.72	557.79	557.49	557.19
5	556.03	555.89	556.84	558.61	558.64	558.05	557.88	557.22	556.90
10	555.31	555.82	557.26	558.53	558.99	558.14	558.30	557.06	556.53
15	553.92	554.93	556.94	557.58	559.55	556.15	557.05	555.05	554.10
20	553.41	554.52	554.94	557.31	558.61	558.45	557.30	556.20	556.61
25	549.75	553.87	552.25	554.81	555.85	555.55	554.52	554.87	553.08
30	553.26	550.08	553.74	552.40	553.88	548.50	552.92	555.39	553.18

QUADRANT = RIGHT

ANGLE OF ATTACK (AOA)	ANGLE OF SIDESLIP (AOS)								
	-20	-15	-10	-5	0	5	10	15	20
0	552.59	554.94	555.53	557.31	557.80	558.94	558.10	558.15	557.96
5	553.62	555.18	556.86	557.43	557.91	558.83	559.21	558.65	556.88
10	553.53	555.27	556.64	556.65	558.29	558.20	557.99	557.38	556.63
15	553.58	554.19	555.10	554.22	556.80	556.71	556.92	557.64	556.39
20	551.39	552.82	552.13	553.78	556.71	554.90	554.83	552.75	549.59
25	548.47	551.91	550.75	547.54	547.84	544.84	548.74	544.81	544.91
30	549.87	552.24	551.83	547.63	547.11	548.36	541.93	543.02	542.43

QUADRANT = BOTTOM

ANGLE OF ATTACK (AOA)	ANGLE OF SIDESLIP (AOS)								
	-20	-15	-10	-5	0	5	10	15	20
0	556.31	557.08	557.88	558.60	558.32	558.35	557.75	557.48	556.97
5	556.52	557.19	558.31	558.25	557.95	557.66	556.92	556.67	556.28
10	556.74	557.87	557.96	558.24	557.83	557.64	556.65	556.49	556.52
15	557.60	558.09	558.01	556.41	553.94	550.96	551.76	553.54	553.23
20	555.57	555.53	553.21	553.07	551.33	553.21	553.74	547.66	548.18
25	554.16	553.99	552.03	546.50	549.35	547.73	549.71	546.61	548.15
30	546.26	551.76	552.91	545.60	549.22	550.03	546.83	546.60	543.49

QUADRANT = LEFT

ANGLE OF ATTACK (AOA)	ANGLE OF SIDESLIP (AOS)								
	-20	-15	-10	-5	0	5	10	15	20
0	558.22	559.28	559.33	559.17	558.58	557.18	556.57	555.28	554.47
5	559.07	558.38	559.42	558.88	558.11	556.78	555.66	554.44	554.39
10	559.07	559.43	559.86	559.64	557.74	557.22	555.97	555.45	554.62
15	557.77	559.42	559.46	559.04	554.76	551.85	551.26	552.10	553.22
20	557.35	556.48	558.23	558.84	557.69	557.05	556.10	553.97	552.07
25	558.77	554.83	554.64	555.44	549.87	547.33	548.30	547.22	546.40
30	551.40	554.23	556.94	553.98	547.56	548.13	542.67	543.61	542.57

Total Temperature--Starboard Side

MN = 0.6

ALT = 10000

QUADRANT = TOP

ANGLE OF ATTACK (AOA) \ ANGLE OF SIDESLIP (AOS)	-20	-15	-10	-5	0	5	10	15	20
0	517.12	517.91	518.33	518.84	519.58	519.37	519.43	519.15	518.88
5	517.80	517.66	518.55	520.20	520.22	519.67	519.52	518.90	518.60
10	517.13	517.60	518.94	520.12	520.55	519.76	519.91	518.75	518.26
15	515.83	516.77	518.64	519.24	521.08	517.91	518.75	516.88	515.98
20	515.36	516.39	516.79	518.98	520.18	520.03	518.96	517.93	518.31
25	511.93	515.79	514.27	516.63	517.60	517.33	516.37	516.70	515.03
30	515.19	512.22	515.65	514.39	515.77	510.76	514.88	517.18	515.13

QUADRANT = RIGHT

ANGLE OF ATTACK (AOA) \ ANGLE OF SIDESLIP (AOS)	-20	-15	-10	-5	0	5	10	15	20
0	514.60	516.79	517.33	518.99	519.44	520.51	519.72	519.77	519.59
5	515.55	517.00	518.57	519.10	519.55	520.40	520.76	520.23	518.59
10	515.47	517.09	518.36	518.37	519.90	519.81	519.62	519.05	518.35
15	515.51	516.08	516.93	516.11	518.51	518.43	518.63	519.29	518.12
20	513.47	514.80	514.17	515.69	518.41	516.72	516.66	514.72	511.77
25	510.73	513.95	512.87	509.86	510.15	507.35	510.98	507.33	507.42
30	512.03	514.24	513.87	509.95	509.46	510.62	504.63	505.66	505.10

QUADRANT = BOTTOM

ANGLE OF ATTACK (AOA) \ ANGLE OF SIDESLIP (AOS)	-20	-15	-10	-5	0	5	10	15	20
0	518.06	518.77	519.52	520.19	519.93	519.95	519.40	519.15	518.67
5	518.25	518.87	519.92	519.87	519.58	519.31	518.63	518.40	518.03
10	518.46	519.51	519.59	519.86	519.47	519.29	518.38	518.23	518.25
15	519.26	519.71	519.63	518.15	515.84	513.07	513.82	515.47	515.17
20	517.36	517.33	515.17	515.02	513.39	515.15	515.64	509.98	510.45
25	516.04	515.90	514.05	508.90	511.55	510.04	511.89	509.00	510.43
30	508.67	513.80	514.87	508.05	511.42	512.18	509.20	508.99	506.09

QUADRANT = LEFT

ANGLE OF ATTACK (AOA) \ ANGLE OF SIDESLIP (AOS)	-20	-15	-10	-5	0	5	10	15	20
0	519.83	520.82	520.87	520.72	520.17	518.86	518.30	517.10	516.34
5	520.62	519.98	520.95	520.45	519.73	518.49	517.45	516.32	516.27
10	520.62	520.96	521.36	521.15	519.39	518.91	517.74	517.26	516.49
15	519.42	520.96	520.99	520.60	516.61	513.90	513.35	514.12	515.16
20	519.02	518.21	519.84	520.40	519.32	518.72	517.84	515.85	514.09
25	520.34	516.67	516.49	517.22	512.04	509.67	510.57	509.57	508.81
30	513.46	516.10	518.63	515.87	509.88	510.41	505.33	506.20	505.24

Total Temperature—Starboard Side

MN = 0.6

ALT = 20000

QUADRANT = TOP

ANGLE OF ATTACK (AOA) \ ANGLE OF SIDESLIP (AOS)	-20	-15	-10	-5	0	5	10	15	20
0	478.98	479.71	480.10	480.57	481.26	481.06	481.12	480.86	480.60
5	479.60	479.48	480.30	481.83	481.85	481.34	481.20	480.62	480.35
10	478.98	479.42	480.66	481.76	482.16	481.42	481.56	480.49	480.03
15	477.78	478.66	480.39	480.94	482.64	479.71	480.49	478.75	477.92
20	477.35	478.30	478.67	480.70	481.81	481.67	480.68	479.72	480.08
25	474.17	477.75	476.34	478.52	479.42	479.16	478.28	478.58	477.04
30	477.19	474.44	477.62	476.45	477.73	473.09	476.90	479.03	477.13

QUADRANT = RIGHT

ANGLE OF ATTACK (AOA) \ ANGLE OF SIDESLIP (AOS)	-20	-15	-10	-5	0	5	10	15	20
0	476.64	478.67	479.17	480.71	481.13	482.11	481.39	481.43	481.27
5	477.53	478.87	480.32	480.81	481.23	482.02	482.35	481.86	480.34
10	477.45	478.95	480.13	480.13	481.55	481.47	481.29	480.77	480.12
15	477.49	478.02	478.80	478.04	480.27	480.19	480.37	480.99	479.90
20	475.60	476.83	476.24	477.66	480.17	478.61	478.55	476.75	474.02
25	473.05	476.04	475.04	472.25	472.51	469.92	473.29	469.90	469.99
30	474.26	476.31	475.96	472.33	471.88	472.96	467.41	468.36	467.84

QUADRANT = BOTTOM

ANGLE OF ATTACK (AOA) \ ANGLE OF SIDESLIP (AOS)	-20	-15	-10	-5	0	5	10	15	20
0	479.84	480.50	481.20	481.82	481.58	481.60	481.09	480.86	480.41
5	480.03	480.60	481.57	481.52	481.26	481.01	480.38	480.16	479.82
10	480.22	481.19	481.26	481.51	481.16	480.99	480.14	480.00	480.03
15	480.95	481.38	481.31	479.93	477.79	475.23	475.92	477.44	477.17
20	479.20	479.17	477.17	477.03	475.52	477.14	477.60	472.36	472.80
25	477.97	477.84	476.14	471.36	473.81	472.41	474.13	471.45	472.78
30	471.15	475.90	476.89	470.57	473.70	474.40	471.64	471.44	468.75

QUADRANT = LEFT

ANGLE OF ATTACK (AOA) \ ANGLE OF SIDESLIP (AOS)	-20	-15	-10	-5	0	5	10	15	20
0	481.49	482.41	482.45	482.31	481.80	480.59	480.07	478.96	478.26
5	482.22	481.63	482.52	482.06	481.40	480.25	479.29	478.23	478.19
10	482.22	482.54	482.90	482.71	481.08	480.63	479.55	479.11	478.39
15	481.10	482.53	482.56	482.20	478.50	475.99	475.49	476.19	477.16
20	480.73	479.98	481.49	482.01	481.01	480.45	479.64	477.80	476.16
25	481.95	478.56	478.39	479.07	474.27	472.08	472.91	471.98	471.27
30	475.58	478.03	480.37	477.81	472.27	472.76	468.05	468.86	467.97

Total Temperature--Starboard Side

MN = 0.6

ALT = 30000

QUADRANT = TOP

ANGLE OF ATTACK (AOA) \ ANGLE OF SIDESLIP (AOS)	-20	-15	-10	-5	0	5	10	15	20
0	440.86	441.53	441.89	442.32	442.95	442.77	442.83	442.59	442.35
5	441.43	441.32	442.07	443.48	443.50	443.03	442.90	442.37	442.12
10	440.86	441.27	442.40	443.42	443.78	443.11	443.24	442.25	441.83
15	439.75	440.56	442.15	442.66	444.23	441.53	442.25	440.65	439.89
20	439.35	440.23	440.57	442.45	443.47	443.35	442.43	441.56	441.88
25	436.44	439.72	438.43	440.45	441.28	441.04	440.22	440.51	439.08
30	439.23	436.69	439.61	438.54	439.72	435.45	438.95	440.91	439.16

QUADRANT = RIGHT

ANGLE OF ATTACK (AOA) \ ANGLE OF SIDESLIP (AOS)	-20	-15	-10	-5	0	5	10	15	20
0	438.70	440.57	441.03	442.45	442.84	443.74	443.07	443.11	442.96
5	439.52	440.75	442.09	442.54	442.92	443.65	443.96	443.51	442.11
10	439.45	440.83	441.91	441.92	443.22	443.15	442.99	442.50	441.91
15	439.48	439.97	440.69	439.99	442.04	441.97	442.14	442.71	441.71
20	437.75	438.88	438.33	439.64	441.96	440.53	440.47	438.82	436.31
25	435.42	438.16	437.24	434.68	434.92	432.53	435.64	432.52	432.60
30	436.53	438.41	438.09	434.75	434.34	435.33	430.22	431.09	430.62

QUADRANT = BOTTOM

ANGLE OF ATTACK (AOA) \ ANGLE OF SIDESLIP (AOS)	-20	-15	-10	-5	0	5	10	15	20
0	441.65	442.26	442.90	443.47	443.25	443.27	442.80	442.58	442.17
5	441.82	442.35	443.24	443.20	442.96	442.72	442.14	441.94	441.63
10	442.00	442.89	442.96	443.19	442.86	442.71	441.93	441.80	441.82
15	442.68	443.06	443.00	441.73	439.77	437.41	438.04	439.45	439.20
20	441.06	441.03	439.19	439.07	437.69	439.18	439.60	434.78	435.19
25	439.94	439.81	438.25	433.86	436.12	434.83	436.41	433.95	435.16
30	433.66	438.03	438.95	433.14	436.01	436.66	434.12	433.94	431.46

QUADRANT = LEFT

ANGLE OF ATTACK (AOA) \ ANGLE OF SIDESLIP (AOS)	-20	-15	-10	-5	0	5	10	15	20
0	443.17	444.01	444.05	443.92	443.46	442.34	441.86	440.83	440.19
5	443.84	443.30	444.12	443.70	443.08	442.02	441.14	440.17	440.13
10	443.84	444.13	444.47	444.29	442.79	442.38	441.38	440.97	440.32
15	442.81	444.12	444.15	443.82	440.42	438.11	437.65	438.30	439.19
20	442.47	441.78	443.17	443.66	442.74	442.23	441.48	439.79	438.28
25	443.60	440.48	440.32	440.95	436.54	434.52	435.28	434.43	433.78
30	437.74	439.99	442.15	439.79	434.69	435.14	430.81	431.56	430.74

Total Temperature--Starboard Side

MN = 0.6

ALT = 36000

QUADRANT = TOP

ANGLE OF ATTACK (AOA) \ ANGLE OF SIDESLIP (AOS)	-20	-15	-10	-5	0	5	10	15	20
0	418.01	418.64	418.98	419.40	420.00	419.83	419.87	419.65	419.43
5	418.55	418.44	419.16	420.50	420.51	420.07	419.94	419.45	419.20
10	418.01	418.39	419.47	420.43	420.78	420.14	420.26	419.32	418.93
15	416.96	417.72	419.23	419.72	421.20	418.64	419.32	417.82	417.10
20	416.58	417.41	417.73	419.52	420.50	420.38	419.51	418.69	419.00
25	413.83	416.93	415.71	417.64	418.42	418.20	417.42	417.69	416.34
30	416.48	414.08	416.84	415.83	416.94	412.90	416.22	418.07	416.41

QUADRANT = RIGHT

ANGLE OF ATTACK (AOA) \ ANGLE OF SIDESLIP (AOS)	-20	-15	-10	-5	0	5	10	15	20
0	415.96	417.73	418.17	419.51	419.88	420.74	420.11	420.15	420.01
5	416.74	417.91	419.18	419.60	419.97	420.66	420.95	420.52	419.20
10	416.67	417.98	419.01	419.01	420.25	420.18	420.03	419.57	419.01
15	416.70	417.17	417.85	417.19	419.13	419.06	419.23	419.77	418.83
20	415.06	416.13	415.61	416.86	419.07	417.71	417.66	416.09	413.71
25	412.87	415.45	414.58	412.17	412.40	410.13	413.08	410.12	410.19
30	413.92	415.71	415.40	412.24	411.85	412.79	407.94	408.77	408.32

QUADRANT = BOTTOM

ANGLE OF ATTACK (AOA) \ ANGLE OF SIDESLIP (AOS)	-20	-15	-10	-5	0	5	10	15	20
0	418.76	419.34	419.95	420.49	420.27	420.29	419.85	419.64	419.26
5	418.92	419.42	420.27	420.23	420.00	419.78	419.22	419.03	418.74
10	419.09	419.94	420.00	420.22	419.90	419.76	419.02	418.90	418.92
15	419.73	420.10	420.04	418.84	416.98	414.74	415.34	416.68	416.45
20	418.21	418.18	416.43	416.33	415.02	416.44	416.84	412.26	412.65
25	417.15	417.02	415.55	411.39	413.54	412.31	413.81	411.47	412.63
30	411.21	415.35	416.21	410.71	413.43	414.05	411.64	411.46	409.12

QUADRANT = LEFT

ANGLE OF ATTACK (AOA) \ ANGLE OF SIDESLIP (AOS)	-20	-15	-10	-5	0	5	10	15	20
0	420.20	421.00	421.04	420.92	420.47	419.41	418.95	417.98	417.37
5	420.84	420.32	421.10	420.70	420.12	419.11	418.27	417.35	417.32
10	420.84	421.11	421.43	421.27	419.84	419.45	418.50	418.12	417.49
15	419.86	421.11	421.13	420.82	417.59	415.41	414.96	415.60	416.44
20	419.54	418.89	420.21	420.67	419.81	419.32	418.61	417.01	415.58
25	420.62	417.65	417.51	418.11	413.93	412.01	412.74	411.93	411.31
30	415.07	417.20	419.25	417.01	412.18	412.61	408.50	409.21	408.43

Total Pressure--Starboard Side

MN = 0.2

ALT = 0

QUADRANT = TOP

ANGLE OF ATTACK (AOA)	ANGLE OF SIDESLIP (AOS)								
	-20	-15	-10	-5	0	5	10	15	20
0	14.95	14.97	14.99	15.00	15.01	15.02	15.02	15.02	15.01
5	14.95	14.97	14.99	15.01	15.02	15.03	15.03	15.03	15.02
10	14.94	14.97	14.99	15.01	15.03	15.03	15.03	15.03	15.02
15	14.93	14.95	14.98	15.01	15.03	15.03	15.02	15.01	14.99
20	14.90	14.93	14.96	14.98	14.95	14.88	14.78	14.70	14.69
25	14.87	14.87	14.92	14.82	14.72	14.67	14.71	14.76	14.78
30	14.65	14.82	14.82	14.73	14.71	14.84	14.87	14.88	14.90

QUADRANT = RIGHT

ANGLE OF ATTACK (AOA)	ANGLE OF SIDESLIP (AOS)								
	-20	-15	-10	-5	0	5	10	15	20
0	14.89	14.92	14.96	14.98	15.01	15.01	15.02	15.03	15.03
5	14.91	14.94	14.97	14.99	15.00	15.01	15.02	15.02	15.02
10	14.90	14.94	14.97	14.98	15.00	15.01	15.01	15.00	15.00
15	14.90	14.92	14.94	14.96	14.99	15.00	14.99	14.96	14.94
20	14.87	14.89	14.91	14.94	14.94	14.89	14.79	14.75	14.71
25	14.80	14.83	14.85	14.78	14.67	14.62	14.62	14.63	14.65
30	14.63	14.72	14.71	14.62	14.58	14.55	14.56	14.59	14.62

QUADRANT = BOTTOM

ANGLE OF ATTACK (AOA)	ANGLE OF SIDESLIP (AOS)								
	-20	-15	-10	-5	0	5	10	15	20
0	14.96	14.98	15.00	15.01	15.01	15.00	14.99	14.99	14.98
5	14.96	14.99	15.00	15.00	15.00	14.98	14.97	14.95	14.93
10	14.96	14.98	14.99	14.99	14.97	14.94	14.92	14.89	14.86
15	14.94	14.96	14.97	14.98	14.95	14.91	14.86	14.82	14.78
20	14.92	14.95	14.94	14.93	14.85	14.78	14.70	14.65	14.61
25	14.90	14.89	14.85	14.71	14.61	14.55	14.49	14.46	14.41
30	14.71	14.76	14.69	14.58	14.48	14.46	14.43	14.43	14.39

QUADRANT = LEFT

ANGLE OF ATTACK (AOA)	ANGLE OF SIDESLIP (AOS)								
	-20	-15	-10	-5	0	5	10	15	20
0	14.99	15.00	15.01	15.01	15.02	15.00	14.97	14.93	14.88
5	14.98	15.00	15.01	15.01	15.01	14.99	14.96	14.92	14.87
10	14.97	14.99	15.01	15.01	15.00	14.97	14.94	14.89	14.83
15	14.96	14.98	15.00	15.00	14.98	14.94	14.89	14.82	14.76
20	14.94	14.97	14.96	14.94	14.80	14.74	14.69	14.68	14.70
25	14.93	14.92	14.88	14.73	14.73	14.74	14.72	14.67	14.63
30	14.78	14.86	14.78	14.78	14.77	14.68	14.64	14.61	14.59

Total Pressure--Starboard Side

MN = 0.2

ALT = 10000

QUADRANT = TOP

ANGLE OF ATTACK (AOA)	ANGLE OF SIDESLIP (AOS)								
	-20	-15	-10	-5	0	5	10	15	20
0	10.28	10.29	10.31	10.32	10.33	10.33	10.33	10.33	10.33
5	10.28	10.30	10.31	10.32	10.33	10.34	10.33	10.33	10.33
10	10.28	10.29	10.31	10.32	10.33	10.34	10.34	10.33	10.33
15	10.27	10.28	10.30	10.32	10.33	10.34	10.33	10.32	10.31
20	10.25	10.27	10.29	10.30	10.28	10.23	10.17	10.11	10.10
25	10.22	10.23	10.26	10.19	10.13	10.09	10.12	10.15	10.16
30	10.07	10.20	10.19	10.13	10.12	10.21	10.23	10.24	10.25

QUADRANT = RIGHT

ANGLE OF ATTACK (AOA)	ANGLE OF SIDESLIP (AOS)								
	-20	-15	-10	-5	0	5	10	15	20
0	10.24	10.26	10.29	10.30	10.32	10.33	10.33	10.34	10.34
5	10.25	10.28	10.29	10.31	10.32	10.33	10.33	10.33	10.33
10	10.25	10.28	10.29	10.30	10.31	10.32	10.32	10.32	10.31
15	10.24	10.26	10.28	10.29	10.31	10.32	10.31	10.29	10.28
20	10.23	10.24	10.25	10.28	10.28	10.24	10.17	10.14	10.12
25	10.18	10.20	10.21	10.17	10.09	10.05	10.06	10.06	10.08
30	10.06	10.12	10.12	10.06	10.03	10.01	10.02	10.03	10.05

QUADRANT = BOTTOM

ANGLE OF ATTACK (AOA)	ANGLE OF SIDESLIP (AOS)								
	-20	-15	-10	-5	0	5	10	15	20
0	10.29	10.31	10.32	10.32	10.32	10.32	10.31	10.31	10.30
5	10.29	10.31	10.32	10.32	10.31	10.30	10.29	10.28	10.27
10	10.29	10.30	10.31	10.31	10.30	10.28	10.26	10.24	10.22
15	10.28	10.29	10.30	10.30	10.28	10.25	10.22	10.19	10.17
20	10.26	10.28	10.28	10.27	10.21	10.16	10.11	10.08	10.05
25	10.24	10.24	10.21	10.11	10.05	10.00	9.96	9.95	9.91
30	10.11	10.15	10.10	10.03	9.96	9.94	9.93	9.92	9.90

QUADRANT = LEFT

ANGLE OF ATTACK (AOA)	ANGLE OF SIDESLIP (AOS)								
	-20	-15	-10	-5	0	5	10	15	20
0	10.31	10.32	10.33	10.33	10.33	10.31	10.30	10.27	10.24
5	10.30	10.32	10.32	10.33	10.32	10.31	10.29	10.26	10.22
10	10.30	10.31	10.32	10.32	10.32	10.30	10.27	10.24	10.20
15	10.29	10.30	10.32	10.32	10.31	10.27	10.24	10.19	10.15
20	10.28	10.30	10.29	10.28	10.18	10.14	10.10	10.10	10.11
25	10.27	10.26	10.23	10.13	10.13	10.14	10.12	10.09	10.06
30	10.16	10.22	10.17	10.16	10.16	10.10	10.07	10.05	10.03

Total Pressure--Starboard Side

MN = 0.2

ALT = 20000

QUADRANT = TOP

ANGLE OF ATTACK (AOA) \ ANGLE OF SIDESLIP (AOS)	-20	-15	-10	-5	0	5	10	15	20
0	6.87	6.88	6.89	6.90	6.90	6.91	6.91	6.91	6.90
5	6.88	6.89	6.89	6.90	6.91	6.91	6.91	6.91	6.91
10	6.87	6.88	6.89	6.90	6.91	6.91	6.91	6.91	6.91
15	6.87	6.87	6.89	6.90	6.91	6.91	6.91	6.90	6.89
20	6.85	6.86	6.88	6.89	6.87	6.84	6.80	6.76	6.76
25	6.84	6.84	6.86	6.82	6.77	6.75	6.76	6.79	6.80
30	6.74	6.82	6.82	6.78	6.76	6.83	6.84	6.84	6.85

QUADRANT = RIGHT

ANGLE OF ATTACK (AOA) \ ANGLE OF SIDESLIP (AOS)	-20	-15	-10	-5	0	5	10	15	20
0	6.85	6.86	6.88	6.89	6.90	6.90	6.91	6.91	6.91
5	6.86	6.87	6.88	6.89	6.90	6.90	6.91	6.91	6.91
10	6.85	6.87	6.88	6.89	6.90	6.90	6.90	6.90	6.90
15	6.85	6.86	6.87	6.88	6.89	6.90	6.89	6.88	6.87
20	6.84	6.85	6.85	6.87	6.87	6.85	6.80	6.78	6.76
25	6.81	6.82	6.83	6.80	6.74	6.72	6.72	6.73	6.74
30	6.73	6.77	6.77	6.73	6.70	6.69	6.70	6.71	6.72

QUADRANT = BOTTOM

ANGLE OF ATTACK (AOA) \ ANGLE OF SIDESLIP (AOS)	-20	-15	-10	-5	0	5	10	15	20
0	6.88	6.89	6.90	6.90	6.90	6.90	6.90	6.89	6.89
5	6.88	6.89	6.90	6.90	6.90	6.89	6.88	6.87	6.87
10	6.88	6.89	6.89	6.89	6.88	6.87	6.86	6.85	6.83
15	6.87	6.88	6.89	6.89	6.88	6.86	6.83	6.81	6.80
20	6.86	6.87	6.87	6.87	6.83	6.80	6.76	6.74	6.72
25	6.85	6.85	6.83	6.76	6.72	6.69	6.66	6.65	6.63
30	6.76	6.79	6.75	6.71	6.66	6.65	6.64	6.64	6.62

QUADRANT = LEFT

ANGLE OF ATTACK (AOA) \ ANGLE OF SIDESLIP (AOS)	-20	-15	-10	-5	0	5	10	15	20
0	6.89	6.90	6.90	6.90	6.91	6.90	6.89	6.87	6.84
5	6.89	6.90	6.90	6.90	6.90	6.89	6.88	6.86	6.84
10	6.88	6.90	6.90	6.90	6.90	6.89	6.87	6.85	6.82
15	6.88	6.89	6.90	6.90	6.89	6.87	6.85	6.82	6.79
20	6.87	6.89	6.88	6.87	6.81	6.78	6.76	6.75	6.76
25	6.87	6.86	6.84	6.77	6.77	6.78	6.77	6.75	6.73
30	6.79	6.83	6.80	6.79	6.79	6.75	6.73	6.72	6.71

Total Pressure--Starboard Side

MN = 0.2

ALT = 30000

QUADRANT = TOP

ANGLE OF ATTACK (AOA) \ ANGLE OF SIDESLIP (AOS)	-20	-15	-10	-5	0	5	10	15	20
0	4.45	4.45	4.46	4.46	4.47	4.47	4.47	4.47	4.47
5	4.45	4.45	4.46	4.47	4.47	4.47	4.47	4.47	4.47
10	4.45	4.45	4.46	4.47	4.47	4.47	4.47	4.47	4.47
15	4.44	4.45	4.46	4.46	4.47	4.47	4.47	4.46	4.46
20	4.43	4.44	4.45	4.46	4.45	4.43	4.40	4.37	4.37
25	4.42	4.43	4.44	4.41	4.38	4.36	4.38	4.39	4.40
30	4.36	4.41	4.41	4.38	4.38	4.42	4.42	4.43	4.43

QUADRANT = RIGHT

ANGLE OF ATTACK (AOA) \ ANGLE OF SIDESLIP (AOS)	-20	-15	-10	-5	0	5	10	15	20
0	4.43	4.44	4.45	4.46	4.46	4.47	4.47	4.47	4.47
5	4.44	4.45	4.45	4.46	4.46	4.47	4.47	4.47	4.47
10	4.43	4.44	4.45	4.46	4.46	4.46	4.46	4.46	4.46
15	4.43	4.44	4.45	4.45	4.46	4.46	4.46	4.45	4.45
20	4.42	4.43	4.43	4.45	4.45	4.43	4.40	4.39	4.38
25	4.40	4.41	4.42	4.40	4.36	4.35	4.35	4.35	4.36
30	4.35	4.38	4.38	4.35	4.34	4.33	4.33	4.34	4.35

QUADRANT = BOTTOM

ANGLE OF ATTACK (AOA) \ ANGLE OF SIDESLIP (AOS)	-20	-15	-10	-5	0	5	10	15	20
0	4.45	4.46	4.46	4.47	4.47	4.46	4.46	4.46	4.45
5	4.45	4.46	4.46	4.46	4.46	4.46	4.45	4.45	4.44
10	4.45	4.46	4.46	4.46	4.45	4.45	4.44	4.43	4.42
15	4.45	4.45	4.45	4.46	4.45	4.44	4.42	4.41	4.40
20	4.44	4.45	4.44	4.44	4.42	4.40	4.37	4.36	4.35
25	4.43	4.43	4.42	4.37	4.35	4.33	4.31	4.30	4.29
30	4.38	4.39	4.37	4.34	4.31	4.30	4.29	4.29	4.28

QUADRANT = LEFT

ANGLE OF ATTACK (AOA) \ ANGLE OF SIDESLIP (AOS)	-20	-15	-10	-5	0	5	10	15	20
0	4.46	4.46	4.47	4.47	4.47	4.46	4.45	4.44	4.43
5	4.46	4.46	4.46	4.47	4.47	4.46	4.45	4.44	4.42
10	4.45	4.46	4.46	4.46	4.46	4.45	4.44	4.43	4.41
15	4.45	4.46	4.46	4.46	4.46	4.44	4.43	4.41	4.39
20	4.45	4.45	4.45	4.45	4.40	4.38	4.37	4.37	4.37
25	4.44	4.44	4.43	4.38	4.38	4.38	4.38	4.36	4.35
30	4.40	4.42	4.40	4.40	4.39	4.37	4.35	4.35	4.34

Total Pressure--Starboard Side

MN = 0.2

ALT = 36000

QUADRANT = TOP

ANGLE OF ATTACK (AOA) \ ANGLE OF SIDESLIP (AOS)	-20	-15	-10	-5	0	5	10	15	20
0	3.36	3.37	3.37	3.37	3.38	3.38	3.38	3.38	3.38
5	3.36	3.37	3.37	3.38	3.38	3.38	3.38	3.38	3.38
10	3.36	3.37	3.37	3.38	3.38	3.38	3.38	3.38	3.38
15	3.36	3.36	3.37	3.38	3.38	3.38	3.38	3.38	3.37
20	3.35	3.36	3.36	3.37	3.36	3.35	3.33	3.31	3.30
25	3.34	3.35	3.36	3.33	3.31	3.30	3.31	3.32	3.32
30	3.30	3.33	3.33	3.31	3.31	3.34	3.35	3.35	3.35

QUADRANT = RIGHT

ANGLE OF ATTACK (AOA) \ ANGLE OF SIDESLIP (AOS)	-20	-15	-10	-5	0	5	10	15	20
0	3.35	3.36	3.36	3.37	3.38	3.38	3.38	3.38	3.38
5	3.35	3.36	3.37	3.37	3.38	3.38	3.38	3.38	3.38
10	3.35	3.36	3.37	3.37	3.37	3.38	3.38	3.37	3.37
15	3.35	3.36	3.36	3.37	3.37	3.37	3.37	3.37	3.36
20	3.34	3.35	3.35	3.36	3.36	3.35	3.33	3.32	3.31
25	3.33	3.34	3.34	3.33	3.30	3.29	3.29	3.29	3.30
30	3.29	3.31	3.31	3.29	3.28	3.27	3.28	3.28	3.29

QUADRANT = BOTTOM

ANGLE OF ATTACK (AOA) \ ANGLE OF SIDESLIP (AOS)	-20	-15	-10	-5	0	5	10	15	20
0	3.37	3.37	3.37	3.38	3.38	3.37	3.37	3.37	3.37
5	3.37	3.37	3.37	3.37	3.37	3.37	3.37	3.36	3.36
10	3.36	3.37	3.37	3.37	3.37	3.36	3.36	3.35	3.34
15	3.36	3.37	3.37	3.37	3.36	3.35	3.34	3.33	3.33
20	3.36	3.36	3.36	3.36	3.34	3.32	3.31	3.30	3.29
25	3.35	3.35	3.34	3.31	3.29	3.27	3.26	3.25	3.24
30	3.31	3.32	3.30	3.28	3.26	3.25	3.25	3.25	3.24

QUADRANT = LEFT

ANGLE OF ATTACK (AOA) \ ANGLE OF SIDESLIP (AOS)	-20	-15	-10	-5	0	5	10	15	20
0	3.37	3.37	3.38	3.38	3.38	3.37	3.37	3.36	3.35
5	3.37	3.37	3.38	3.38	3.38	3.37	3.37	3.36	3.34
10	3.37	3.37	3.38	3.38	3.37	3.37	3.36	3.35	3.34
15	3.37	3.37	3.37	3.37	3.37	3.36	3.35	3.33	3.32
20	3.36	3.37	3.37	3.36	3.33	3.32	3.31	3.30	3.31
25	3.36	3.36	3.35	3.31	3.31	3.32	3.31	3.30	3.29
30	3.32	3.34	3.33	3.32	3.32	3.30	3.29	3.29	3.28

Total Pressure--Starboard Side

MN = 0.4

ALT = 0

QUADRANT = TOP

ANGLE OF ATTACK (AOA)	ANGLE OF SIDESLIP (AOS)								
	-20	-15	-10	-5	0	5	10	15	20
0	15.86	15.95	16.01	16.06	16.09	16.11	16.12	16.11	16.08
5	15.89	15.96	16.03	16.09	16.13	16.13	16.13	16.13	16.09
10	15.86	15.93	16.03	16.09	16.12	16.13	16.12	16.12	16.12
15	15.78	15.86	15.94	16.12	16.12	16.09	16.10	15.98	15.20
20	15.52	15.64	15.87	15.76	15.38	14.99	14.68	14.70	15.10
25	15.24	15.57	15.47	15.02	14.63	15.06	15.20	15.28	15.36
30	14.12	14.60	15.31	14.76	15.52	15.42	15.26	15.59	15.55

QUADRANT = RIGHT

ANGLE OF ATTACK (AOA)	ANGLE OF SIDESLIP (AOS)								
	-20	-15	-10	-5	0	5	10	15	20
0	15.56	15.74	15.89	15.98	16.04	16.07	16.10	16.11	16.11
5	15.67	15.84	15.94	16.00	16.05	16.09	16.10	16.10	16.08
10	15.70	15.84	15.92	15.97	16.03	16.09	16.08	16.06	16.08
15	15.65	15.76	15.81	16.03	15.97	16.11	15.97	15.78	15.58
20	15.36	15.58	15.64	15.62	15.23	14.74	14.55	14.54	14.75
25	14.75	15.21	15.23	14.72	14.40	14.31	14.30	14.34	14.50
30	14.23	14.40	14.77	14.37	14.12	14.13	14.00	14.27	14.27

QUADRANT = BOTTOM

ANGLE OF ATTACK (AOA)	ANGLE OF SIDESLIP (AOS)								
	-20	-15	-10	-5	0	5	10	15	20
0	15.89	15.97	16.03	16.07	16.07	16.06	16.02	15.98	15.91
5	15.89	15.97	16.03	16.06	16.03	16.01	15.94	15.86	15.79
10	15.88	15.96	15.99	16.01	15.98	15.90	15.78	15.67	15.58
15	15.85	15.90	15.90	16.06	15.89	15.51	15.34	15.04	15.07
20	15.86	15.92	15.58	15.17	14.71	14.41	14.29	14.02	13.97
25	15.55	15.46	14.84	14.41	14.07	13.95	14.01	13.82	13.84
30	14.02	14.62	14.63	14.02	13.84	13.94	13.84	13.72	13.65

QUADRANT = LEFT

ANGLE OF ATTACK (AOA)	ANGLE OF SIDESLIP (AOS)								
	-20	-15	-10	-5	0	5	10	15	20
0	16.00	16.04	16.07	16.08	16.09	16.03	15.97	15.81	15.58
5	15.96	16.03	16.06	16.08	16.09	16.01	15.91	15.74	15.51
10	15.94	16.01	16.06	16.09	16.05	15.98	15.82	15.65	15.35
15	15.90	15.98	16.00	16.05	15.96	15.59	15.38	14.93	14.61
20	15.88	15.89	15.62	15.13	14.79	14.70	14.83	14.92	14.67
25	15.78	15.67	15.08	14.92	15.06	14.79	14.52	14.35	14.33
30	14.27	15.19	15.11	15.33	14.80	14.46	14.17	14.29	14.12

Total Pressure--Starboard Side

MN = 0.4

ALT = 10000

QUADRANT = TOP

ANGLE OF ATTACK (AOA) \ ANGLE OF SIDESLIP (AOS)	-20	-15	-10	-5	0	5	10	15	20
0	10.91	10.97	11.01	11.04	11.07	11.08	11.09	11.08	11.06
5	10.93	10.98	11.03	11.06	11.09	11.09	11.09	11.09	11.07
10	10.91	10.96	11.02	11.07	11.09	11.09	11.09	11.08	11.09
15	10.85	10.91	10.96	11.09	11.09	11.06	11.07	10.99	10.45
20	10.67	10.76	10.92	10.84	10.57	10.31	10.10	10.11	10.38
25	10.48	10.71	10.64	10.33	10.06	10.36	10.46	10.51	10.56
30	9.71	10.04	10.53	10.15	10.68	10.61	10.50	10.72	10.70

QUADRANT = RIGHT

ANGLE OF ATTACK (AOA) \ ANGLE OF SIDESLIP (AOS)	-20	-15	-10	-5	0	5	10	15	20
0	10.70	10.83	10.93	10.99	11.03	11.05	11.07	11.08	11.08
5	10.77	10.89	10.96	11.00	11.04	11.06	11.07	11.07	11.06
10	10.80	10.90	10.95	10.99	11.02	11.06	11.06	11.05	11.06
15	10.76	10.84	10.87	11.02	10.98	11.08	10.98	10.85	10.72
20	10.56	10.72	10.75	10.74	10.48	10.14	10.01	10.00	10.14
25	10.14	10.46	10.48	10.12	9.90	9.84	9.83	9.86	9.97
30	9.78	9.90	10.16	9.89	9.71	9.71	9.63	9.82	9.81

QUADRANT = BOTTOM

ANGLE OF ATTACK (AOA) \ ANGLE OF SIDESLIP (AOS)	-20	-15	-10	-5	0	5	10	15	20
0	10.93	10.98	11.03	11.05	11.05	11.05	11.02	10.99	10.94
5	10.93	10.99	11.02	11.05	11.02	11.01	10.96	10.91	10.86
10	10.92	10.98	11.00	11.01	10.99	10.93	10.85	10.78	10.71
15	10.90	10.94	10.94	11.05	10.93	10.67	10.55	10.35	10.37
20	10.91	10.95	10.72	10.43	10.11	9.91	9.83	9.64	9.61
25	10.70	10.63	10.21	9.91	9.67	9.60	9.64	9.51	9.52
30	9.64	10.05	10.06	9.64	9.52	9.59	9.52	9.44	9.39

QUADRANT = LEFT

ANGLE OF ATTACK (AOA) \ ANGLE OF SIDESLIP (AOS)	-20	-15	-10	-5	0	5	10	15	20
0	11.00	11.03	11.05	11.06	11.06	11.02	10.98	10.87	10.72
5	10.98	11.02	11.05	11.06	11.06	11.01	10.94	10.83	10.67
10	10.96	11.01	11.04	11.06	11.04	10.99	10.88	10.76	10.55
15	10.93	10.99	11.00	11.03	10.98	10.72	10.58	10.27	10.05
20	10.92	10.93	10.74	10.41	10.17	10.11	10.20	10.26	10.09
25	10.85	10.78	10.37	10.26	10.36	10.17	9.98	9.87	9.85
30	9.81	10.44	10.39	10.54	10.18	9.95	9.75	9.83	9.71

Total Pressure--Starboard Side

MN = 0.4

ALT = 20000

QUADRANT = TOP

ANGLE OF ATTACK (AOA) \ ANGLE OF SIDESLIP (AOS)	-20	-15	-10	-5	0	5	10	15	20
0	7.29	7.33	7.36	7.38	7.40	7.41	7.41	7.41	7.39
5	7.31	7.34	7.37	7.40	7.42	7.42	7.42	7.42	7.40
10	7.29	7.33	7.37	7.40	7.41	7.42	7.41	7.41	7.41
15	7.26	7.29	7.33	7.41	7.41	7.40	7.40	7.35	6.99
20	7.14	7.19	7.30	7.25	7.07	6.89	6.75	6.76	6.94
25	7.01	7.16	7.11	6.91	6.73	6.92	6.99	7.03	7.06
30	6.49	6.71	7.04	6.79	7.14	7.09	7.02	7.17	7.15

QUADRANT = RIGHT

ANGLE OF ATTACK (AOA) \ ANGLE OF SIDESLIP (AOS)	-20	-15	-10	-5	0	5	10	15	20
0	7.15	7.24	7.31	7.35	7.38	7.39	7.40	7.41	7.41
5	7.20	7.28	7.33	7.36	7.38	7.40	7.40	7.40	7.40
10	7.22	7.29	7.32	7.35	7.37	7.40	7.39	7.39	7.39
15	7.20	7.25	7.27	7.37	7.34	7.41	7.34	7.25	7.17
20	7.06	7.17	7.19	7.18	7.00	6.78	6.69	6.69	6.78
25	6.78	7.00	7.00	6.77	6.62	6.58	6.57	6.60	6.67
30	6.54	6.62	6.79	6.61	6.49	6.50	6.44	6.56	6.56

QUADRANT = BOTTOM

ANGLE OF ATTACK (AOA) \ ANGLE OF SIDESLIP (AOS)	-20	-15	-10	-5	0	5	10	15	20
0	7.31	7.34	7.37	7.39	7.39	7.39	7.37	7.35	7.32
5	7.31	7.35	7.37	7.39	7.37	7.36	7.33	7.29	7.26
10	7.30	7.34	7.35	7.36	7.35	7.31	7.26	7.21	7.16
15	7.29	7.31	7.31	7.39	7.31	7.13	7.05	6.92	6.93
20	7.29	7.32	7.16	6.98	6.76	6.63	6.57	6.45	6.42
25	7.15	7.11	6.83	6.63	6.47	6.42	6.44	6.36	6.36
30	6.45	6.72	6.73	6.45	6.36	6.41	6.37	6.31	6.28

QUADRANT = LEFT

ANGLE OF ATTACK (AOA) \ ANGLE OF SIDESLIP (AOS)	-20	-15	-10	-5	0	5	10	15	20
0	7.36	7.38	7.39	7.39	7.40	7.37	7.34	7.27	7.17
5	7.34	7.37	7.39	7.39	7.40	7.36	7.32	7.24	7.13
10	7.33	7.36	7.38	7.40	7.38	7.35	7.28	7.19	7.06
15	7.31	7.35	7.36	7.38	7.34	7.17	7.07	6.87	6.72
20	7.30	7.31	7.18	6.96	6.80	6.76	6.82	6.86	6.75
25	7.26	7.21	6.94	6.86	6.93	6.80	6.68	6.60	6.59
30	6.56	6.98	6.95	7.05	6.81	6.65	6.52	6.57	6.49

Total Pressure--Starboard Side

MN = 0.4

ALT = 30000

QUADRANT = TOP

ANGLE OF ATTACK (AOA) \ ANGLE OF SIDESLIP (AOS)	-20	-15	-10	-5	0	5	10	15	20
0	4.72	4.74	4.76	4.78	4.79	4.79	4.80	4.79	4.78
5	4.73	4.75	4.77	4.79	4.80	4.80	4.80	4.80	4.79
10	4.72	4.74	4.77	4.79	4.80	4.80	4.80	4.79	4.80
15	4.69	4.72	4.74	4.80	4.80	4.79	4.79	4.75	4.52
20	4.62	4.65	4.72	4.69	4.57	4.46	4.37	4.37	4.49
25	4.53	4.63	4.60	4.47	4.35	4.48	4.52	4.55	4.57
30	4.20	4.34	4.56	4.39	4.62	4.59	4.54	4.64	4.63

QUADRANT = RIGHT

ANGLE OF ATTACK (AOA) \ ANGLE OF SIDESLIP (AOS)	-20	-15	-10	-5	0	5	10	15	20
0	4.63	4.68	4.73	4.75	4.77	4.78	4.79	4.79	4.79
5	4.66	4.71	4.74	4.76	4.78	4.79	4.79	4.79	4.78
10	4.67	4.71	4.74	4.75	4.77	4.79	4.78	4.78	4.78
15	4.66	4.69	4.70	4.77	4.75	4.79	4.75	4.69	4.64
20	4.57	4.64	4.65	4.65	4.53	4.38	4.33	4.33	4.39
25	4.39	4.53	4.53	4.38	4.28	4.26	4.25	4.27	4.31
30	4.23	4.28	4.39	4.28	4.20	4.20	4.17	4.25	4.24

QUADRANT = BOTTOM

ANGLE OF ATTACK (AOA) \ ANGLE OF SIDESLIP (AOS)	-20	-15	-10	-5	0	5	10	15	20
0	4.73	4.75	4.77	4.78	4.78	4.78	4.77	4.75	4.73
5	4.73	4.75	4.77	4.78	4.77	4.76	4.74	4.72	4.70
10	4.72	4.75	4.76	4.76	4.75	4.73	4.69	4.66	4.63
15	4.72	4.73	4.73	4.78	4.73	4.62	4.56	4.48	4.48
20	4.72	4.74	4.63	4.51	4.38	4.29	4.25	4.17	4.16
25	4.63	4.60	4.42	4.29	4.18	4.15	4.17	4.11	4.12
30	4.17	4.35	4.35	4.17	4.12	4.15	4.12	4.08	4.06

QUADRANT = LEFT

ANGLE OF ATTACK (AOA) \ ANGLE OF SIDESLIP (AOS)	-20	-15	-10	-5	0	5	10	15	20
0	4.76	4.77	4.78	4.78	4.79	4.77	4.75	4.70	4.64
5	4.75	4.77	4.78	4.78	4.79	4.76	4.73	4.68	4.61
10	4.74	4.76	4.78	4.79	4.78	4.75	4.71	4.65	4.57
15	4.73	4.75	4.76	4.77	4.75	4.64	4.58	4.44	4.35
20	4.72	4.73	4.65	4.50	4.40	4.37	4.41	4.44	4.36
25	4.69	4.66	4.49	4.44	4.48	4.40	4.32	4.27	4.26
30	4.24	4.52	4.50	4.56	4.40	4.30	4.22	4.25	4.20

Total Pressure--Starboard Side

MN = 0.4

ALT = 36000

QUADRANT = TOP

ANGLE OF ATTACK (AOA) \ ANGLE OF SIDESLIP (AOS)	-20	-15	-10	-5	0	5	10	15	20
0	3.57	3.59	3.60	3.61	3.62	3.62	3.63	3.62	3.62
5	3.58	3.59	3.61	3.62	3.63	3.63	3.63	3.63	3.62
10	3.57	3.58	3.61	3.62	3.63	3.63	3.63	3.63	3.63
15	3.55	3.57	3.59	3.63	3.63	3.62	3.62	3.59	3.42
20	3.49	3.52	3.57	3.55	3.46	3.37	3.30	3.31	3.40
25	3.43	3.50	3.48	3.38	3.29	3.39	3.42	3.44	3.46
30	3.18	3.28	3.44	3.32	3.49	3.47	3.43	3.51	3.50

QUADRANT = RIGHT

ANGLE OF ATTACK (AOA) \ ANGLE OF SIDESLIP (AOS)	-20	-15	-10	-5	0	5	10	15	20
0	3.50	3.54	3.57	3.59	3.61	3.62	3.62	3.62	3.62
5	3.52	3.56	3.59	3.60	3.61	3.62	3.62	3.62	3.62
10	3.53	3.56	3.58	3.59	3.61	3.62	3.62	3.61	3.62
15	3.52	3.55	3.56	3.61	3.59	3.62	3.59	3.55	3.51
20	3.45	3.51	3.52	3.51	3.43	3.32	3.27	3.27	3.32
25	3.32	3.42	3.43	3.31	3.24	3.22	3.22	3.23	3.26
30	3.20	3.24	3.32	3.23	3.18	3.18	3.15	3.21	3.21

QUADRANT = BOTTOM

ANGLE OF ATTACK (AOA) \ ANGLE OF SIDESLIP (AOS)	-20	-15	-10	-5	0	5	10	15	20
0	3.58	3.59	3.61	3.62	3.61	3.61	3.60	3.59	3.58
5	3.57	3.59	3.61	3.61	3.61	3.60	3.58	3.57	3.55
10	3.57	3.59	3.60	3.60	3.60	3.58	3.55	3.53	3.50
15	3.57	3.58	3.58	3.61	3.57	3.49	3.45	3.38	3.39
20	3.57	3.58	3.50	3.41	3.31	3.24	3.21	3.15	3.14
25	3.50	3.48	3.34	3.24	3.16	3.14	3.15	3.11	3.11
30	3.15	3.29	3.29	3.15	3.11	3.14	3.11	3.09	3.07

QUADRANT = LEFT

ANGLE OF ATTACK (AOA) \ ANGLE OF SIDESLIP (AOS)	-20	-15	-10	-5	0	5	10	15	20
0	3.60	3.61	3.62	3.62	3.62	3.60	3.59	3.56	3.51
5	3.59	3.60	3.61	3.62	3.62	3.60	3.58	3.54	3.49
10	3.59	3.60	3.61	3.62	3.61	3.59	3.56	3.52	3.45
15	3.58	3.59	3.60	3.61	3.59	3.51	3.46	3.36	3.29
20	3.57	3.58	3.51	3.40	3.33	3.31	3.34	3.36	3.30
25	3.55	3.52	3.39	3.36	3.39	3.33	3.27	3.23	3.22
30	3.21	3.42	3.40	3.45	3.33	3.25	3.19	3.21	3.18

Total Pressure--Starboard Side

MN = 0.6

ALT = 0

QUADRANT = TOP

ANGLE OF ATTACK (AOA)	ANGLE OF SIDESLIP (AOS) -20	-15	-10	-5	0	5	10	15	20
0	17.75	17.99	18.11	18.20	18.27	18.24	18.26	18.25	18.23
5	17.77	17.94	18.10	18.21	18.25	18.25	18.26	18.25	18.23
10	17.68	17.88	18.10	18.18	18.23	18.26	18.26	18.21	18.16
15	17.44	17.67	18.00	17.83	18.40	17.06	17.78	15.87	15.00
20	17.00	17.35	17.39	16.93	15.98	15.20	14.85	14.63	15.47
25	15.51	16.43	16.38	14.57	15.56	16.01	15.80	16.15	16.33
30	13.79	13.50	15.96	14.92	16.38	14.15	15.07	16.87	17.05

QUADRANT = RIGHT

ANGLE OF ATTACK (AOA)	ANGLE OF SIDESLIP (AOS) -20	-15	-10	-5	0	5	10	15	20
0	17.13	17.65	17.93	18.11	18.22	18.19	18.21	18.24	18.28
5	17.34	17.76	17.99	18.15	18.18	18.20	18.25	18.26	18.27
10	17.38	17.71	17.97	18.09	18.14	18.21	18.18	18.28	18.26
15	17.24	17.54	17.74	17.55	17.67	17.20	17.05	16.32	15.60
20	16.66	16.93	16.94	16.63	15.14	14.41	14.32	14.42	14.56
25	14.42	14.93	16.09	14.17	13.46	13.63	13.50	13.56	13.57
30	13.34	13.73	14.36	13.87	13.30	13.25	12.53	13.25	13.68

QUADRANT = BOTTOM

ANGLE OF ATTACK (AOA)	ANGLE OF SIDESLIP (AOS) -20	-15	-10	-5	0	5	10	15	20
0	17.68	17.89	18.06	18.15	18.18	18.18	18.15	18.16	18.13
5	17.70	17.91	18.07	18.14	18.18	18.16	18.12	18.08	18.02
10	17.67	17.90	18.01	18.15	18.13	18.12	17.91	17.93	17.71
15	17.66	17.80	17.85	17.10	16.52	15.43	15.29	14.75	14.23
20	17.28	17.34	16.42	14.99	14.07	13.90	13.52	13.49	13.37
25	16.17	16.50	14.76	13.44	13.17	12.97	13.12	12.67	12.68
30	12.54	13.90	14.66	13.07	12.98	13.26	12.79	12.32	12.05

QUADRANT = LEFT

ANGLE OF ATTACK (AOA)	ANGLE OF SIDESLIP (AOS) -20	-15	-10	-5	0	5	10	15	20
0	17.96	18.02	18.11	18.16	18.25	18.21	18.14	17.98	17.73
5	17.84	17.95	18.11	18.17	18.23	18.19	18.07	17.91	17.58
10	17.75	17.95	18.08	18.17	18.20	18.18	18.04	17.77	17.22
15	17.70	17.93	17.91	17.57	17.24	15.22	15.60	14.63	14.54
20	17.42	17.33	16.31	15.26	14.81	14.76	14.75	15.21	14.78
25	17.40	17.16	15.35	15.48	14.66	14.28	14.11	13.77	13.60
30	14.07	14.67	15.77	16.26	14.06	13.37	12.80	13.37	13.43

Total Pressure--Starboard Side

MN = 0.6

ALT = 10000

QUADRANT = TOP

ANGLE OF ATTACK (AOA) \ ANGLE OF SIDESLIP (AOS)	-20	-15	-10	-5	0	5	10	15	20
0	12.20	12.37	12.45	12.52	12.56	12.54	12.56	12.55	12.54
5	12.22	12.34	12.45	12.53	12.55	12.55	12.56	12.55	12.54
10	12.16	12.30	12.45	12.51	12.54	12.56	12.56	12.53	12.49
15	11.99	12.15	12.38	12.26	12.66	11.73	12.23	10.92	10.32
20	11.69	11.93	11.96	11.64	10.99	10.45	10.21	10.06	10.64
25	10.66	11.30	11.26	10.02	10.70	11.01	10.87	11.11	11.23
30	9.48	9.29	10.98	10.26	11.26	9.73	10.37	11.60	11.72

QUADRANT = RIGHT

ANGLE OF ATTACK (AOA) \ ANGLE OF SIDESLIP (AOS)	-20	-15	-10	-5	0	5	10	15	20
0	11.78	12.14	12.33	12.46	12.53	12.51	12.53	12.54	12.57
5	11.93	12.21	12.37	12.48	12.50	12.51	12.55	12.56	12.57
10	11.95	12.18	12.36	12.44	12.48	12.52	12.50	12.57	12.56
15	11.85	12.06	12.20	12.07	12.15	11.83	11.73	11.22	10.73
20	11.46	11.64	11.65	11.44	10.41	9.91	9.85	9.91	10.01
25	9.92	10.27	11.06	9.74	9.26	9.37	9.28	9.32	9.33
30	9.17	9.45	9.88	9.54	9.15	9.12	8.62	9.11	9.41

QUADRANT = BOTTOM

ANGLE OF ATTACK (AOA) \ ANGLE OF SIDESLIP (AOS)	-20	-15	-10	-5	0	5	10	15	20
0	12.16	12.31	12.42	12.48	12.51	12.50	12.48	12.49	12.47
5	12.18	12.32	12.42	12.48	12.50	12.49	12.46	12.43	12.39
10	12.15	12.31	12.39	12.48	12.47	12.46	12.32	12.33	12.18
15	12.14	12.24	12.27	11.76	11.36	10.61	10.52	10.15	9.79
20	11.89	11.93	11.30	10.31	9.67	9.56	9.30	9.27	9.20
25	11.12	11.34	10.15	9.24	9.06	8.92	9.02	8.72	8.72
30	8.62	9.56	10.08	8.99	8.93	9.12	8.79	8.47	8.29

QUADRANT = LEFT

ANGLE OF ATTACK (AOA) \ ANGLE OF SIDESLIP (AOS)	-20	-15	-10	-5	0	5	10	15	20
0	12.35	12.39	12.46	12.49	12.55	12.52	12.47	12.36	12.19
5	12.27	12.35	12.45	12.49	12.54	12.51	12.42	12.32	12.09
10	12.21	12.35	12.43	12.49	12.52	12.50	12.40	12.22	11.84
15	12.17	12.33	12.32	12.08	11.86	10.47	10.73	10.06	10.00
20	11.98	11.92	11.22	10.50	10.19	10.15	10.15	10.46	10.16
25	11.97	11.80	10.55	10.64	10.08	9.82	9.70	9.47	9.35
30	9.67	10.09	10.84	11.18	9.67	9.20	8.81	9.20	9.24

Total Pressure--Starboard Side

MN = 0.6

ALT = 20000

QUADRANT = TOP

ANGLE OF ATTACK (AOA) \ SIDE SLIP ANGLE (SSA)	-20	-15	-10	-5	0	5	10	15	20
0	8.16	8.27	8.33	8.37	8.40	8.39	8.40	8.39	8.38
5	8.17	8.25	8.32	8.38	8.39	8.39	8.40	8.39	8.38
10	8.13	8.22	8.32	8.36	8.38	8.40	8.40	8.37	8.35
15	8.02	8.12	8.28	8.20	8.46	7.85	8.18	7.30	6.90
20	7.82	7.98	8.00	7.78	7.35	6.99	6.83	6.73	7.12
25	7.13	7.55	7.53	6.70	7.16	7.36	7.27	7.43	7.51
30	6.34	6.21	7.34	6.86	7.53	6.51	6.93	7.76	7.84

QUADRANT = RIGHT

ANGLE OF ATTACK (AOA) \ SIDE SLIP ANGLE (SSA)	-20	-15	-10	-5	0	5	10	15	20
0	7.88	8.12	8.25	8.33	8.38	8.36	8.37	8.39	8.40
5	7.98	8.17	8.27	8.35	8.36	8.37	8.39	8.39	8.40
10	7.99	8.15	8.27	8.32	8.34	8.37	8.36	8.41	8.40
15	7.93	8.06	8.16	8.07	8.12	7.91	7.84	7.50	7.17
20	7.66	7.79	7.79	7.65	6.96	6.63	6.58	6.63	6.69
25	6.63	6.87	7.40	6.52	6.19	6.27	6.21	6.23	6.24
30	6.13	6.32	6.60	6.38	6.12	6.09	5.76	6.09	6.29

QUADRANT = BOTTOM

ANGLE OF ATTACK (AOA) \ SIDE SLIP ANGLE (SSA)	-20	-15	-10	-5	0	5	10	15	20
0	8.13	8.23	8.30	8.35	8.36	8.36	8.35	8.35	8.34
5	8.14	8.24	8.31	8.34	8.36	8.35	8.33	8.31	8.29
10	8.12	8.23	8.28	8.35	8.34	8.33	8.23	8.24	8.14
15	8.12	8.18	8.21	7.86	7.60	7.09	7.03	6.78	6.54
20	7.95	7.98	7.55	6.90	6.47	6.39	6.22	6.20	6.15
25	7.44	7.59	6.79	6.18	6.06	5.96	6.03	5.83	5.83
30	5.77	6.39	6.74	6.01	5.97	6.10	5.88	5.66	5.54

QUADRANT = LEFT

ANGLE OF ATTACK (AOA) \ SIDE SLIP ANGLE (SSA)	-20	-15	-10	-5	0	5	10	15	20
0	8.26	8.29	8.33	8.35	8.39	8.37	8.34	8.27	8.15
5	8.21	8.26	8.33	8.35	8.38	8.37	8.31	8.24	8.08
10	8.16	8.26	8.31	8.35	8.37	8.36	8.29	8.17	7.92
15	8.14	8.25	8.24	8.08	7.93	7.00	7.17	6.73	6.69
20	8.01	7.97	7.50	7.02	6.81	6.79	6.78	6.99	6.80
25	8.00	7.89	7.06	7.12	6.74	6.57	6.49	6.33	6.25
30	6.47	6.74	7.25	7.48	6.47	6.15	5.89	6.15	6.18

Total Pressure--Starboard Side

MN = 0.6

ALT = 30000

QUADRANT = TOP

ANGLE OF ATTACK (AOA) \ ANGLE OF SIDESLIP (AOS)	-20	-15	-10	-5	0	5	10	15	20
0	5.28	5.35	5.39	5.41	5.43	5.43	5.43	5.43	5.42
5	5.29	5.34	5.38	5.42	5.43	5.43	5.43	5.43	5.42
10	5.26	5.32	5.38	5.41	5.42	5.43	5.43	5.42	5.40
15	5.19	5.26	5.35	5.31	5.47	5.08	5.29	4.72	4.46
20	5.06	5.16	5.17	5.04	4.75	4.52	4.42	4.35	4.60
25	4.61	4.89	4.87	4.34	4.63	4.76	4.70	4.80	4.86
30	4.10	4.02	4.75	4.44	4.87	4.21	4.48	5.02	5.07

QUADRANT = RIGHT

ANGLE OF ATTACK (AOA) \ ANGLE OF SIDESLIP (AOS)	-20	-15	-10	-5	0	5	10	15	20
0	5.10	5.25	5.33	5.39	5.42	5.41	5.42	5.43	5.44
5	5.16	5.28	5.35	5.40	5.41	5.41	5.43	5.43	5.44
10	5.17	5.27	5.35	5.38	5.40	5.42	5.41	5.44	5.43
15	5.13	5.22	5.28	5.22	5.26	5.12	5.07	4.86	4.64
20	4.96	5.04	5.04	4.95	4.50	4.29	4.26	4.29	4.33
25	4.29	4.44	4.79	4.22	4.01	4.05	4.02	4.03	4.04
30	3.97	4.09	4.27	4.13	3.96	3.94	3.73	3.94	4.07

QUADRANT = BOTTOM

ANGLE OF ATTACK (AOA) \ ANGLE OF SIDESLIP (AOS)	-20	-15	-10	-5	0	5	10	15	20
0	5.26	5.32	5.37	5.40	5.41	5.41	5.40	5.40	5.39
5	5.27	5.33	5.37	5.40	5.41	5.40	5.39	5.38	5.36
10	5.26	5.32	5.36	5.40	5.39	5.39	5.33	5.33	5.27
15	5.25	5.30	5.31	5.09	4.91	4.59	4.55	4.39	4.23
20	5.14	5.16	4.89	4.46	4.18	4.13	4.02	4.01	3.98
25	4.81	4.91	4.39	4.00	3.92	3.86	3.90	3.77	3.77
30	3.73	4.14	4.36	3.89	3.86	3.95	3.80	3.66	3.59

QUADRANT = LEFT

ANGLE OF ATTACK (AOA) \ ANGLE OF SIDESLIP (AOS)	-20	-15	-10	-5	0	5	10	15	20
0	5.34	5.36	5.39	5.40	5.43	5.42	5.40	5.35	5.27
5	5.31	5.34	5.39	5.40	5.42	5.41	5.37	5.33	5.23
10	5.28	5.34	5.38	5.40	5.42	5.41	5.37	5.29	5.12
15	5.27	5.33	5.33	5.23	5.13	4.53	4.64	4.35	4.33
20	5.18	5.16	4.85	4.54	4.41	4.39	4.39	4.52	4.40
25	5.18	5.11	4.57	4.60	4.36	4.25	4.20	4.10	4.04
30	4.18	4.36	4.69	4.84	4.18	3.98	3.81	3.98	3.99

Total Pressure--Starboard Side

MN = 0.6

ALT = 36000

QUADRANT = TOP

ANGLE OF ATTACK (AOA)	ANGLE OF SIDESLIP (AOS)								
	-20	-15	-10	-5	0	5	10	15	20
0	3.99	4.05	4.07	4.09	4.11	4.10	4.11	4.11	4.10
5	4.00	4.04	4.07	4.10	4.11	4.10	4.11	4.10	4.10
10	3.98	4.02	4.07	4.09	4.10	4.11	4.11	4.10	4.09
15	3.92	3.97	4.05	4.01	4.14	3.84	4.00	3.57	3.37
20	3.82	3.90	3.91	3.81	3.60	3.42	3.34	3.29	3.48
25	3.49	3.70	3.68	3.28	3.50	3.60	3.55	3.63	3.67
30	3.10	3.04	3.59	3.36	3.68	3.18	3.39	3.80	3.83

QUADRANT = RIGHT

ANGLE OF ATTACK (AOA)	ANGLE OF SIDESLIP (AOS)								
	-20	-15	-10	-5	0	5	10	15	20
0	3.85	3.97	4.03	4.08	4.10	4.09	4.10	4.10	4.11
5	3.90	3.99	4.05	4.08	4.09	4.09	4.11	4.11	4.11
10	3.91	3.99	4.04	4.07	4.08	4.10	4.09	4.11	4.11
15	3.88	3.95	3.99	3.95	3.97	3.87	3.84	3.67	3.51
20	3.75	3.81	3.81	3.74	3.41	3.24	3.22	3.24	3.27
25	3.24	3.36	3.62	3.19	3.03	3.07	3.04	3.05	3.05
30	3.00	3.09	3.23	3.12	2.99	2.98	2.82	2.98	3.08

QUADRANT = BOTTOM

ANGLE OF ATTACK (AOA)	ANGLE OF SIDESLIP (AOS)								
	-20	-15	-10	-5	0	5	10	15	20
0	3.98	4.03	4.06	4.08	4.09	4.09	4.08	4.08	4.08
5	3.98	4.03	4.06	4.08	4.09	4.09	4.08	4.07	4.05
10	3.97	4.03	4.05	4.08	4.08	4.08	4.03	4.03	3.98
15	3.97	4.00	4.01	3.85	3.72	3.47	3.44	3.32	3.20
20	3.89	3.90	3.69	3.37	3.16	3.13	3.04	3.03	3.01
25	3.64	3.71	3.32	3.02	2.96	2.92	2.95	2.85	2.85
30	2.82	3.13	3.30	2.94	2.92	2.98	2.88	2.77	2.71

QUADRANT = LEFT

ANGLE OF ATTACK (AOA)	ANGLE OF SIDESLIP (AOS)								
	-20	-15	-10	-5	0	5	10	15	20
0	4.04	4.05	4.07	4.09	4.11	4.10	4.08	4.04	3.99
5	4.01	4.04	4.07	4.09	4.10	4.09	4.06	4.03	3.95
10	3.99	4.04	4.07	4.09	4.10	4.09	4.06	4.00	3.87
15	3.98	4.03	4.03	3.95	3.88	3.42	3.51	3.29	3.27
20	3.92	3.90	3.67	3.43	3.33	3.32	3.32	3.42	3.32
25	3.91	3.86	3.45	3.48	3.30	3.21	3.17	3.10	3.06
30	3.16	3.30	3.55	3.66	3.16	3.01	2.88	3.01	3.02

References

1. "Loss of Control on Approach, Colgan Air, Inc., Operating as Continental Connection Flight 3407, Bombardier DHC-8-400, N200WQ, Clarence Center, New York, February 12, 2009," Accident Report NTSB/AAR-10/01, National Transportation Safety Board, Washington DC, Feb. 2010.
2. "SE209: Airplane State Awareness - Simulator Fidelity (R-D)," October 2021https://skybrary.aero/articles/se209-airplane-state-awareness-simulator-fidelity-r-d, accessed 3/30/2022.
3. Schroeder, Jeffery A. and Burke, Robert H., "Upset Prevention and Recovery Training – A Regulator Update," AIAA 2016-1429, 4 January 2016.
4. Cunningham, K., Shah, G.H., Murphy, P.C., Hill, M.A., and Pickering, B.P., "Pilot Sensitivity to Simulator Flight Dynamics Model Formulation for Stall Training," AIAA-2019-0717, AIAA SciTech Forum, 7–11 January 2019, San Diego, CA.
5. Cunningham, K., Shah, GH., Hill, M.A., Pickering, B.P., Litt, J.S., Norin, S.B., "A Generic T-tail Transport Airplane Simulation for High-Angle-of-Attack Dynamics Modeling Investigations," AIAA 2018-1168, AIAA Modeling and Simulation Technologies Conference, AIAA SciTech Forum, January, 2018.
6. Anon., "Loss of Control In-Flight Accident Analysis Report, Edition 2019, Guidance Material and Best Practices," International Air Transport Association (IATA), 2019. https://www.iata.org/contentassets/b6eb2adc248c484192101edd1ed36015/loc-i_2019.pdf, accessed 1/14/2022.
7. Cashman, John E., Kelly, Brian D., Nield, Brian N., "Operational Use of Angle of Attack on Modern Commercial Jet Airplanes," Aero Magazine, No. 12, Oct. 2000. http://www.boeing.com/commercial/aeromagazine/aero_12/attack_story.html, accessed 2/27/2019.
8. Fuller, J.W., "Integrated Flight and Propulsion Control for Loss-of Control Prevention," AIAA 2012-4896, AIAA Guidance, Navigation, and Control Conference, 13-16 August 2012, Minneapolis, MN.
9. Walsh, P.P., and Fletcher, P., *Gas Turbine Performance*, Blackwell Science/ASME, 2004, p. 459.
10. Zhou H., Yu F., and Yang K., "Study on Design Compliance of Civil Turbofan Engine with the Requirements Defined in FAR 33.65," 3rd International Symposium on Aircraft Airworthiness, ISAA 2013, Procedia Engineering 80 (2014) 183–192, p. 188.
11. Raymer, Daniel P., Aircraft Design: A Conceptual Approach, 3rd Edition, AIAA Education Series, 1999, pp. 247–248.
12. Loftin, L.K., Jr., "Quest for Performance: The Evolution of Modern Aircraft," NASA SP-468, 1985, pp. 423–426.
13. "Anatomy of a Flameout," http://pop.h-cdn.co/assets/cm/15/06/54d1538f3923d_-_WWWrong106.pdf, accessed 10/25/2018.
14. Dennis A. Crider, "The Use of Data from Aviation Accident Investigations in Development of Flight Simulator Training Scenarios," AIAA-2017-1078, AIAA SciTech Forum, 9–13 January 2017, Grapevine, Texas.
15. National Transportation Safety Board, Crash of Pinnacle Airlines Flight 3701 Bombardier CL-600-2B19, N8396A Jefferson City, Missouri October 14, 2004, Accident Report NTSB/AAR-07/01, adopted January 9, 2007.
16. Simon, D.L., Rinehart, A.W., and Jones, S.M., "A Dynamic Model for the Evaluation of Aircraft Engine Icing Detection and Control-Based Mitigation Strategies," GT2017-65128, Proceedings of ASME Turbo Expo 2017: Turbomachinery Technical Conference and Exposition GT2017 June 26–30, 2017, Charlotte, NC.

17. Oates, Gordon C., ed., Aircraft Propulsion Systems Technology and Design, AIAA Education Series, American Institute of Aeronautics and Astronautics, 1989, pp. 373–376.
18. Liu, Yuan, Claus, Russell W., Litt, Jonathan S., Guo, Ten-Huei, "Simulating Effects of High Angle of Attack on Turbofan Engine Performance," AIAA 2013-1075, 51st AIAA Aerospace Sciences Meeting including the New Horizons Forum and Aerospace Exposition, Grapevine, TX, January 7–10, 2013, also NASA/TM—2013-217846, February 2013.
19. Agon, A., Abeynayake, A., and Smart, M., "Applicability of Viscous and Inviscid Flow Solvers to the Hypersonic REST Inlet," 18th Australasian Fluid Mechanics Conference, Launceston, Australia, 3–7 December 2012.
20. Bombardier CRJ700, https://customer.aero.bombardier.com/webd/BAG/CustSite/BRAD/RACSDocument.nsf/51aae8b2b3bfdf6685256c300045ff31/ec63f8639ff3ab9d85257c1500635bd8/$FILE/ATTE8Q23.pdf/CRJ700APMR15.pdf, accessed 3/30/2022
21. GE's CF34 Engine Family https://www.geaviation.com/bga/engines/cf34-engine, accessed 10/30/2018
22. Bombardier Challenger 605 – Power Plant, pp. 5–6, https://www.smartcockpit.com/docs/CL605-POWER_PLANT.pdf
23. EPR vs. N1, http://www.dj-airways.com/epr-vs-n1/
24. The Aircraft Gas Turbine Engine and its Operation, Pratt & Whitney Aircraft Group, 1980, pp. 152–156.
25. Jones, S.M., "Steady-State Modeling of Gas Turbine Engines Using the Numerical Propulsion System Simulation Code," GT2010-22350, Proceedings of ASME Turbo Expo 2010: Power for Land, Sea and Air, GT2010, June 14–18, 2010, Glasgow, UK.
26. Chapman, Jeffryes W., Lavelle, Thomas M., May, Ryan D., Litt, Jonathan S., Guo, Ten-Huei, "Propulsion System Simulation Using the Toolbox for the Modeling and Analysis of Thermodynamic Systems (T-MATS)," AIAA 2014-3929, 50th AIAA/ASME/SAE/ASEE Joint Propulsion Conference, Cleveland, OH, July 28–30, 2014, also NASA/TM—2014-218410, November 2014.
27. Chapman, Jeffryes W., Lavelle, Thomas M., Litt, Jonathan S., Guo, Ten-Huei, "A Process for the Creation of T-MATS Propulsion System Models from NPSS data," AIAA 2014-3931, 50th AIAA/ASME/SAE/ASEE Joint Propulsion Conference, Cleveland, OH, July 28–30, 2014, also NASA/TM—2014-218409, November 2014.
28. Chapman, Jeffryes W., Lavelle, Thomas M., May, Ryan D., Litt, Jonathan S., Guo, Ten-Huei, "Toolbox for the Modeling and Analysis of Thermodynamic Systems (T-MATS) User's Guide," NASA/TM—2014-216638, January 2014, p. 18.
29. https://www.nasa.gov/sites/default/files/atoms/files/arc-14275-1_cart3d.pdf, accessed 4/12/2019.
30. Aeronautical Vestpocket Handbook, 20th Ed., United Technologies, Pratt & Whitney, 1986.
31. Kerrebrock, Jack L., Aircraft Engines and Gas Turbines, The MIT Press, 1977, pp. 78–80.
32. Anderson, J.D., *Introduction to Flight*, McGraw-Hill, Inc., 1985, pp. 117–118.
33. Hill, Philip G., and Peterson, Carl R., Mechanics and Thermodynamics of Propulsion, Second Edition, Addison Wesley, 1992, pp. 170–171.
34. Triantafyllou, T., Nikolaidis,T., Diakostefanis, M., Pilidis, P., "Stability Assessment of an Airflow Distorted Military Engine's FAN," Proceedings of the Institution of Mechanical Engineers, Part G: Journal of Aerospace Engineering 232(13), 2018, pp. 2584–2592.
35. Williams, J.G., Steenken, W.G., Yuhas, A.G., "Estimating Engine Airflow in Gas-Turbine Powered Aircraft with Clean and Distorted Inlet Flows," NASA Contractor Report 198052, September 1996, pp. 41–44.

36. Culley, D., Garg, S., et al., “More Intelligent Gas Turbine Engines,” RTO TECHNICAL REPORT TR-AVT-128, April 2009.
37. Siller, H.A., Bassetti, A., Hage, W., and Funke, S., “Measurements of the noise generated by a V2500 engine in flight and in static measurements on the ground,” AIAA 2017-3844, AVIATION Forum, Denver, Colorado, 5–9 June 2017.
38. Airbus A320-232, G-EUUI p. 5 https://assets.publishing.service.gov.uk/media/5422ef18ed915d1374000269/dft_avsafety_pdf_032607.pdf, accessed 11/2/2018.
39. Sallee, G.P., “Performance Deterioration Based on Existing (Historical) Data; JT9D Jet Engine Diagnostics Program,” NASA Contractor Report 135448, 1978, pp. 156–159.
40. Volponi, A.J., “Gas Turbine Parameter Corrections,” Journal of Engineering for Gas Turbines and Power, vol. 121, October 1999, pp. 613–621.
41. Kurzke J., “Effects of Inlet Flow Distortion on the Performance of Aircraft Gas Turbines,” Journal of Engineering for Gas Turbines and Power, 130 (4), July 2008, p. 5.